NASA CR-54330
AVCO RAD-TR-65-13

THIRD QUARTERLY PROGRESS REPORT

RESISTOJET RESEARCH AND DEVELOPMENT - PHASE II

by

Richard D. John

prepared for

NATIONAL AERONAUTICS AND SPACE ADMINISTRATION

10 June 1965

CONTRACT NAS 3-5908

Technical Management
NASA Lewis Research Center
Cleveland, Ohio
Electric Propulsion Office
Henry Hunczak

RESEARCH AND ADVANCED DEVELOPMENT DIVISION
AVCO CORPORATION
Wilmington, Massachusetts

This document consists of 134 pages,
101 copies, Series A

THIRD QUARTERLY PROGRESS REPORT

RESISTOJET RESEARCH AND DEVELOPMENT - PHASE II

by

Richard D. John

prepared for

NATIONAL AERONAUTICS AND SPACE ADMINISTRATION

10 June 1965

CONTRACT NAS 3-5908

Technical Management
NASA Lewis Research Center
Cleveland, Ohio
Electric Propulsion Office
Henry Hunczak

RESEARCH AND ADVANCED DEVELOPMENT DIVISION
AVCO CORPORATION
Wilmington, Massachusetts

ABSTRACT

Descriptions are presented of an operational wire-in-tension thrust stand, and an operational impulse table. The thrust stand has a sensitivity of ± 5 micropounds and the impulse table has a sensitivity of ± 1 micropound. Thrust data obtained on a simple 5-mil diameter orifice indicate that the ratio of actual to ideal specific impulse is between 0.60 to 0.70 in the thrust range from 10^{-5} to 10^{-4} pounds. The Model I Single-Axis Resistojet Attitude Control System, including thrustors, a propellant storage and feed system, control logic, signal and power conditioning package, and an on-board position sensor has been successfully operated on the air bearing facility at NASA Lewis. Operation of the sytem has been demonstrated in the acquisition mode, and in both soft and hard limit-cycle operation.

CONTENTS

CONTENTS (Cont'd)

CONTENTS (Concl'd)

ILLUSTRATIONS

ILLUSTRATIONS (Concl'd)

ILLUSTRATIONS (Cont'd)

ILLUSTRATIONS (Concl'd)

TABLES

SUMMARY

The overall objective of this program is to carry out research and development on both pulsed and continuous resistojet thrustor systems for operation from 5 to 5000 watts. Work is currently being concentrated on the development of 5- to 50-watt thrustors suitable for the attitude and orbit control of satellites in the 500- to 1000-pound class.

During the past quarter work has been completed on the development of both a wire-in-tension thrust stand and an impulse table. The thrust stand has a thrust measurement capability of ±5 micropounds, and the impulse table has a thrust measurement capability of ±1 micropound. The basic measurement device in the thrust stand is a direct displacement transducer; the angular velocity change of the impulse table is measured with on-board rate gyroscopes. Thrust stand data obtained with a 5-mil diameter orifice, using ammonia as a propellant, indicate that the ratio of the actual to the ideal impulse is between 0.60 and 0.70 in the thrust range from 10^{-5} to 10^{-4} pound.

The Model I Resistojet Attitude Control System has been successfully operated on the air bearing attitude control system (ACS) test bed located at NASA Lewis. The ACS contains an ammonia feed system and resistojet thrustors, control logic package, power and signal conditioning packages, and a position sensor. The control system demonstrated acquisition, and both soft and hard limit-cycle operation over a range of input disturbance torques from 200 to 1000 dyne-cm.

Preliminary studies have been completed on the design of a three-axis ACS for application to satellites in the 500- to 1000-pound class. Power conditioning for the low-resistance (order of 0.10 ohm) resistojet engines is accomplished by inverting the dc power from the power supply into 1000 cps ac, and stepping down the voltage (24 volts to 1 volt) with a lightweight transformer located at the thrustor. In this manner power lead losses are minimized.

I. INTRODUCTION

This is the third quarterly progress report submitted under contract NAS 3-5908, entitled, Resistojet Research and Development - Phase II. This report covers the period 1 January 1965 through 31 March 1965.

A. PROGRAM OBJECTIVES

The overall objectives of this program are to pursue research and development of electrothermal thrustor systems of the resistance type in the power range from 5 to 5000 watts. During the third quarter, attention has continued to be focused on resistojets operating at power inputs less than 50 watts and at thrust levels below 10^{-3} pounds. A single-axis breadboard resistojet attitude control system, developed as part of the present program, has been successfully operated on the air bearing facility at NASA Lewis. The resistojet ACS includes propellant feed, power conditioning, control logic, sensor, and engine packages. The single-axis resistojet ACS technology will be applied to the development of a breadboard three-axis resistojet ACS. The ultimate objective of this phase of the program is to provide the technology required to develop flight-qualified, three-axis resistojet ACS and station-keeping systems.

B. PROGRAM ORGANIZATION

This program originates from the Electric Propulsion Office of the NASA Lewis Research Center. Mr. Henry Hunczak is Project Manager for the NASA Lewis Research Center. The Project Director at Avco RAD is Dr. R. R. John. Other participants in this program and their principal areas of contribution are: Dr. S. Bennett, and Dr. D. Morgan, Mr. W. Huss and Mr. J. Malenda, Thrustor and Test System Design and Development; Mr. J. T. Smith, Materials Development; Mr. R. Coulombre, Mr. H. D'Auriol, and Mr. J. Olbrych, System Design and Development.

C. PROGRAM SCHEDULING

This is the third quarterly progress report and summarizes technical progress under contract NAS 3-5908. Data on contract costs and manpower have been previously submitted in Monthly Letter Reports 7 (10 February), 8 (10 March), and 9 (10 April).

II. RESISTOJET ENGINE DEVELOPMENT

The engine development program is currently concentrated on the development of fast heat-up resistojets for operation in the thrust range from 10^{-5} to 10^{-4} pounds and at power levels of the order of 10 watts. Program emphasis during the past quarter has been on continued improvement of the wire-in-tension thrust stand described previously,[1,3] and on the development of an impulse table; fabrication techniques have been developed for the heater-nozzle element which permit close tolerances on the nozzle throat and heater wall thickness; finally, data have been obtained on the nozzle performance in the thrust regime between 10^{-4} and 10^{-5} pounds of thrust.

A. MEASUREMENT OF ENGINE PROPULSION PERFORMANCE

1. Wire-in-Tension Thrust Stand

The wire-in-tension thrust[1,3] development has been completed and two stands are in operation. The thrust stand background noise level has been reduced to about ±5 micropounds without electrical filtering. The final suspension system used to isolate the basic thrust table from the laboratory is shown in figure 2.1. The thrust stand is suspended on a triple-folded spring and ring system. Dampers are located inside each spring. Figure 2.2 shows a photograph of the suspension system and the thrust table in position on the vacuum plate (with the bell jar removed).

The basic thrust table is shown in figure 2.3. The stand consists of an outer ring suspended by the spring suspension system illustrated in figures 2.1 and 2.2. A smaller inner ring is supported from the outer ring by four wires stretched to a high state of tension. The thrustor is mounted on this inner ring with the thrust direction downward. A measurement of the vertical displacement between the inner and outer rings is used to indicate engine thrust. Since very small displacements are involved, a highly sensitive linear differential transformer (Sanborn Model 595D-005BM) is used for the displacement measurement; this unit has an ultimate sensitivity of 10^{-7} inches displacement. One side of the displacement transducer is supported on the large yoke fastened to the outer ring; the other side is supported on the smaller yoke fastened to the inner ring (see figure 2.3). For calibration small weights are placed on the channel mounted on top of the inner ring. A motor-operated lifting device permits remote positioning of known weights on the inner ring; this permits the static determination of the displacement as a function of applied force. Figure 2.4 shows a typical displacement versus force curve showing that the displacement is linear with force.

The thrustor on the inner ring is connected to the ammonia propellant supply by a flexible tube. This tube introduces negligible error in the measurement,

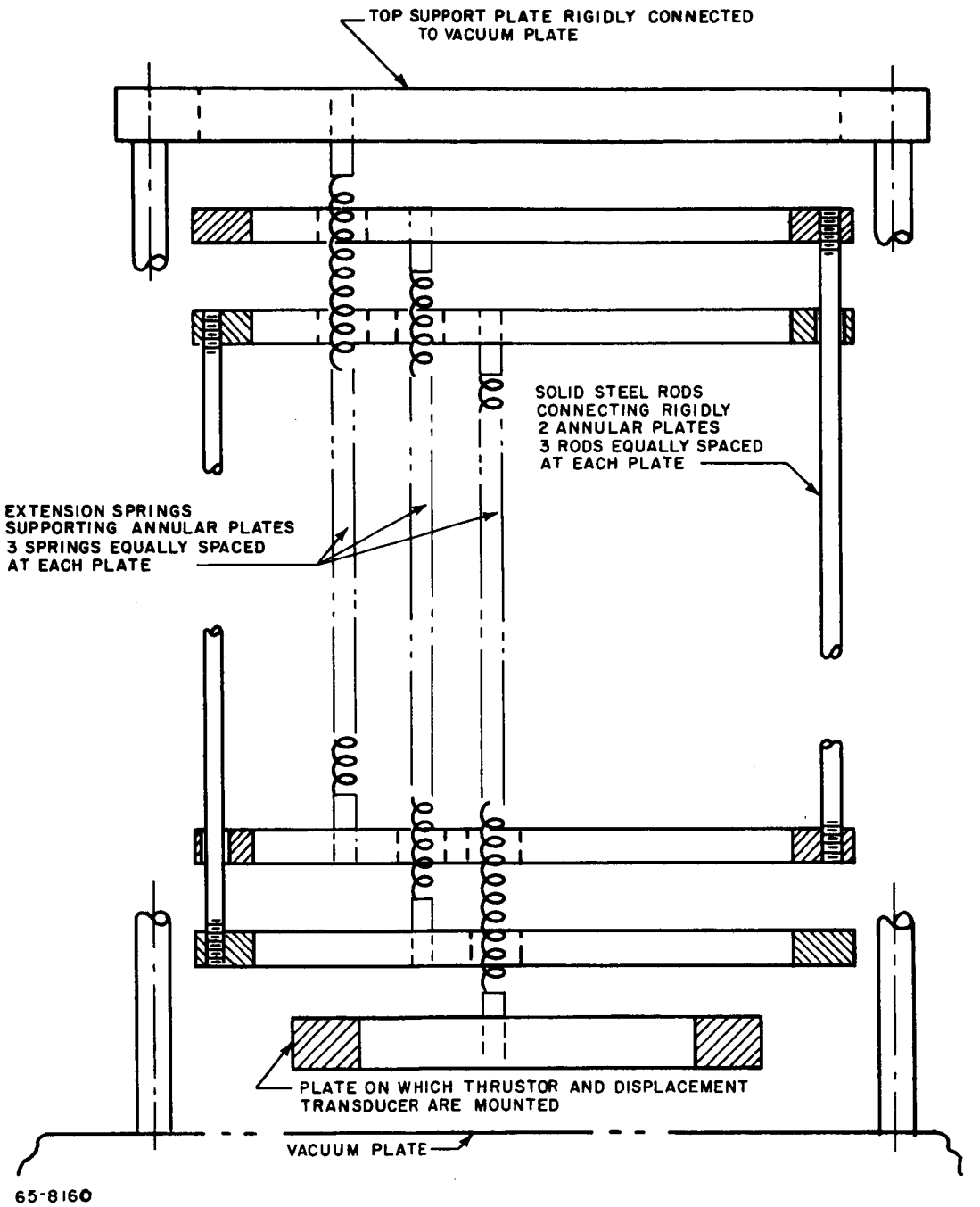

Figure 2.1 SCHEMATIC OF SUSPENSION SYSTEM FOR THE WIRE-IN-TENSION THRUST STAND

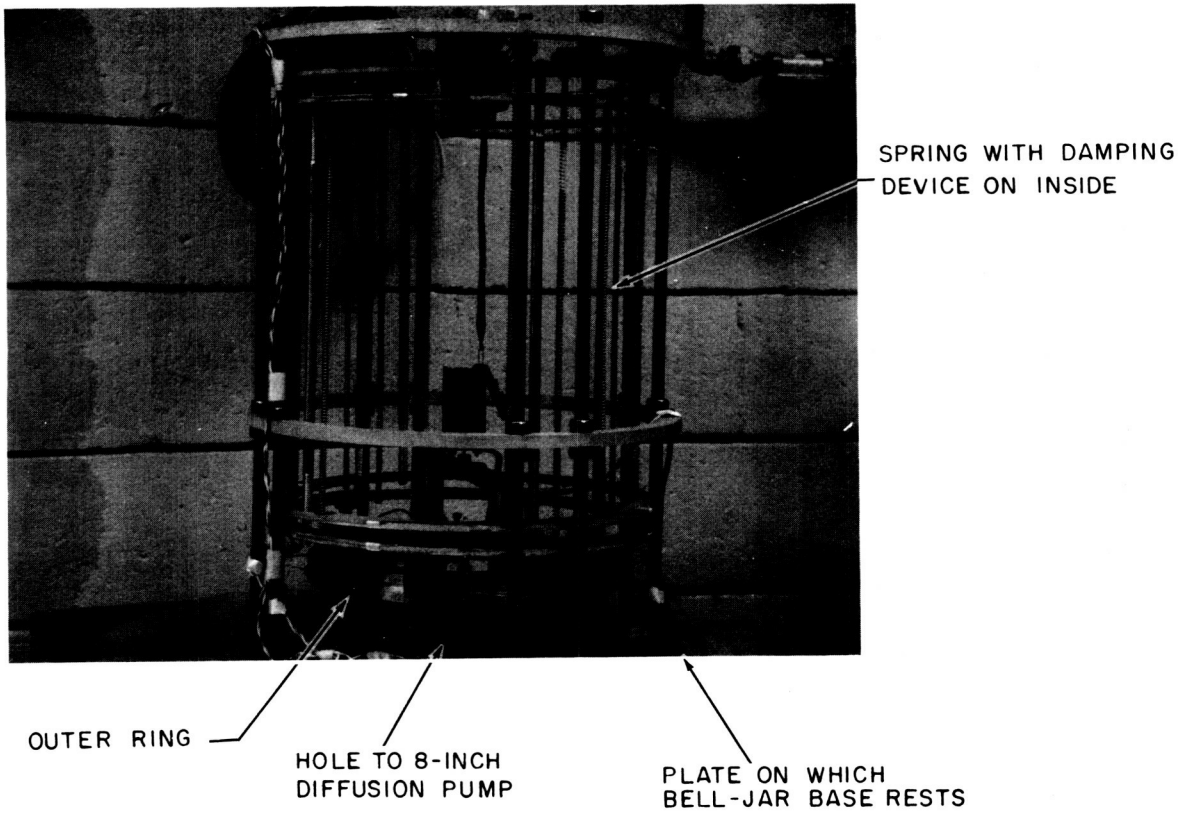

Figure 2.2 PHOTOGRAPH OF THE SUSPENSION SYSTEM AND THRUST PLATE

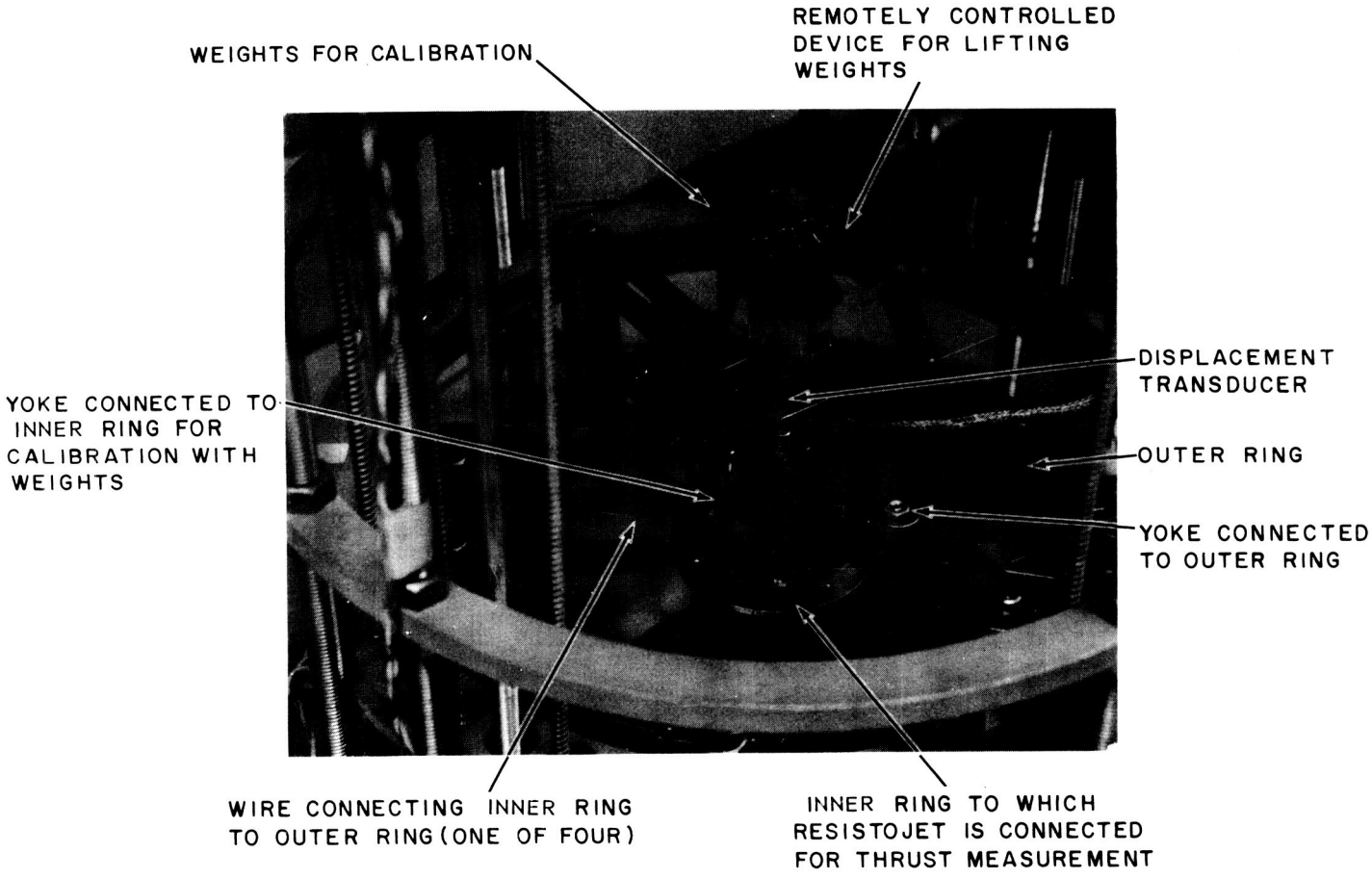

Figure 2.3 PHOTOGRAPH OF BASIC THRUST TABLE

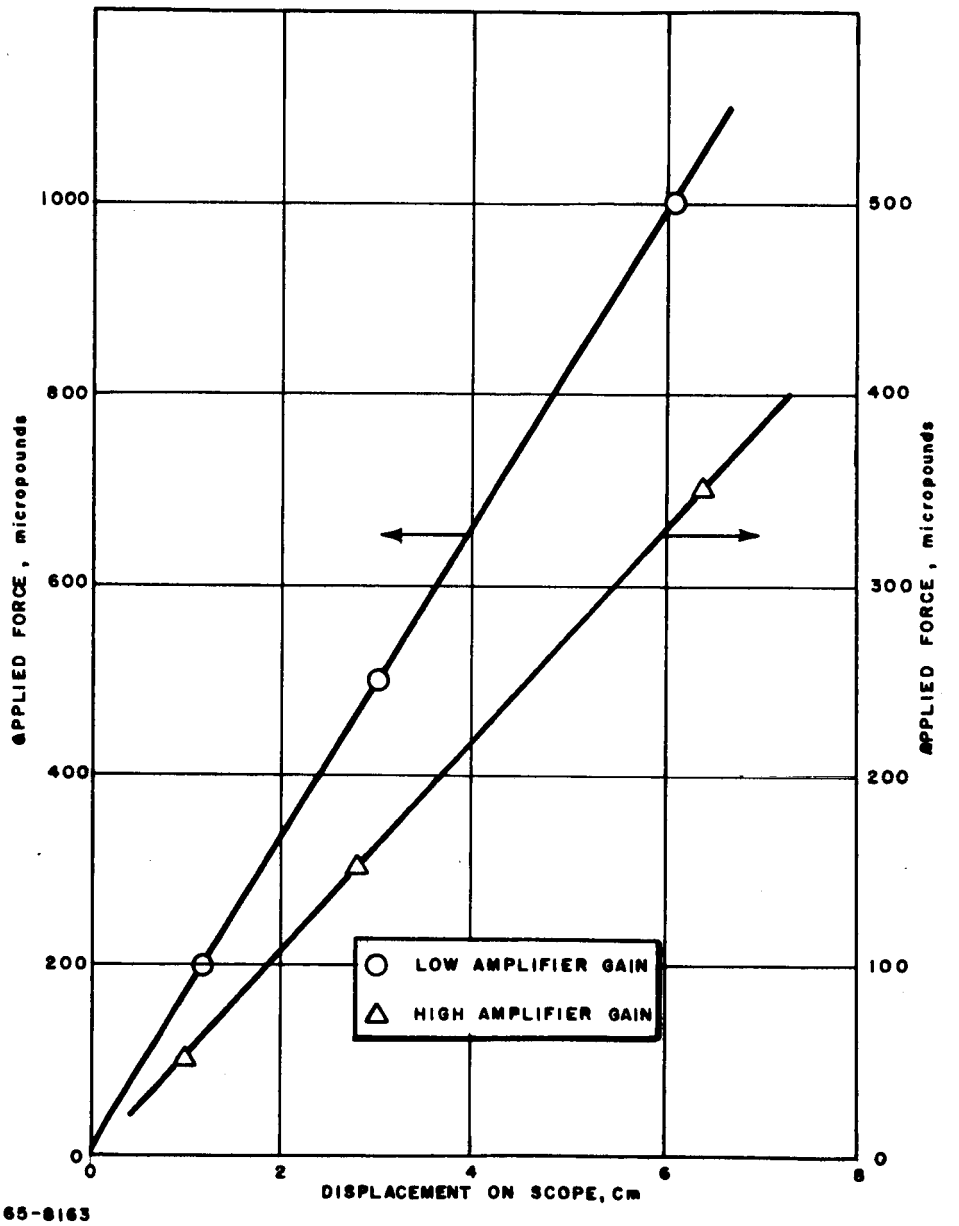

Figure 2.4 THRUST STAND DISPLACEMENT VERSUS APPLIED FORCE

since the calibration techniques include deflection of this tube, and since the flexural force of the tube is orders of magnitude less than that of the four wires supporting the inner ring. The valve controlling the propellant flow is placed on the outer ring.

2. Flow Measurement System

A schematic of the ammonia propellant supply and flow measuring system is given in figure 2.5. The flow measurement involves valving off from the ammonia supply a known volume V_1 and measuring the decrease in pressure in this known volume for a given number of resistojet pulses or, in steady state operation, over a given period of time. The pressure decrease and known volume provide an accurate measurement of the total mass flow and thus provide either the mass per resistojet pulse or the steady state ammonia flow rate. Referring to figure 2.5, the pressure decrease is measured with a differential pressure transducer connected to the volume V_1 and to a reference pressure.

At the beginning of a measurement, solenoid valve V3 is opened and the pressure in V_1 and the pressure reference tank equalized. Valves V1, V2, and V3 are then closed isolating the volume V_1 and the decrease in pressure observed with the differential pressure transducer. Using the ideal gas law, the total expelled gas is given by:

$$m = \Delta P \left(V_1 / \frac{RT}{M} \right) \tag{2.1}$$

where

R = universal gas constant psia, feet^3/lb-mole-°R

M = molecular weight, lb/lb mole

T = gas temperature, °R

m = total mass flow, pounds

V_1 = volume of closed-off system, feet^3

ΔP = pressure decrease, psi

The sensitivity of the pressure transducer used is 0.0775 psi/millivolt; the millivolt output is generally measured on an oscilloscope using a sensitivity of 1 mv/cm. Assuming an accuracy of reading the trace of ±0.1 cm, the pressure decrease can be read with an accuracy of about ±0.01 psia. The time measurement is taken using an electronic timer with an accuracy of ±1 millisecond. With these accuracies and using a standard volume of 84 milliliters, the present mass flow measurement capability for a ΔP of 0.5 psia is 1×10^{-7} lb/sec ±3 percent.

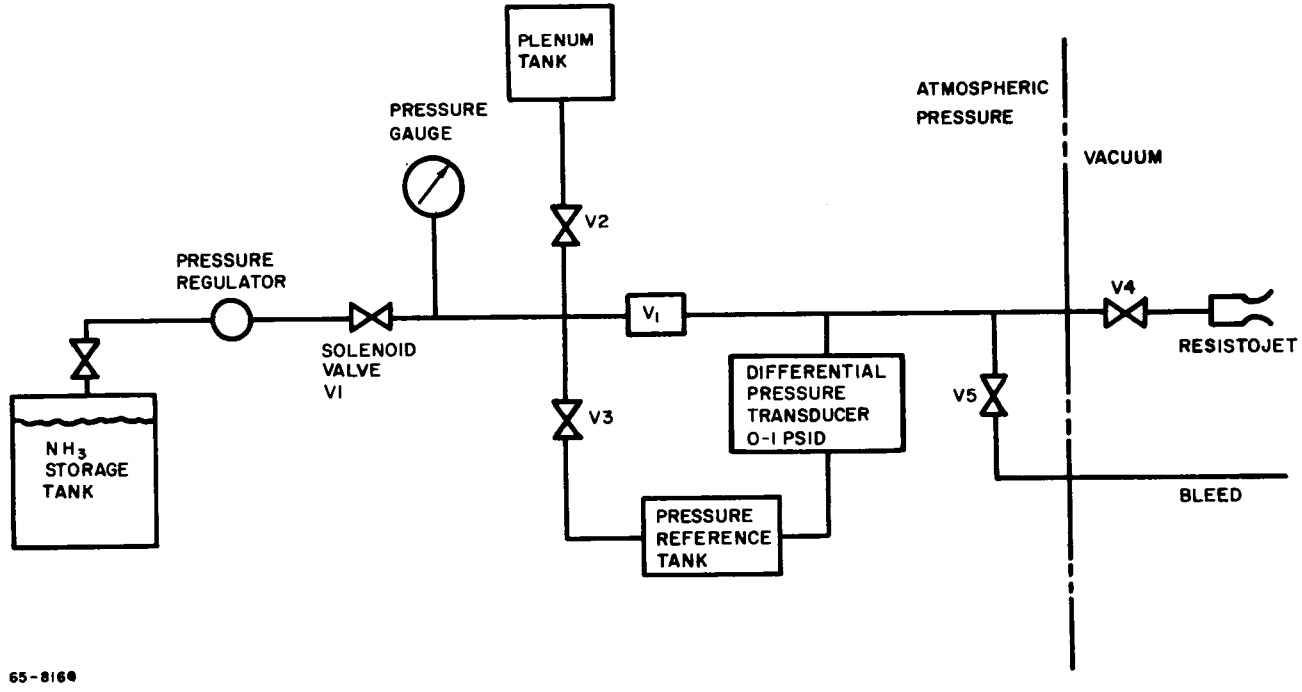

Figure 2.5 LABORATORY AMMONIA PROPELLANT SUPPLY AND FLOW MEASUREMENT SYSTEM

3. Impulse Table

An impulse table has been designed, developed, and tested for measuring the impulse output of microthrust mass expulsion devices operated in the thrust range from 10^{-5} to 10^{-3} pounds and below. The impulse table is shown schematically in figure 2.6. It basically consists of a horizontal table mounted on a vertical wire. Impulse bits (lb-sec) are given to the table by means of a thrustor and observations are made on the change of angular rate of the table. The equation of motion of the table is given by

$$\Delta\dot{\theta} = \frac{\tau_R + \tau_D}{J} t_R \qquad (2.2)$$

where, $\Delta\dot{\theta}$ (radians/sec) is the measured change in angular rate, τ_R (lb-ft) = F (lbs) x r (ft) is the applied torque, τ_D (lb-ft) is the system disturbance torque, t_R (sec) is the time the applied torque acts on the system, and J (lb-ft-sec^2) is the table moment of inertia. In the current tests the measured change in angular rate has been measured both optically and with on-board rate gyros.

The major design goal in the development of the impulse table has been to hold the disturbance torque, τ_D, which primarily arises from wire tension, to as low a value as possible. This has been accomplished by using a stranded cable which has a spring constant of about 300 dyne-cm/deg, and by providing an optical-driven servo system which can hold the table to less than 0.01 degree. Thus, the disturbance torque due to wire tension is less than 5 dyne-cm which corresponds to a thrust of less than 10^{-6} pounds at a moment arm of 2 feet.

During the next quarter, the single-axis table will be mounted in a 6- x 8-foot vacuum chamber and connected to a low-pressure diffusion pump (32-inch diameter) system. The resistojet engines will be operated on the impulse table at back pressures of less than 1 micron. Engine performance data obtained on the impulse table will be compared with results obtained on the wire-in-tension thrust stand.

The impulse table can also serve a secondary function for preliminary checkout of single-axis ACS. The servo system permits systematic variation of disturbance torque, τ_D, acquisition angle, $\theta_{initial}$, and acquisition rate, $\dot{\theta}_{initial}$. The details of the single axis resistojet attitude control system are presented in section III. Typical results, indicative of the application of the impulse table to preliminary checkout of the single-axis ACS are presented in appendix C.

B. ENGINE FABRICATION TECHNIQUES

A major problem in the development of the fast heat-up resistojet has been the fabrication of the relatively small heater nozzle elements. In the engines tested

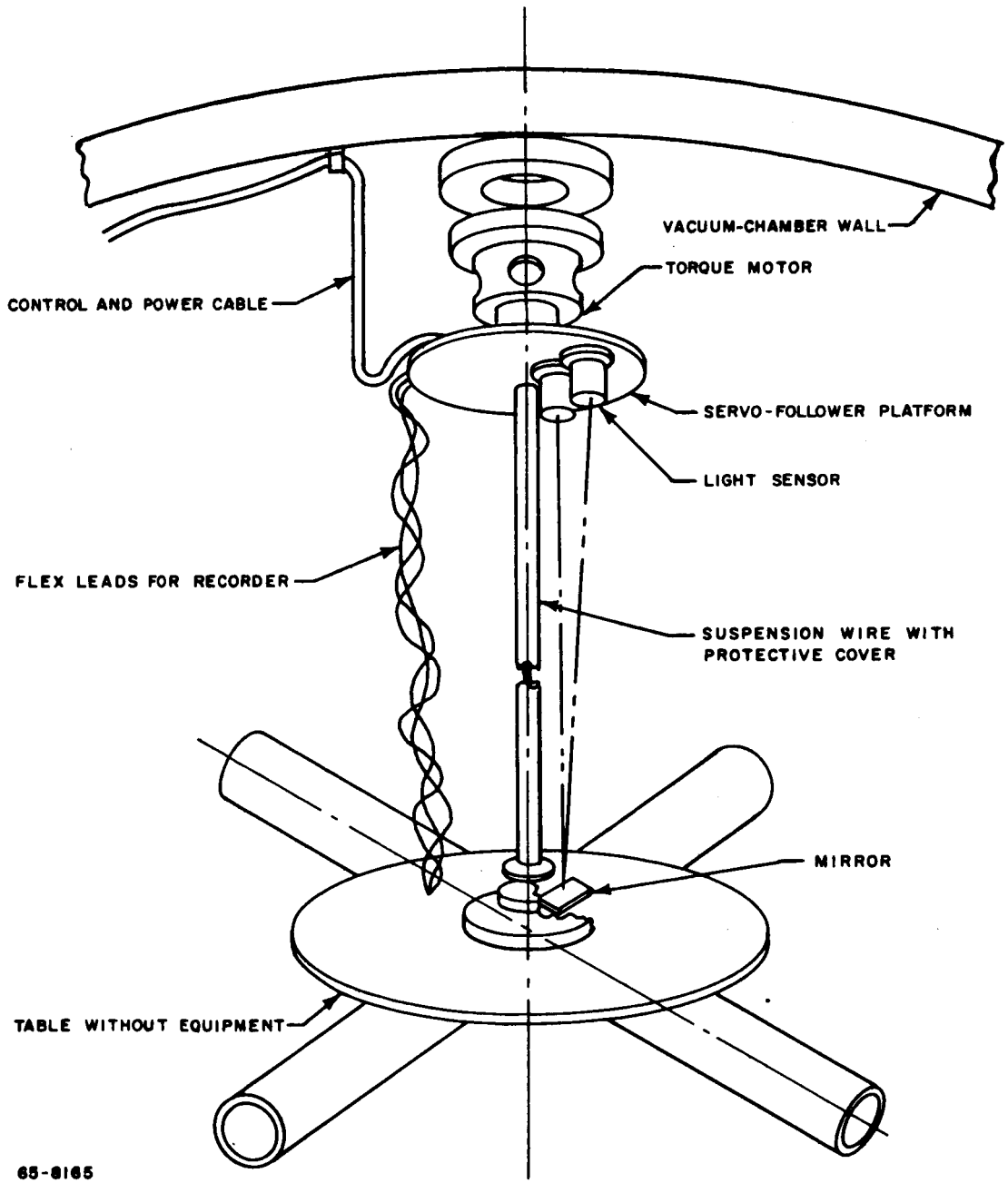

Figure 2.6 SCHEMATIC DIAGRAM OF THE IMPULSE TABLE

to date the heater-nozzle elements have been fabricated directly from thin wall tubing. The nozzle shape has essentially been pressed into the thin wall tubing; this procedure has made it very difficult to control the critical heater-nozzle dimensions.

During the past quarter a process has been developed for the reliable fabrication of the heater-nozzle units. The process consists of deposition of a refractory metal onto a mandrel of the desired shape and dissolving the mandrel in an acid. Close control can be obtained on the resistojet dimensions by machining the mandrel to the desired shape before plating. Molybdenum, which can be dissolved in hot nitric acid has been used as the mandrel for tungsten; titanium, which can be dissolved in hydrofluoric acid, has been used for rhenium. Fused salt electrolysis was used to deposit the tungsten; vapor deposition was used for the rhenium and tungsten-rhenium alloy. Details are presented below.

1. Mandrel Fabrication

Material selection for mandrel fabrication was influenced by operating temperature of the deposition process and acid resistance of the deposited metal. Operating temperatures of the fused salt plating and vapor plating processes were in the range 800 to 1000°C. Thus, molybdenum, which retains strength at these temperatures, was chosen as a substrate for tungsten. However, molybdenum could not be used for rhenium coatings for both are attacked by the same acids. Hence, titanium was chosen as mandrel material for vapor deposited rhenium.

The mandrel is made by cutting 2-inch lengths of 0.070-inch wire, slitting 1/4-inch tabs in the wire, bending the tabs at right angles to the length of the wire, then machining the nozzle, constriction and, shaft on a jewelers lathe using a carbide tipped cutting tool. Figure 2.7 shows the various machining steps. After machining, the mandrel is polished electrochemically in an alcohol-sulfuric acid solution using 20 volts of direct current for one minute. Dimensions are shown in figure 2.8.

2. Fuzed Salt Electrolysis

This is a proprietary process developed by the Parma Research Division of Union Carbide Corporation. The electroplating solution consists of molten tungsten-fluoride, sodium-fluoride, and potassium-fluoride salts. The operating temperature is 800°C. Many articles can be plated simultaneously, as in regular plating. Thickness of the coatings can be controlled from a fraction of a thousandth of an inch to heavy deposits up to a quarter of an inch thick or more. The tungsten coatings used in this investigation were 0.003 to 0.004 inch thick and were fully dense and free of pin-holes; the crystal structure is columnar and radially oriented. At present, rhenium or alloys of rhenium cannot be deposited by this method.

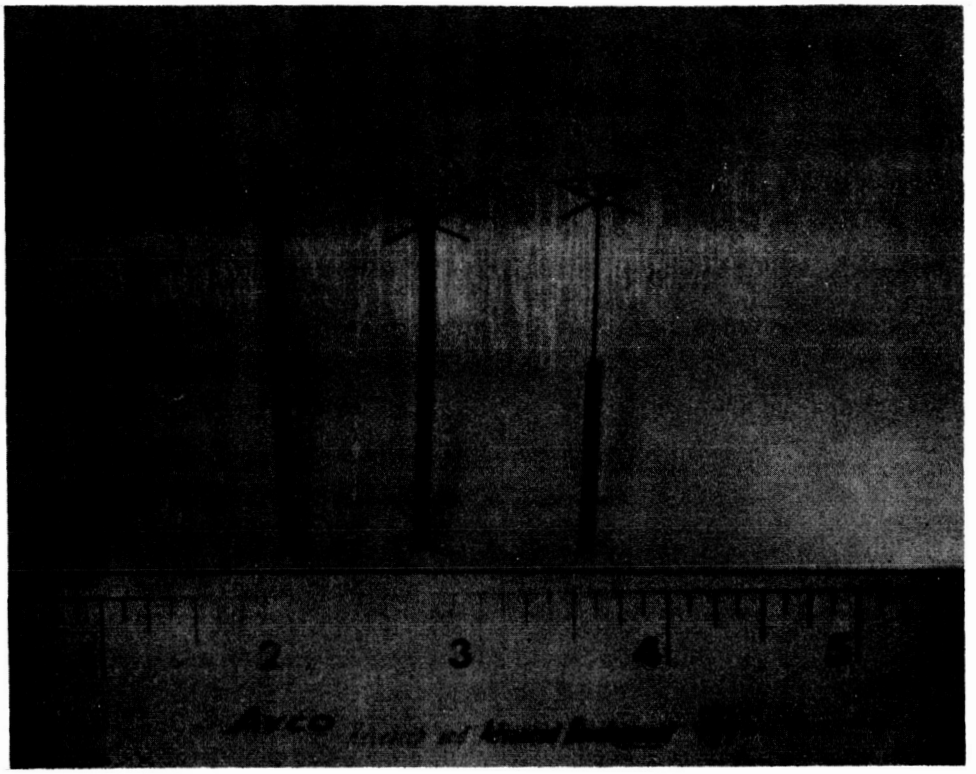

65-8166

Figure 2.7 MANDREL FABRICATION

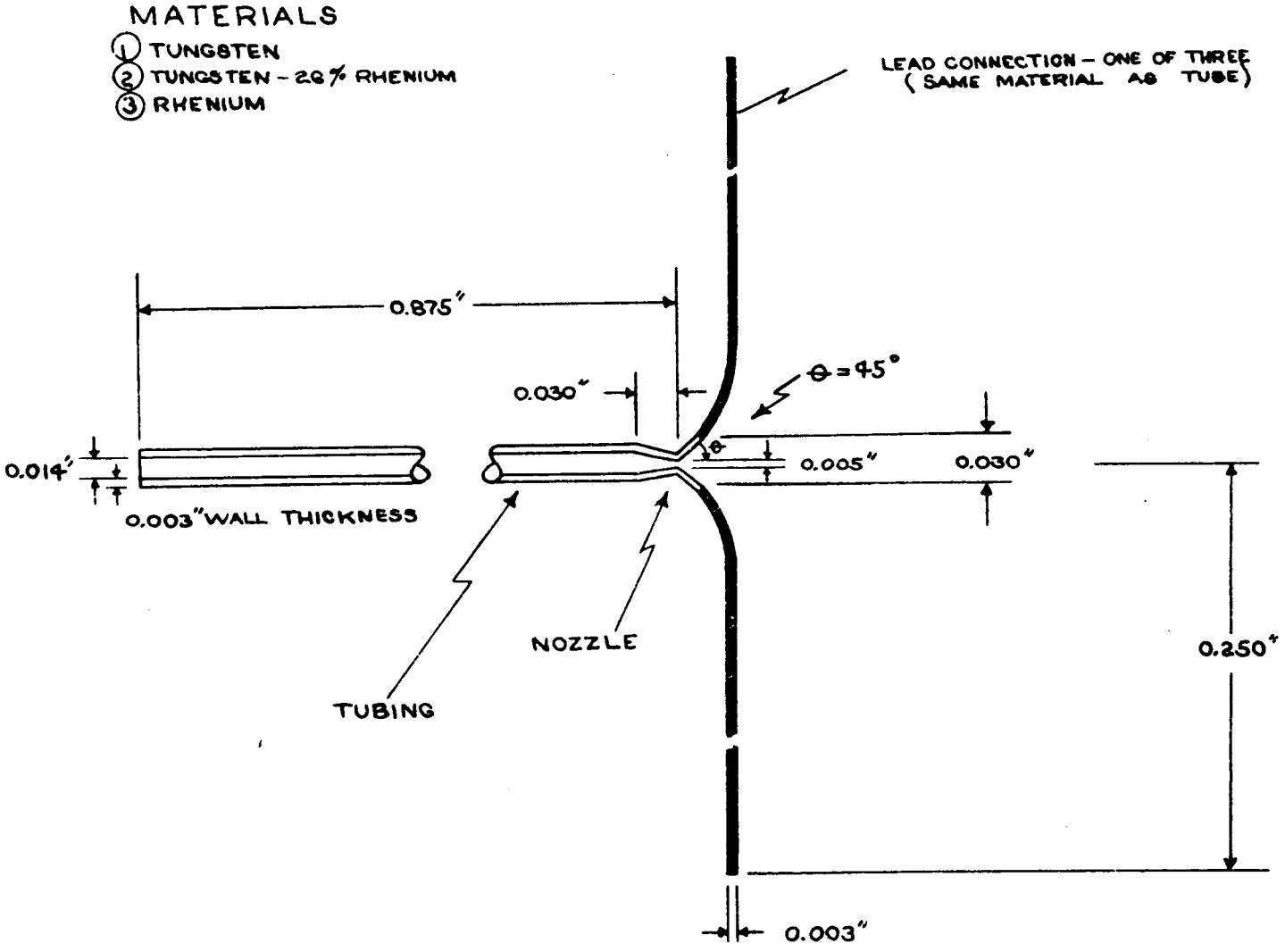

Figure 2.8 BASIC MANDREL DIMENSIONS

3. Vapor Deposition

This process operates on the principle of thermal decomposition of metal halides or carbonyls onto a heated substrate. Operating temperature of the substrate is 900 to 1000°C. Tungsten, rhenium, and alloys of tungsten/rhenium are among the metals which can be deposited. These coatings also are fully dense and free from pin holes. San Fernando Laboratories of Pacoima, California, supplied the coatings for this investigation. Figure 2.9 shows samples of rhenium and rhenium-tungsten alloy deposited by vapor deposition. At present, the process is relatively expensive as only one mandrel at a time can be coated.

4. Dissolving the Mandrel

Molybdenum mandrels were dissolved in a nitric acid (85 percent) sulfuric (15 percent) acid solution operated at 70°C under a pulsating negative pressure cycle as shown in figure 2.10. The time required to dissolve a 1-inch-long mandrel is 16 to 20 hours. It is interesting to note that the dissolution rate of bare molybdenum wire in this solution is very rapid (see figure 2.11).

Titanium mandrels are dissolved in a 50-percent solution of hydrofluoric acid (48-percent HF) at room temperature. In this case, the reaction product is titanium trifluoride (red-violet). The same techniques mentioned above must be used; i.e., pulsating vacuum and careful rinsing. The dissolution rate of exposed titanium wire is shown in figure 2.12. The time required to remove a 1-inch mandrel is, like molybdenum, 16 to 20 hours.

The long acid-leaching time required in the case of the enclosed mandrel is due to the entrapment of hydrogen gas bubbles and reaction products in a very small diameter tube. In the case of molybdenum, the reaction products precipitated on drying out were observed to be a mixture of molybdenum dioxide (lead gray), molybdenum trioxide (whitish yellow) and molybdenum pentoxide (violet blue). These products are formed on the face of the mandrel inside the tube if the tube is allowed to dry without efficient rinsing. If this occurs, restarting the dissolution process becomes very difficult and even impossible in severe cases. During the course of this investigation, it was found necessary to rinse out the tubes with hot distilled water, followed by a rinse in concentrated hydrochloric acid. Both rinses must be carried out under vacuum using the pressure cycle shown in figure 2.10.

C. ENGINE PERFORMANCE

During the past quarter effort in this area was primarily directed to the improvement of the thrust measurement capability of both the wire-in-tension thrust stand and the impulse table. Some data have been obtained, however, on the

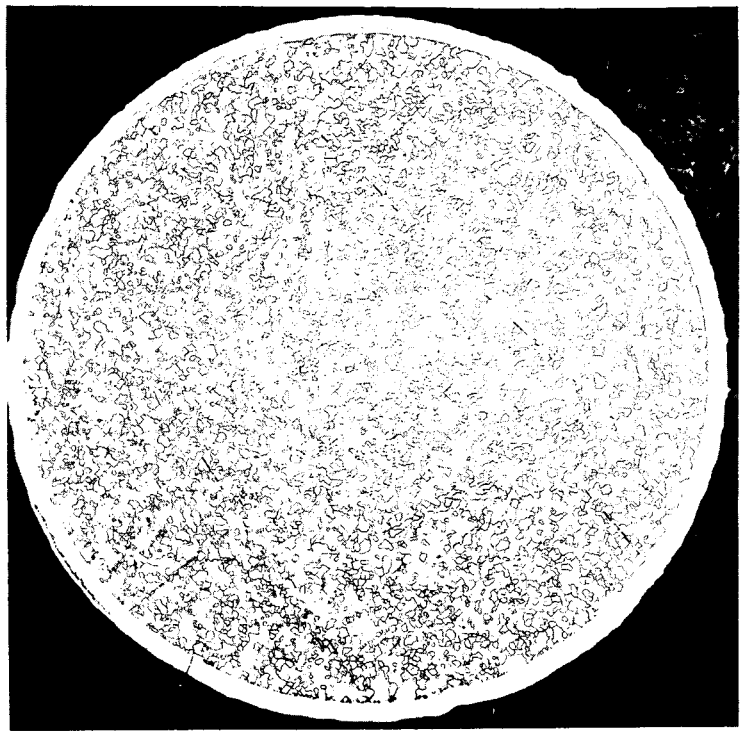

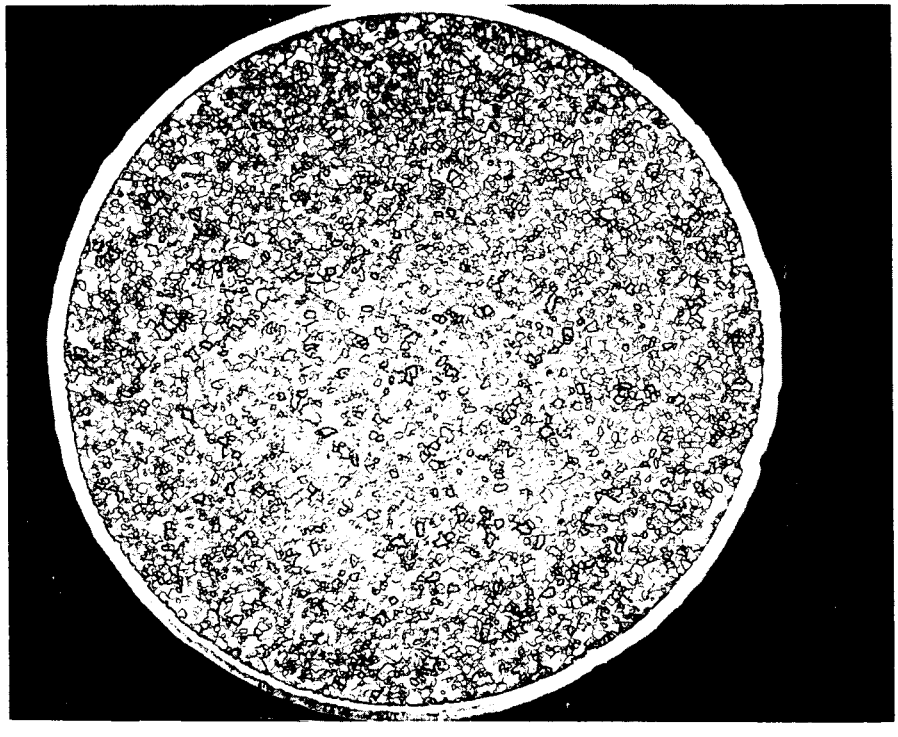

Figure 2.9 PHOTOMICROGRAPHS OF VAPOR-DEPOSITED RHENIUM AND RHENIUM/TUNGSTEN ALLOY

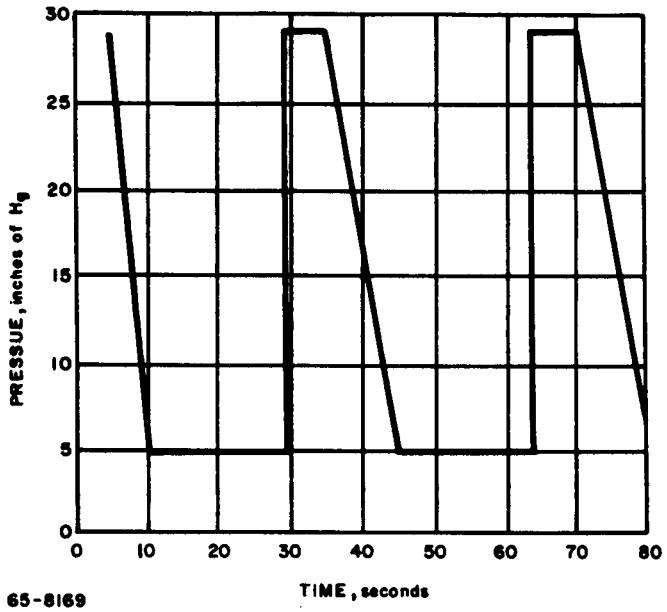

Figure 2.10 PULSATING PRESSURE CYCLE FOR DISSOLVING THE MOLYBDENUM MANDREL

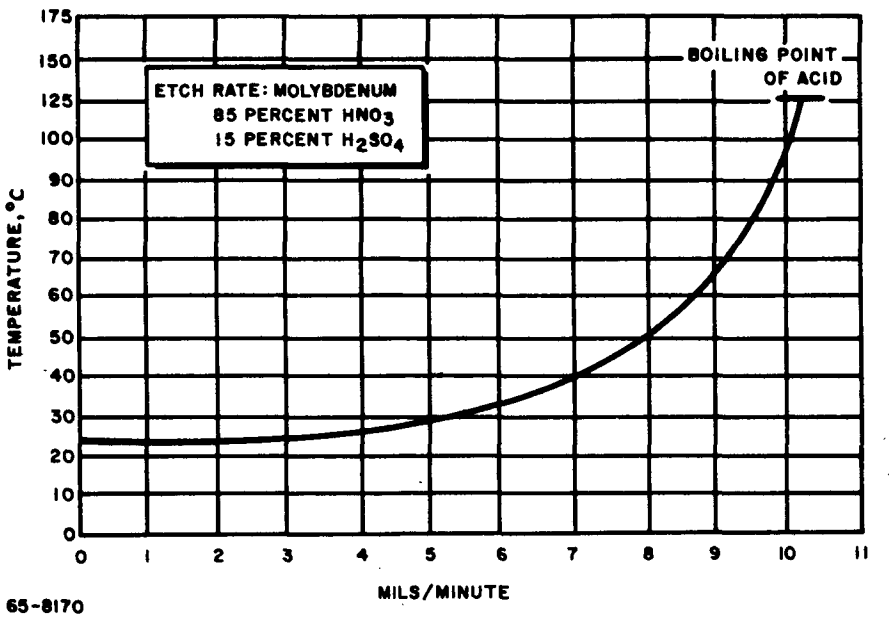

Figure 2.11 DISSOLUTION RATE OF BARE MOLYBDENUM WIRE

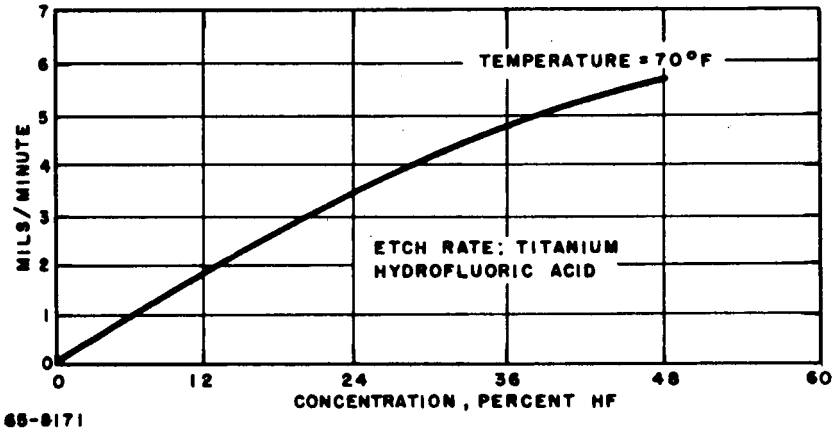

Figure 2.12 DISSOLUTION RATE OF BARE TITANIUM WIRE

performance of a small (5-mil) diameter orifice in ammonia flow. A diagram of the orifice is presented in figure 2.13. The purpose of the tests was to explore orifice and nozzle behavior in the thrust regime between 10^{-6} and 10^{-4} pound of thrust where Tinling[4] originally reported a marked deterioration in cold-gas nozzle performance. The results were obtained using the wire-in-tension thrust stand. The ammonia flow was at room temperature and the nozzle-box pressure was varied over the range from 1 to 5 psia.

Table 2.1 shows the propulsion performance of the orifice. The orifice coefficient defined as the ratio of actual to ideal mass flow is shown as a function of Reynolds number (based on nozzle diameter) in figure 2.14; the experimental results are superimposed on the original results of Tinling (reference 4, figure 6). Figure 2.15 presents the ratio of actual to ideal specific impulse (for orifice flow) as a function of mass flow, again superimposed on the original results of Tinling (reference 4, figure 8). The nozzle-orifice coefficients for both sets of experiments are essentially identical. In the case of the specific impulse, however, there is no evidence of the sharp falloff in performance originally reported by Tinling. As indicated in the previous quarterly (reference 1, page 37) Tinling has recently found that the original reported dropoff in specific impulse could be attributed to operation at a relatively high (30 micron) back pressure. The data reported in table 2.1, which indicate no significant falloff in specific impulse at low-thrust levels is in accord with Tinling's most recent results. Similarly, recent work by Jonath[5] in the 10^{-4} to 10^{-5} range indicates a recovery of nearly 90 percent of theoretical specific impulse.

The above data strongly suggests that there is not a marked deterioration of nozzle performance in the thrust regime between 10^{-5} to 10^{-4} pound, even though the orifice coefficient of 0.50 to 0.60 suggests strong viscous-flow effects. This area, however, is still under active investigation.

TABLE 2.1

PROPULSION PERFORMANCE OF A 5-MIL DIAMETER ORIFICE WITH AMMONIA FLOW

Chamber Pressure (psia)	Meas. Thrust (μlbs)	Ammonia Flow (μlbs/sec)	Specific Impulse (sec)
5	90	1.9	49
4	73	1.4	54
3	43	0.93	47
2	27	0.71	38
1	20	0.40	50

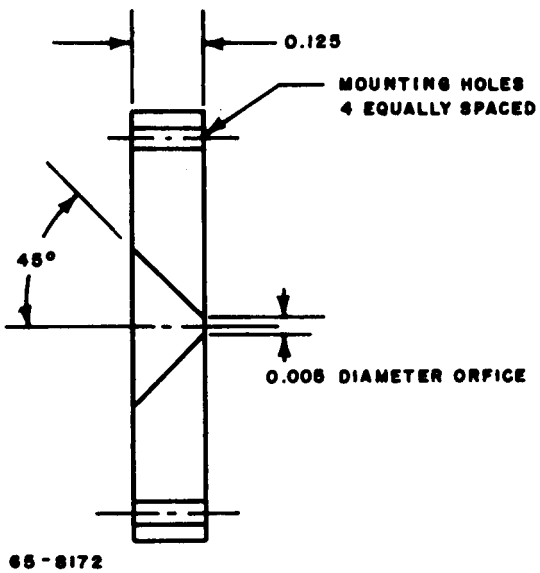

Figure 2.13 SHARP-EDGED ORIFICE EXIT NOZZLE

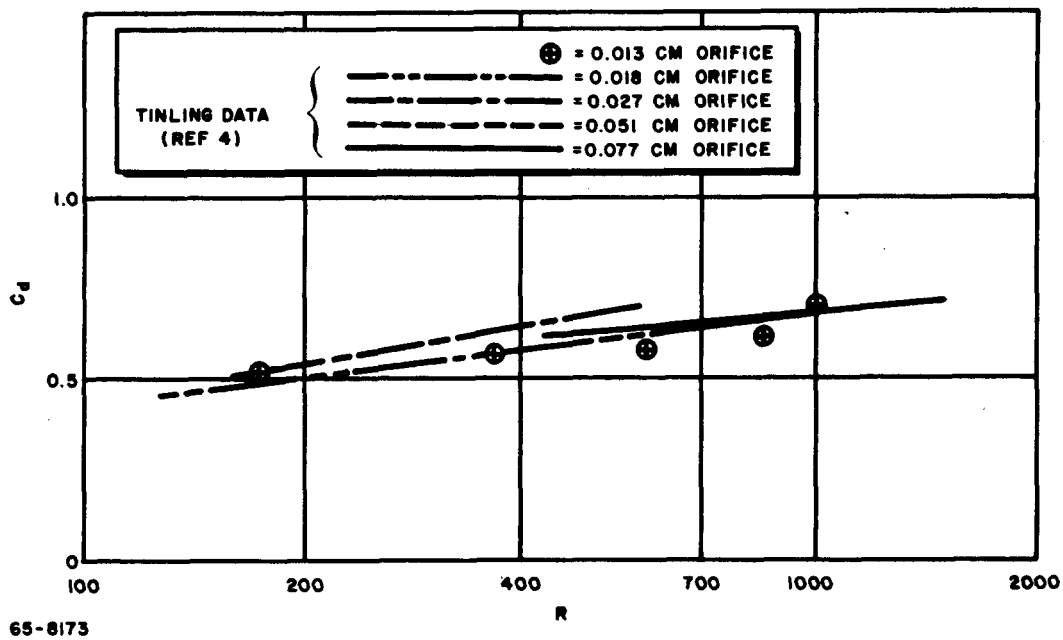

Figure 2.14 ORIFICE COEFFICIENT VERSUS NOZZLE REYNOLDS NUMBER

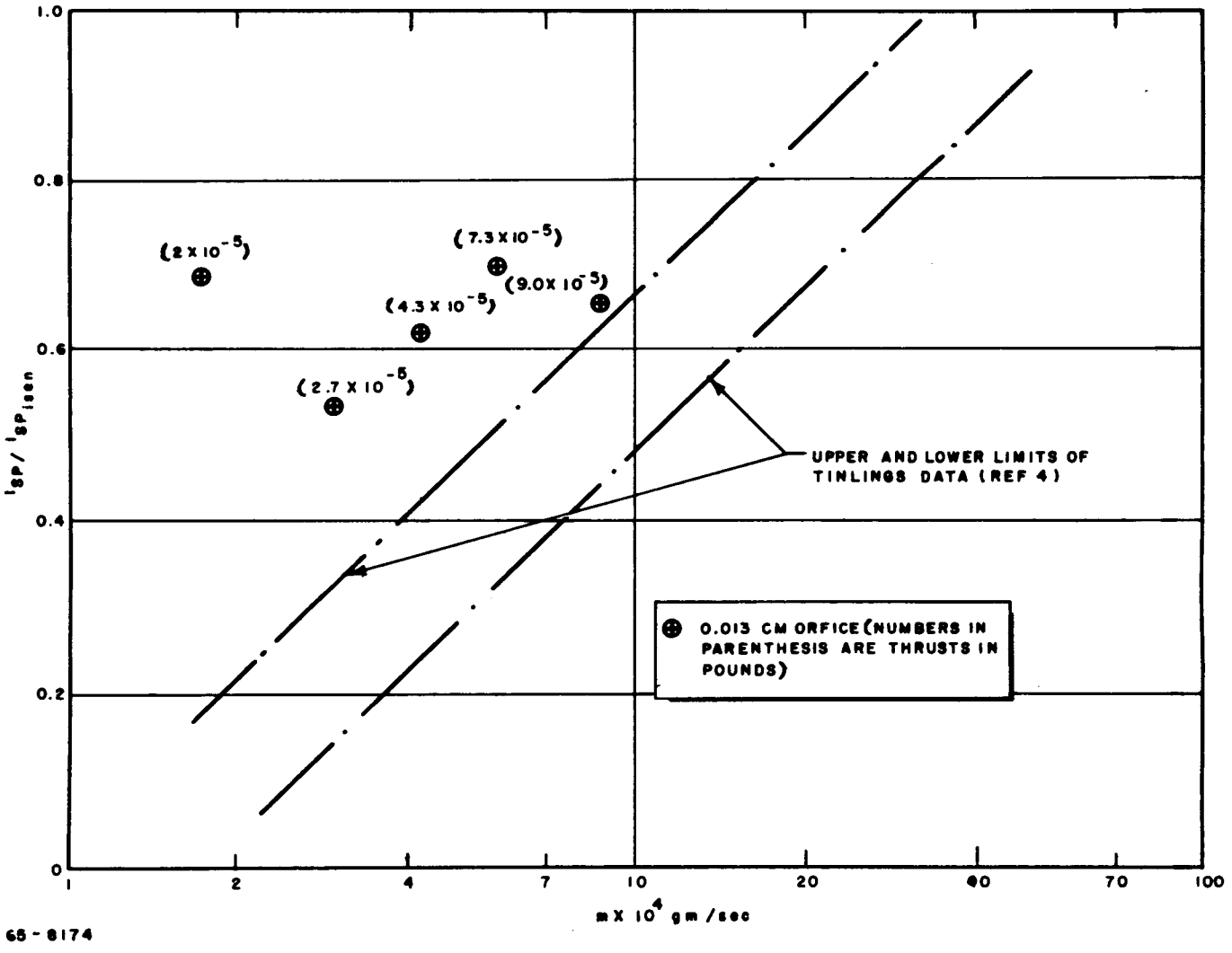

Figure 2.15 RATIO ACTUAL TO IDEAL SPECIFIC IMPULSE VERSUS AMMONIA FLOW RATE

III. SINGLE-AXIS LABORATORY ATTITUDE CONTROL SYSTEM

A. INTRODUCTION AND BACKGROUND

As part of the present program a series of system tests are being carried out on a complete resistojet ACS on an ACS test bed which has recently been installed at NASA, Lewis Research Center. The ACS test bed is shown in figure 3.1. The test bed is mounted on an air bearing in a large vacuum chamber. During a typical ACS test, the test bed is completely isolated from the laboratory and completely self-contained. Power is supplied from on-board batteries; propellant is supplied from an on-board propellant supply; and, finally, communication to and from the test bed is accomplished by on-board telemetry equipment. The test bed and test setup are readily adaptable to the checkout and testing of a variety of three-axis attitude control systems based on gas and particle-expulsion devices. The air-bearing test facility is thus ideally suited for comparing the overall performance of different attitude control systems.

The air-bearing test facility has been designed to test complete three-axis attitude control systems. There is the possibility of complete 360-degree angular freedom about the test-bed vertical axis, and about ±10-degree angular freedom about each of the test-bed horizontal axis. To simplify the control problem the initial resistojet ACS air-bearing tests have been single rather than three axis. Future tests are planned, however, of a complete three axis resistojet ACS.

The primary purpose of the initial single-axis resistojet ACS tests has been to demonstrate hardware feasibility and to identify and solve subsystem interface problems. A secondary objective has been to measure overall system performance. The resistojet single-axis ACS has been described previously[1] and consists of a control logic package and sensor, power conditioning equipment, resistojet engines and propellant storage and feed system, and finally a signal conditioning package. The overall behavior of the resistojet ACS is established by the initial angle, $\theta_{initial}$, and angular rate, $\dot{\theta}_{initial}$, of the test bed, and by the external disturbance torque, τ_D. The initial table angle and rate can be preset by means of the on-board engines. The external disturbance torque can be varied by operating the air bearing at different pressures.

During the past quarter, the Model-I Resistojet ACS, described previously,[1] was delivered to NASA, Lewis, and successfully checked-out and tested on the ACS test bed. The control system was operated in the acquisition mode, and in both hard and soft limit cycles.

B. MODEL I SINGLE-AXIS RESISTOJET ACS

The single-axis resistojet ACS has been described in some detail in the previous quarterly.[1]

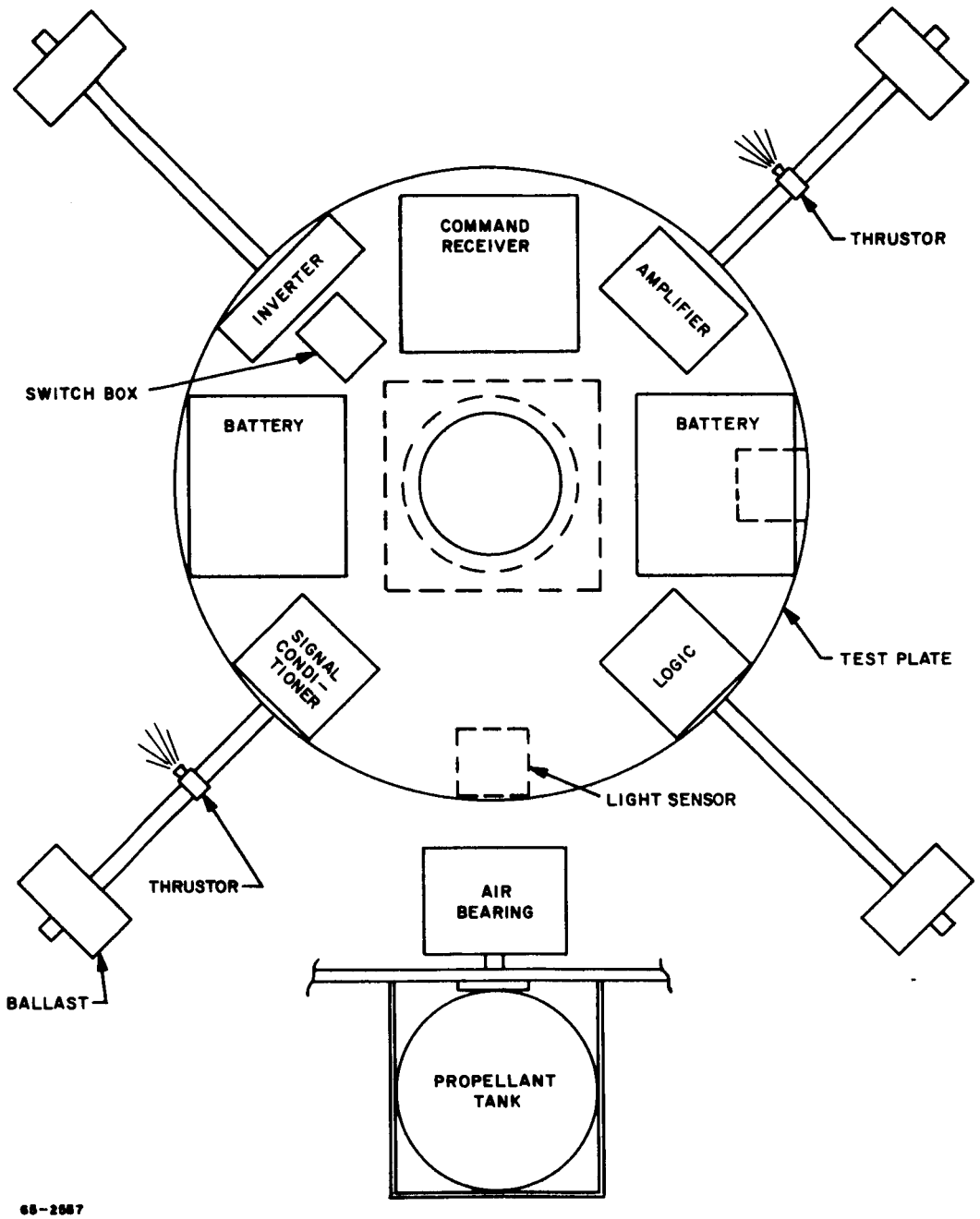

Figure 3.1 ATTITUDE CONTROL SYSTEM TEST BED

1. Control Logic Circuitry

A functional diagram of the control logic system is shown in figure 3.2. The control function, $Z(t)$, is generated by the lead network. The lead network takes the sensor signal, $\theta(t)$, and generates a control function, $Z(t)$, which is proportional to the sum of the vehicle position, $\theta(t)$, and rate, $\dot{\theta}(t)$. The lead network is described in appendix A. The control function, $Z(t)$, is then fed into a switching network which controls the operation of the appropriate engine.

The control method, which governs the design of both the lead and switching networks, is based on a method proposed by Vaeth.[1,2] The Vaeth method uses two sets of engine control commands. Whenever, the control function, $Z(t)$ exceeds the smaller, i.e., θ_{inner}, of two preset values, the appropriate engine is pulsed for a preset time producing an impulse bit, $\int F dt$, which if the angular rate is small enough, reverses the direction of rotation of the table. The system thus oscillates between the preset limits resulting in limit cycle control. If the rate of rotation is too large, however, the impulse bit will not be sufficiently large to reverse the rotation. With this condition, the control function will reach and exceed the larger of the two preset values, and the engine will be turned on and remains on continuously until the control function again drops below the larger preset value. This set of commands is used for acquisition and as a backup to the limit-cycle control lines. For the resistojet ACS the switching network also provides a finite heat-up time before the gas flow is pulsed.

A schematic of the switching network is presented in figure 3.3. A reset circuit (shown in dashed lines) has been added to the switching network, described previously,[1] to prevent two valves from going on simultaneously due to noise signals from the polarity detector.

Analog computer solutions indicating the performance of the control logic system as a function of disturbance torque, τ_D, initial position, $\theta_{initial}$, and initial rate, $\dot{\theta}_{initial}$, are presented in appendix B.

2. Light or Position Sensor

The basic input to the control system lead network is the table position, $\theta(t)$. The initial concept[1] for the optical sensor is shown in figure 3.4.A. Because the center of the source filament was hotter than the ends the original sensor was quite sensitive to vertical motion. To alleviate this problem a sensor of the type shown in figure 3.4.B was constructed. A vertical displacement of the filament on the photocells does not give a differential output even though the filament may be nonuniform. The improved rejection of unwanted signals due to cross-axis motion was obtained, however, at the expense of range. Whereas, the original sensor was linear to about ±3

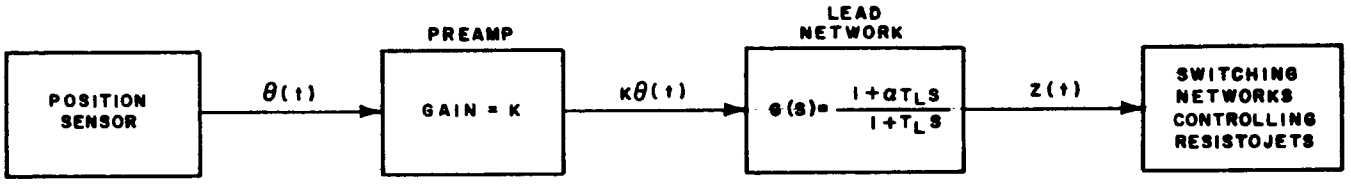

65-8175

Figure 3.2 FUNCTIONAL DIAGRAM OF THE CONTROL LOGIC SYSTEM

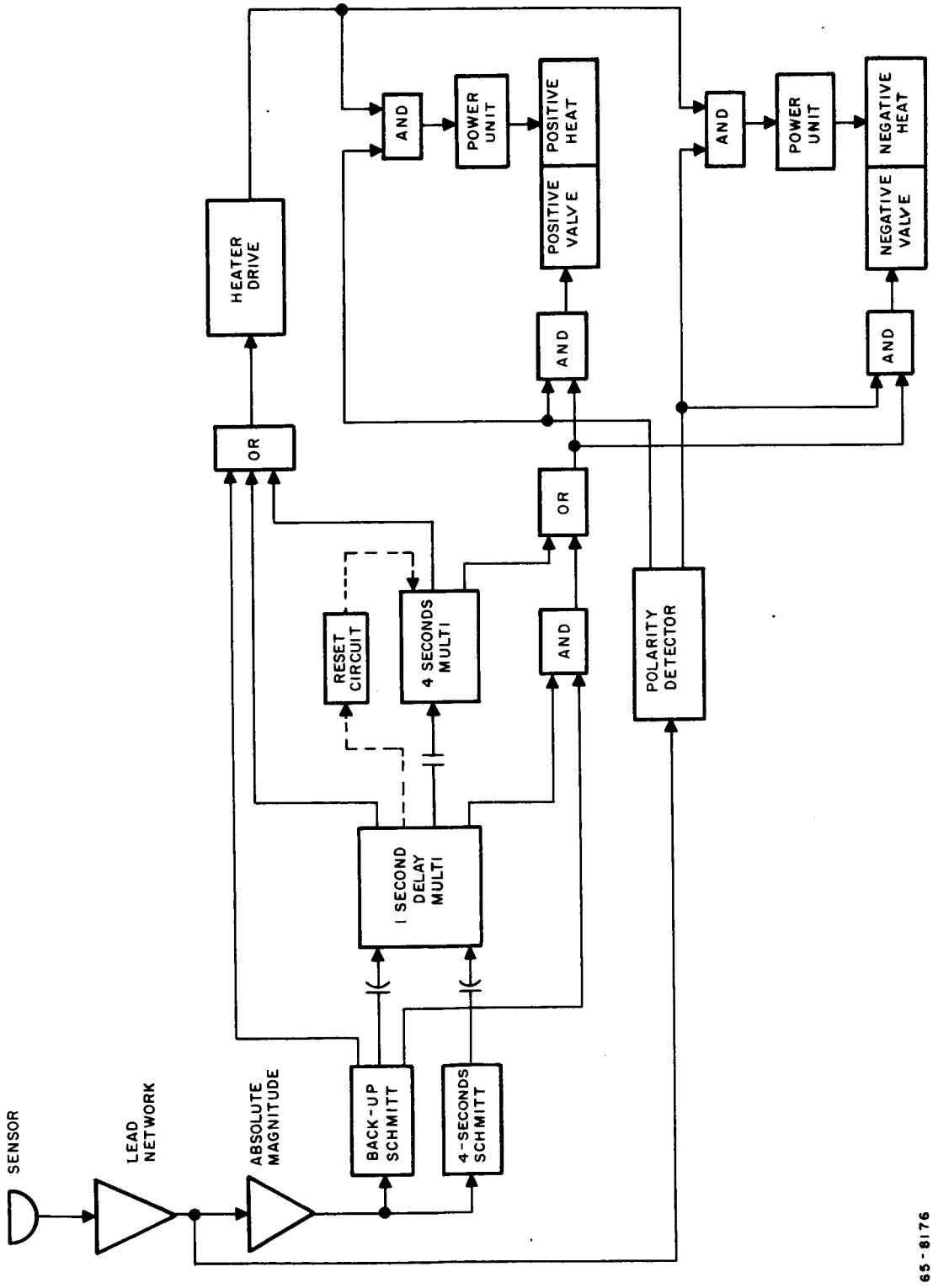

Figure 3.3 FUNCTIONAL DIAGRAM OF THE CONTROL LOGIC SWITCHING NETWORK

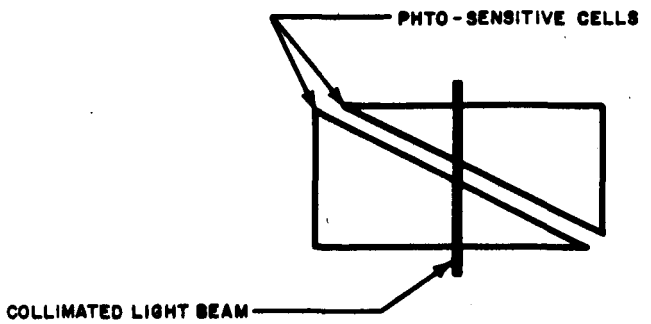

a ORIGINAL CONCEPT FOR SENSOR

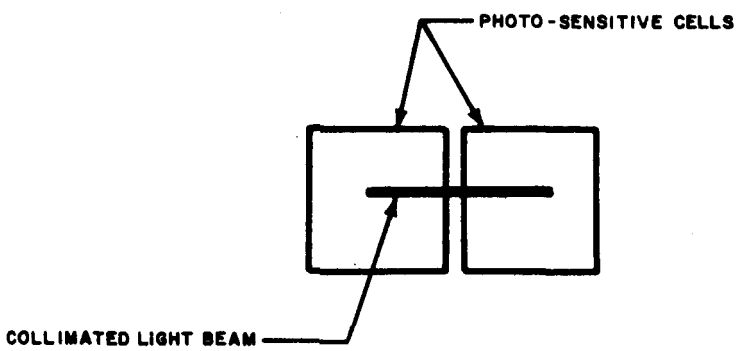

65-8177

b PRESENT POSITION SENSOR

Figure 3.4 OPERATION OF POSITION SENSOR

degrees, the present sensor in linear to only about ±1.0 degree. In each case, however, the maximum angle which could be picked up was about ±8 degrees. However, beyond 1.5 degrees the sensor output is a constant, and beyond 8 degrees falls to zero.

3. Resistojet Engine Flow System

A schematic of the most recent resistojet ammonia flow system is presented in figure 3.5. Originally, a differential pressure orifice and thermocouple were located (see reference 1, figure 45) in each of the propellant lines passing to the attitude control and station-keeping engine. Normally, only one resistojet will be operating at any one time, and the data from one flow measurement can be related to the particular resistojet operating by means of the individual solenoid valve actuation signals. Thus, the three original differential pressure transducers and orifice plates have been replaced by a single orifice plate and transducer located in close proximity to the plenum tank.

Referring to figure 3.5, the plenum-tank pressure is regulated by means of a pressure switch and solenoid valve. During preliminary system tests, it was found that noise generated by operation of the solenoid was sufficient to trigger the thrustor valves. A decoupling circuit consisting of a 20-ohm resistor and a 1000-microfarad capacitor was used in the solenoid circuit to reduce this noise. As an added precaution a 40-cps, low-pass filter also was placed in the error-signal circuit. The combination of the decoupling circuit and low-pass filter eliminated the interference problem.

4. Revised Telemetry Data Transmission Channel List

A revised telemetry data channel list is shown in table 3.1.

C. EVALUATION OF THE MODEL I SINGLE-AXIS RESISTOJET ACS

1. Chronological Summary of System Tests

The Resistojet System - Model I was delivered to NASA Lewis on 4 March 1965. The system electrical checkouts were carried out on 17 and 18 March 1965. A summary of the four single-axis resistojet ACS tests completed during March and April 1965 is shown in table 3.2. In all of the tests described in table 3.2, the resistojet ACS held the position of the test bed to ±0.5 degree for extended periods of time, and with reasonable propellant consumption.

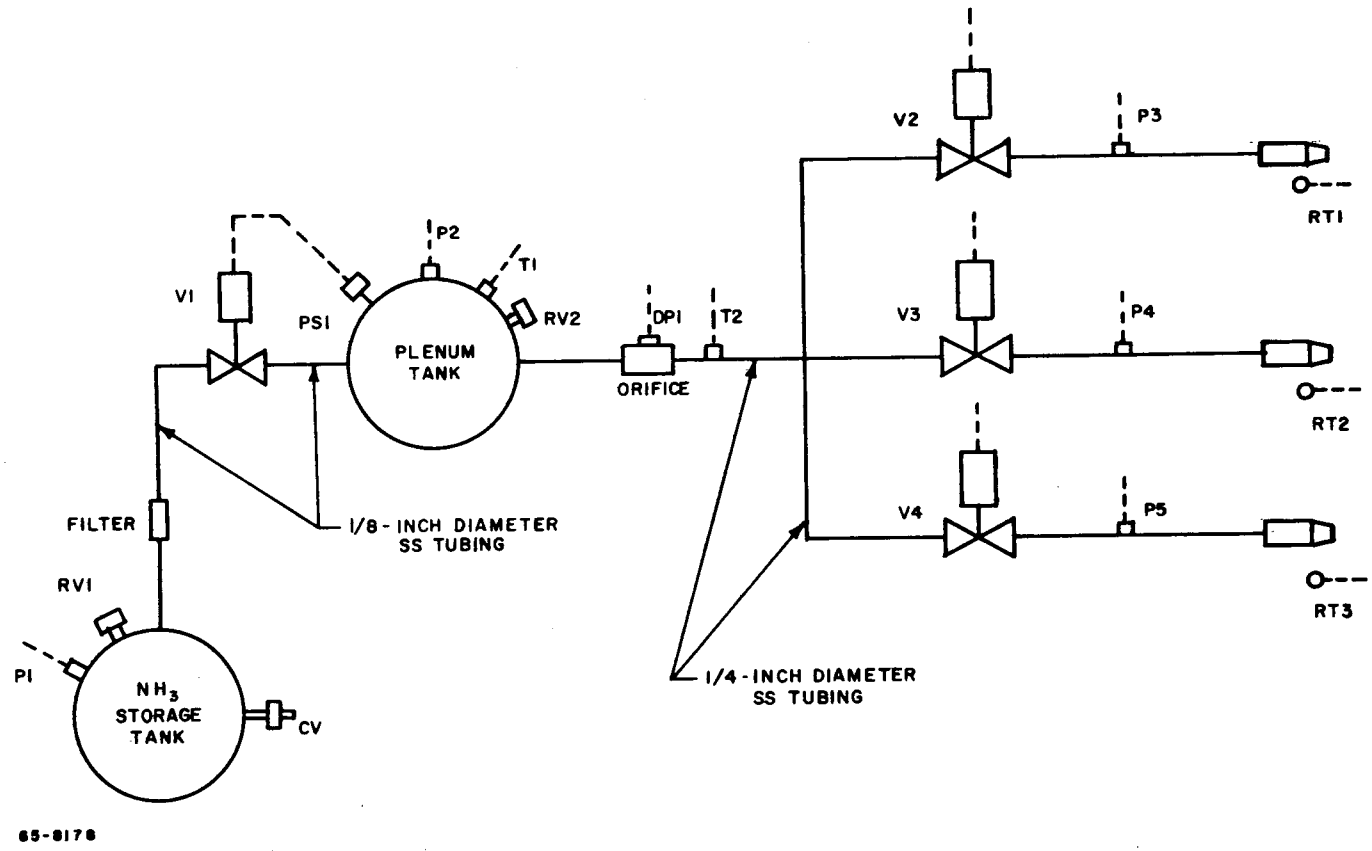

Figure 3.5 SCHEMATIC DIAGRAM OF THE RESISTOJET AMMONIA FLOW SYSTEM

TABLE 3.1

REVISED TELEMETRY DATA CHANNEL LIST FOR MODEL I
RESISTOJET ACS

Channel No.	Commutated Channel No.	Channel Identification	Description	Channel	Range	Telemetry Output (volts)	Instrumentation
1		V_1	Sensor Preamplifier Output (Fine)	C	± 0.5°	-2.5 to 2.5	T, R
2		V_3	Total Error Signal	C	0-0.5°	0-5	T, R
3		V_4	Valve Actuation Signal (Clockwise Rotation)	C	28 vdc	0-5	T
4		V_5	Valve Actuation Signal (C- Clockwise Rotation)	C	28 vdc	0-5	T
5		P_3	Nozzle Box Pressure (Clockwise Rotation)	C	0-50 psi	0-5	T, R
6		P_4	Nozzle Box Pressure (C-Clockwise Rotation)	C	0-50 psi	0-5	T, R
7		DP_1	ACS Differential Pressure (Flow)	C	0-1 psi	0-5	T, M
9	38	P_1	Ammonia Tank Pressure	I	0-250 psi	0-5	T, M
10	39	P_2	Plenum Pressure	I	0-50 psi	0-5	T, M
11	33	T_1	Plenum Temperature	I	0-100°F	0-5	T, M
13	34	T_2	Ammonia Line Temperature at DP_1	I	0-100°F	0-5	T
16	40	P_5	Nozzle Box Pressure (Station Keeping)	I	0-50 psi	0-5	T, R
17	41	RT_1	Resistojet Temperature (Clockwise Rotation)	I	1000-1700K	0-5	T, M
18	42	RT_2	Resistojet Temperature (C-Clockwise Rotation)	I	1000-1700K	0-5	T, M
19	31	RT_3	Resistojet Temperature (Station Keeping)	I	1000-1700K	0-5	T
20	4	V_2	Sensor Preamplifier Output (Coarse)	I	±5°	-2.5 to +2.5	T, R
21	8	V_6	Valve Actuation Signal (Station Keeping)	I	28 vdc	0-5	T
22	7	V_7	Resistojet Heater Voltage CW	I	2 vdc	0-5	T, M
23	6	V_8	Resistojet Heater Voltage CCW	I	2 vdc	0-5	T, M
24	5	V_9	Resistojet Heater Voltage Station Keeping	I	2 vdc	0-5	T

TABLE 3.2

SUMMARY OF SINGLE-AXIS RESISTOJET ACS TESTS AT NASA, LEWIS (MARCH-APRIL, 1965)

Run No.	Date	Comment
1	March 25-26	(i) System Controlled (ii) RF Interference (iii) Valve Chatter
2	April 1-2	(i) System Controlled (ii) Valve Chatter (Inner and Outer Lines)
3	April 12-13	(i) System Controlled (ii) Valve Chatter (Inner and Outer Lines)
4	April 22	(i) System Controlled (ii) Valve Chatter (Outer Lines)

2. Sensor Calibration

Figures 3.6 through 3.9 present the sensor calibration curves. Figure 3.6 shows vehicle position, θ, versus output signal voltage; figures 3.7 and 3.8 show nozzle-box pressure versus output signal voltage for, respectively, the clockwise (CW) and counterclockwise (CCW) thrustors; finally, figure 3.9 shows pressure-normalized orifice mass-flow rate versus output signal voltage.

Typical outputs from the continuous telemetry channels are shown in figures 3.10 through 3.13. Results are presented illustrating the acquisition mode (figure 3.10) and both hard (figure 3.11) and soft (figure 3.12 and figure 3.13) cycle operation. Data are presented for seven continuous telemetry channels. Channel 1 presents vehicle position $\theta(t)$, and channel 2 shows vehicle total error, $Z(t) = \theta(t) + (a - 1) r_L \dot{\theta}(t)$. Channels 3 and 5 show nozzle-box pressure for, respectively, the CCW and CW thrustors, while channels 4 and 6 show the nozzle-valve actuation signals. Finally, channel 7 is the pressure drop across the differential orifice.

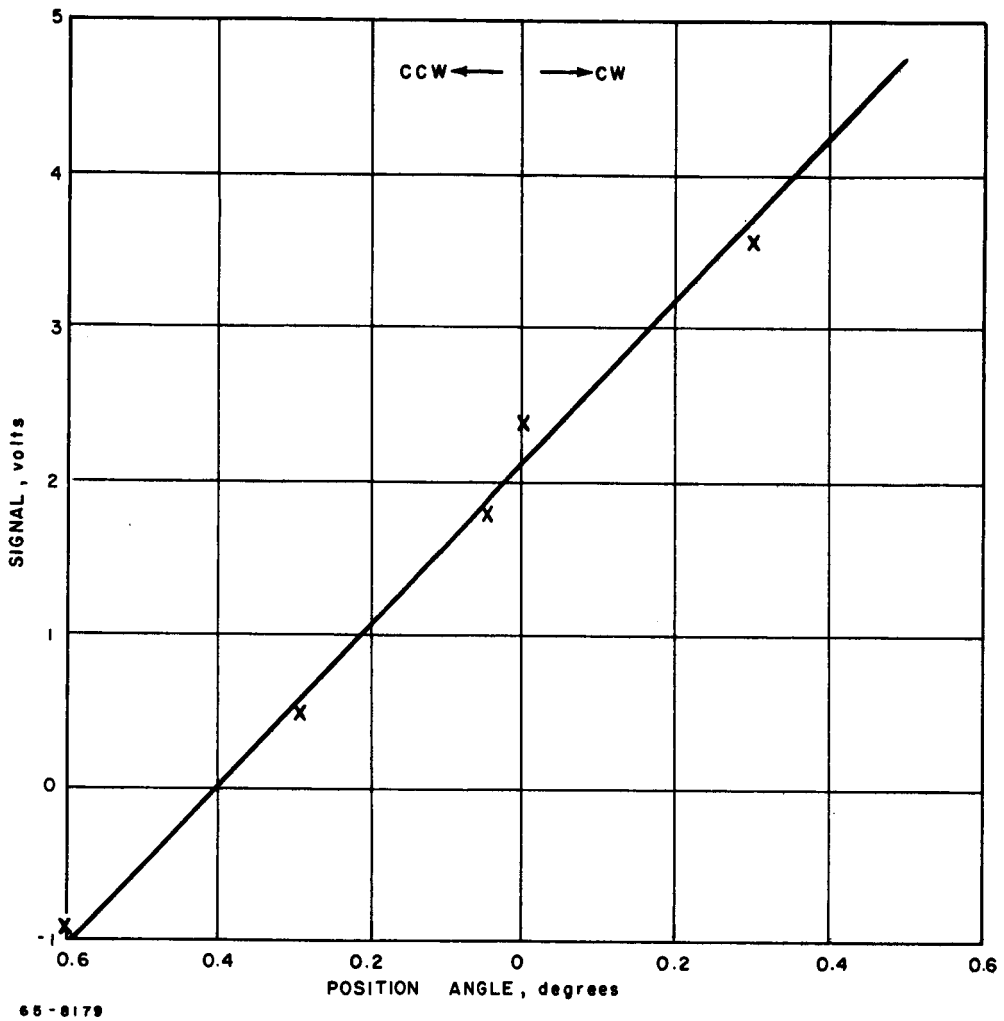

Figure 3.6 VEHICLE POSITION VERSUS OUTPUT SIGNAL VOLTAGE

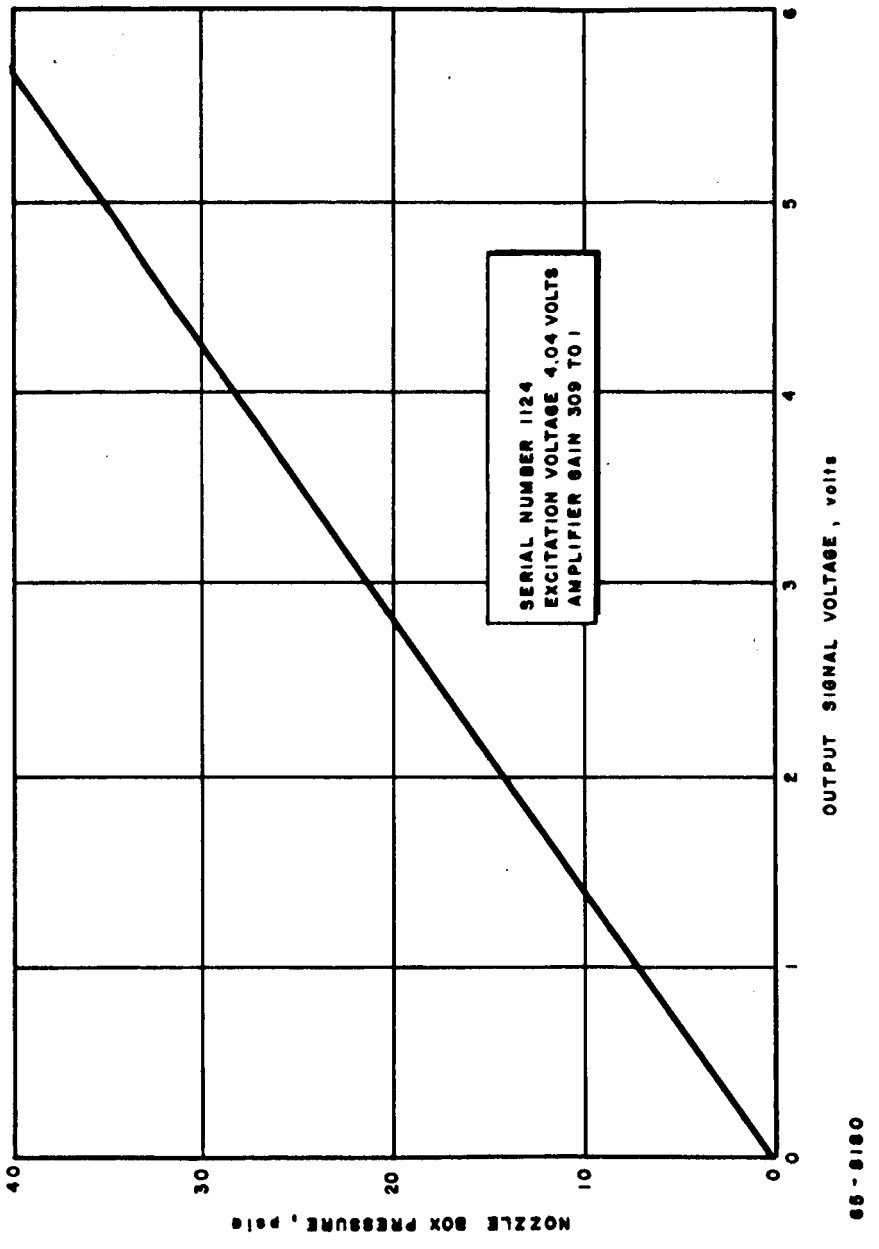

Figure 3.7 NOZZLE-BOX PRESSURE (CLOCKWISE) VERSUS OUTPUT SIGNAL VOLTAGE

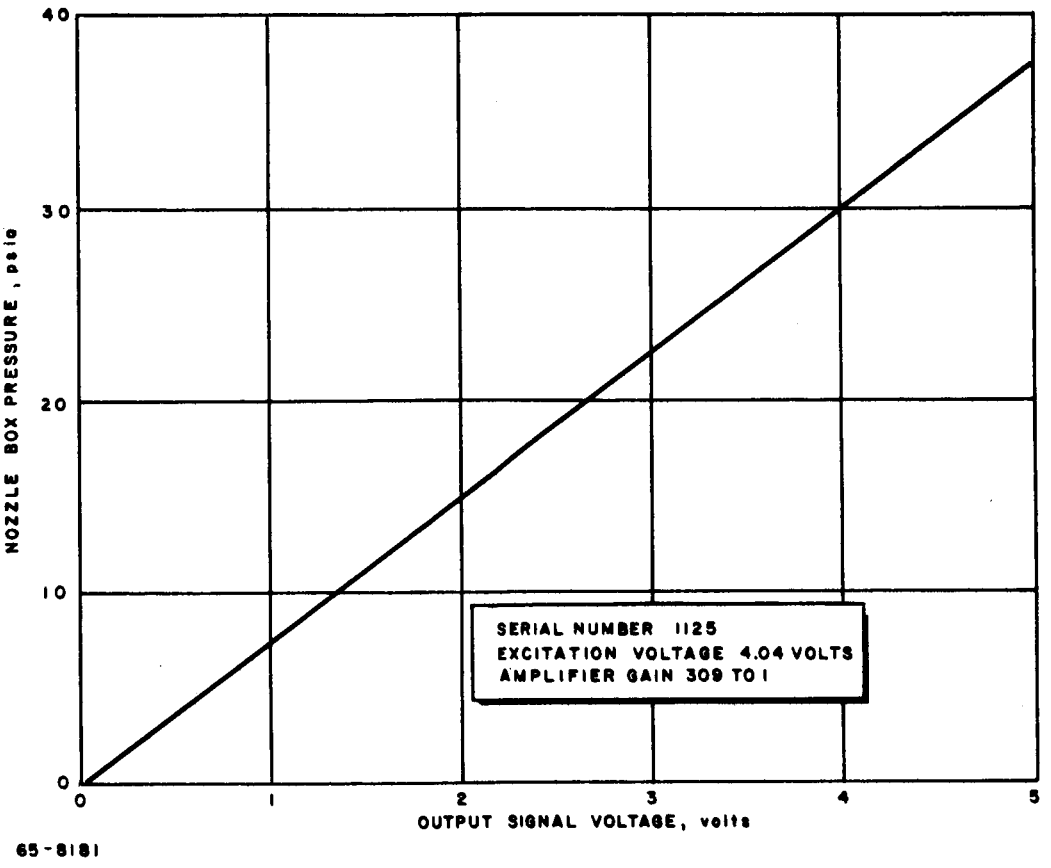

Figure 3.8 NOZZLE-BOX PRESSURE COUNTER CLOCKWISE VERSUS OUTPUT SIGNAL VOLTAGE

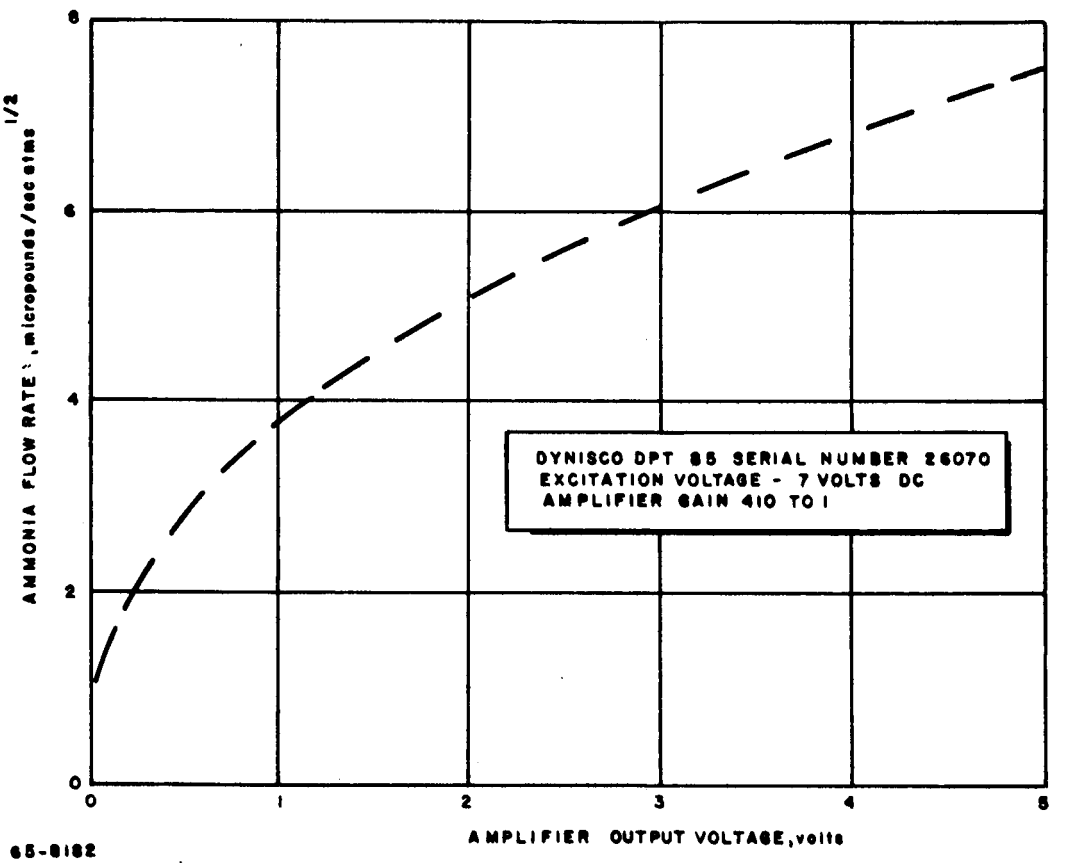

Figure 3.9 PRESSURE NORMALIZED ORIFICE MASS FLOW RATE VERSUS OUTPUT SIGNAL VOLTAGE

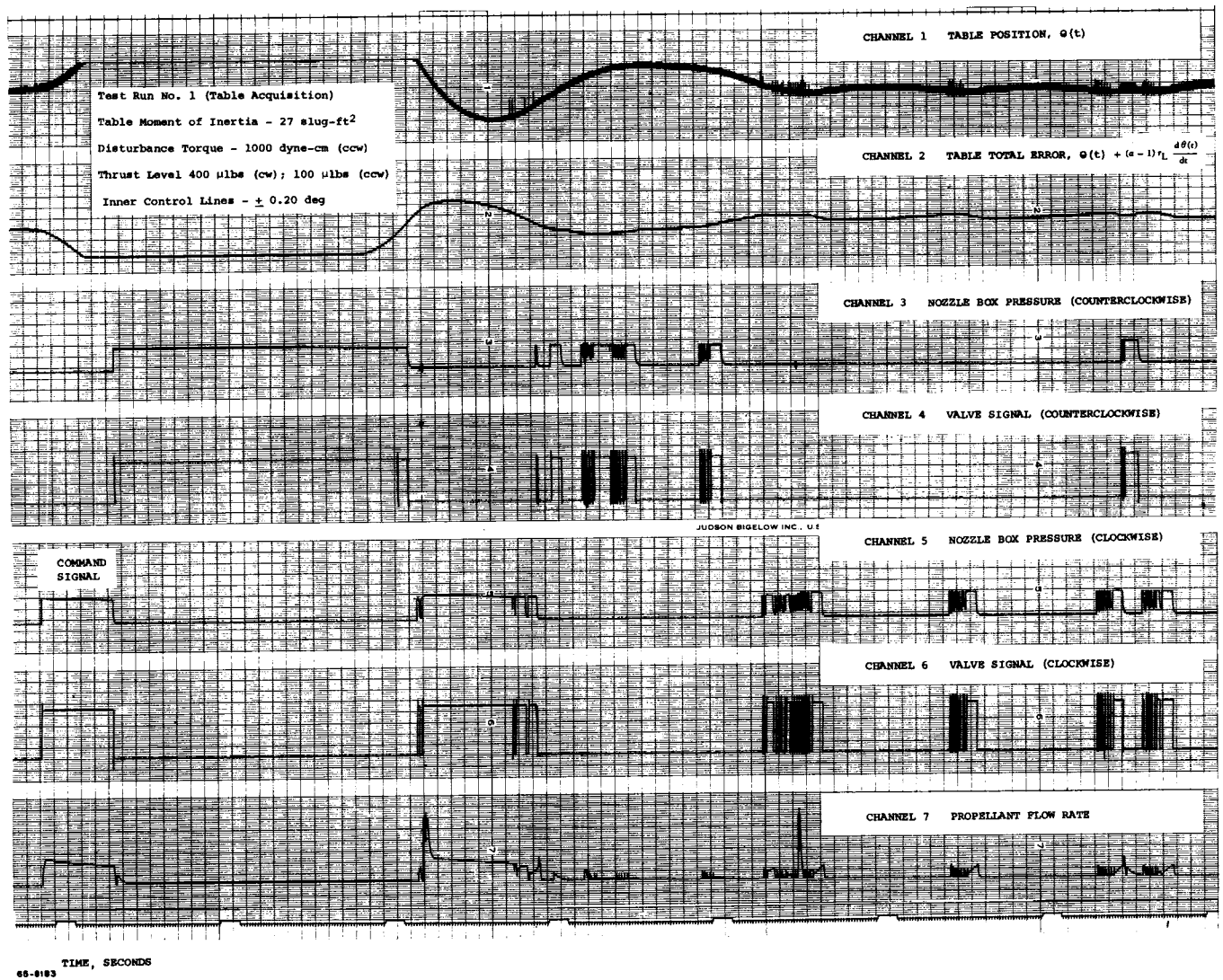

Figure 3.10 OPERATION OF THE SINGLE-AXIS RESISTOJET ACS IN THE ACQUISITION MODE

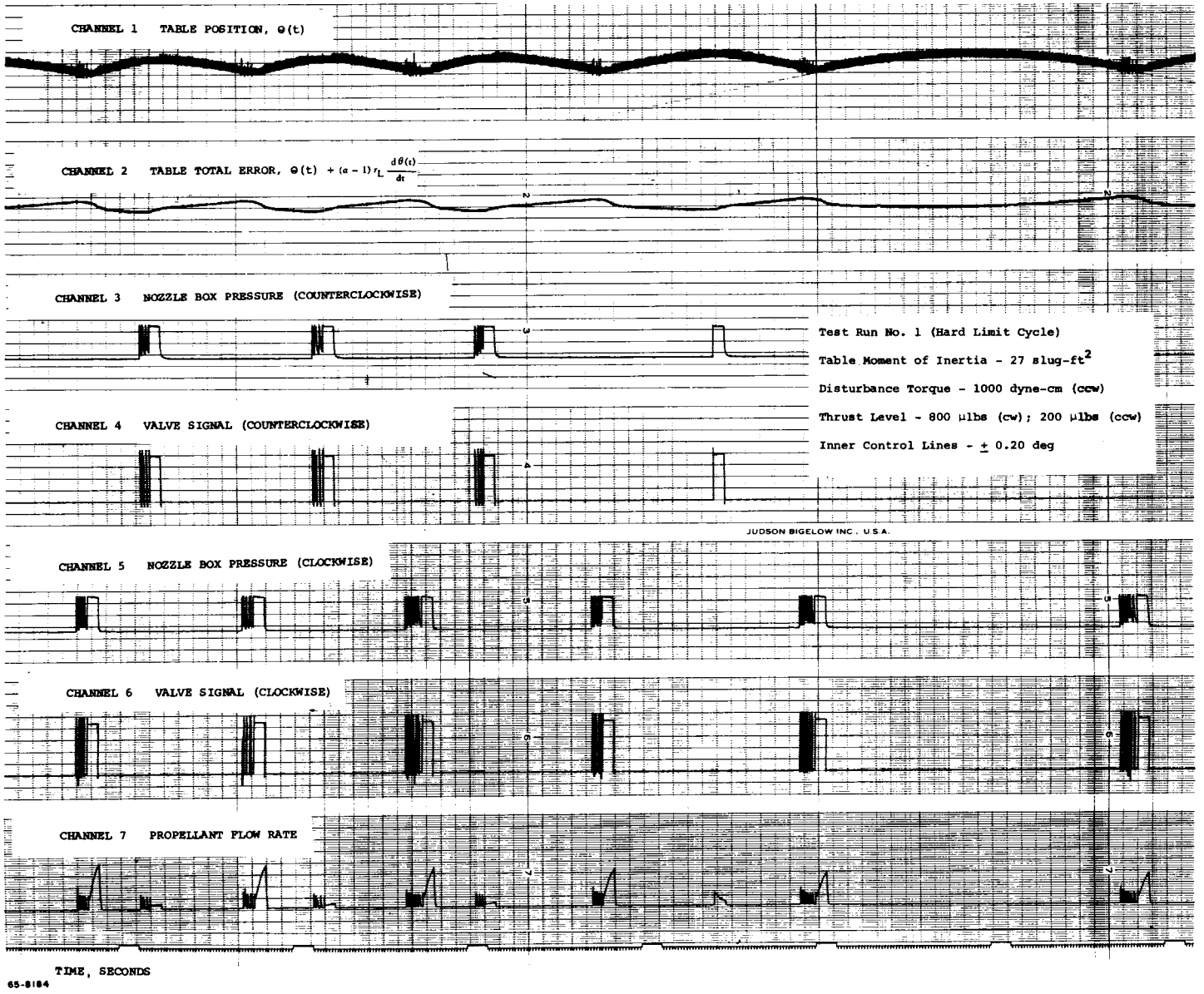

Figure 3.11 OPERATION OF THE SINGLE-AXIS RESISTOJET ACS IN A HARD LIMIT CYCLE

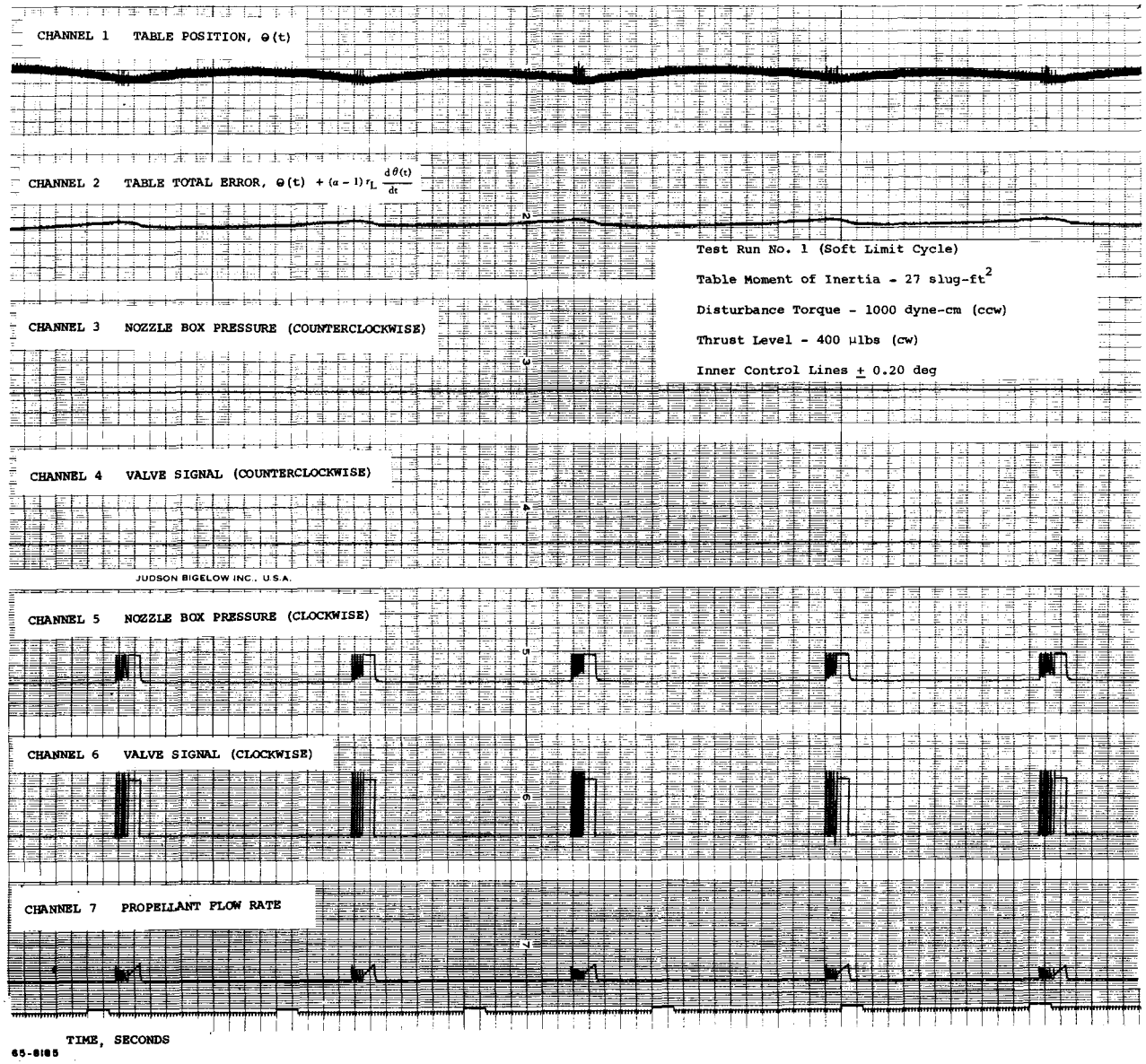

Figure 3.12 OPERATION OF THE SINGLE-AXIS RESISTOJET ACS IN A SOFT LIMIT CYCLE, r_D = 1000 DYNE-CM (CCW)

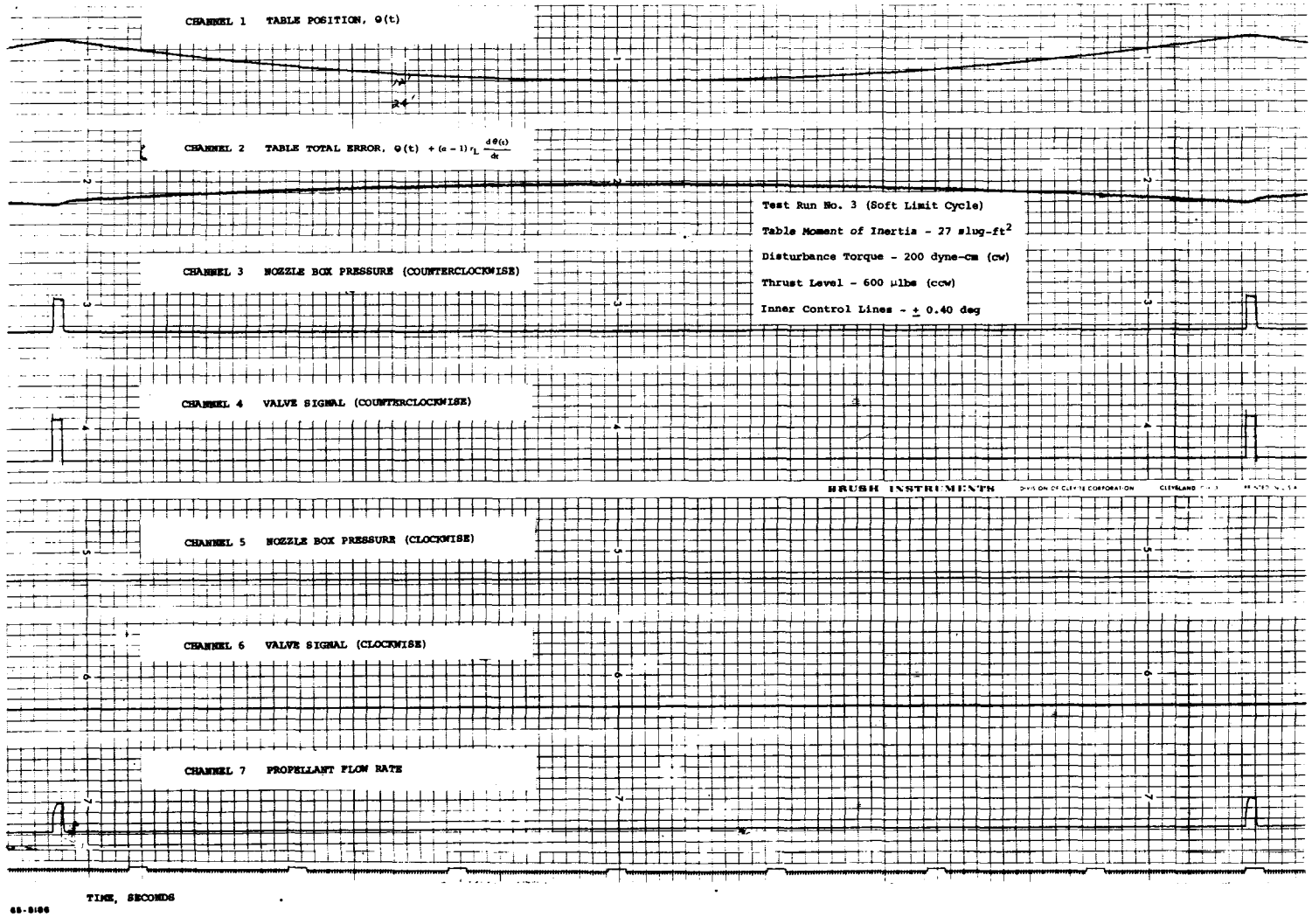

Figure 3.13 OPERATION OF THE SINGLE-AXIS RESISTOJET ACS IN A SOFT LIMIT CYCLE, r_D = 200 DYNE-CM (CW)

3. Thrustor Performance Characteristics

The thrustor design is shown in figure 3.14; the heater element-nozzle combination is removable and can be replaced by other heaters. Table 3.3 shows the nominal characteristics of the heater element-nozzle combinations used in the NASA, Lewis, tests. It is stressed that it is a simple matter to interchange the heater-nozzle elements.

4. Calibration of the Air Bearing

The disturbance torque, τ_D, on the air bearing can be varied both in magnitude and direction by changing the bearing pressure and bearing angular position. The input disturbance torque, τ_D, can be estimated from observations on changes in the table angular rate, $\Delta\theta_D$, during a fixed time period, Δt_D when no other disturbances are acting on the table. The disturbance torque is given by

$$\tau_D = J \Delta \dot{\theta}_D / \Delta t_D \tag{3.1}$$

where, τ_D (lb-ft or 1 lb-ft = 1.36×10^7 dyne-cm), is the disturbance torque, J (lb-ft-sec^2) is the table moment of inertia, $\Delta\dot{\theta}_D$ (rad/sec) is the change in vehicle angular rate over the time period, Δt_D (seconds).

Referring to figure 3.12, the change in vehicle rate, $\Delta\dot{\theta}$, between pulses is about 1.8×10^{-4} rad/sec, the time Δt_D, over which the rate change occurs is about 65 sec, and the table inertia is 27 lb-ft/sec^2, the disturbance torque for this test condition, i.e., air bearing pressure of 45 psia, is thus about 75×10^{-6} lb-ft or about 1000 dyne-cm.

The control torque is given by

$$\tau_c = J \Delta \dot{\theta}_c / \Delta t_c \tag{3.2}$$

where, τ_c (lb-ft) is the control torque, and $\Delta\dot{\theta}_c$ is the change in vehicle angular rate over the period, Δt_c, that the control torque is applied.

The control thrust is given by

$$T_c = \tau_c / \iota \tag{3.3}$$

where ι (ft) is the thrustor moment arm.

For soft cycle operation the control torque is given by

$$\tau_c / \tau_D = \Delta t_D / \Delta t_c \tag{3.4}$$

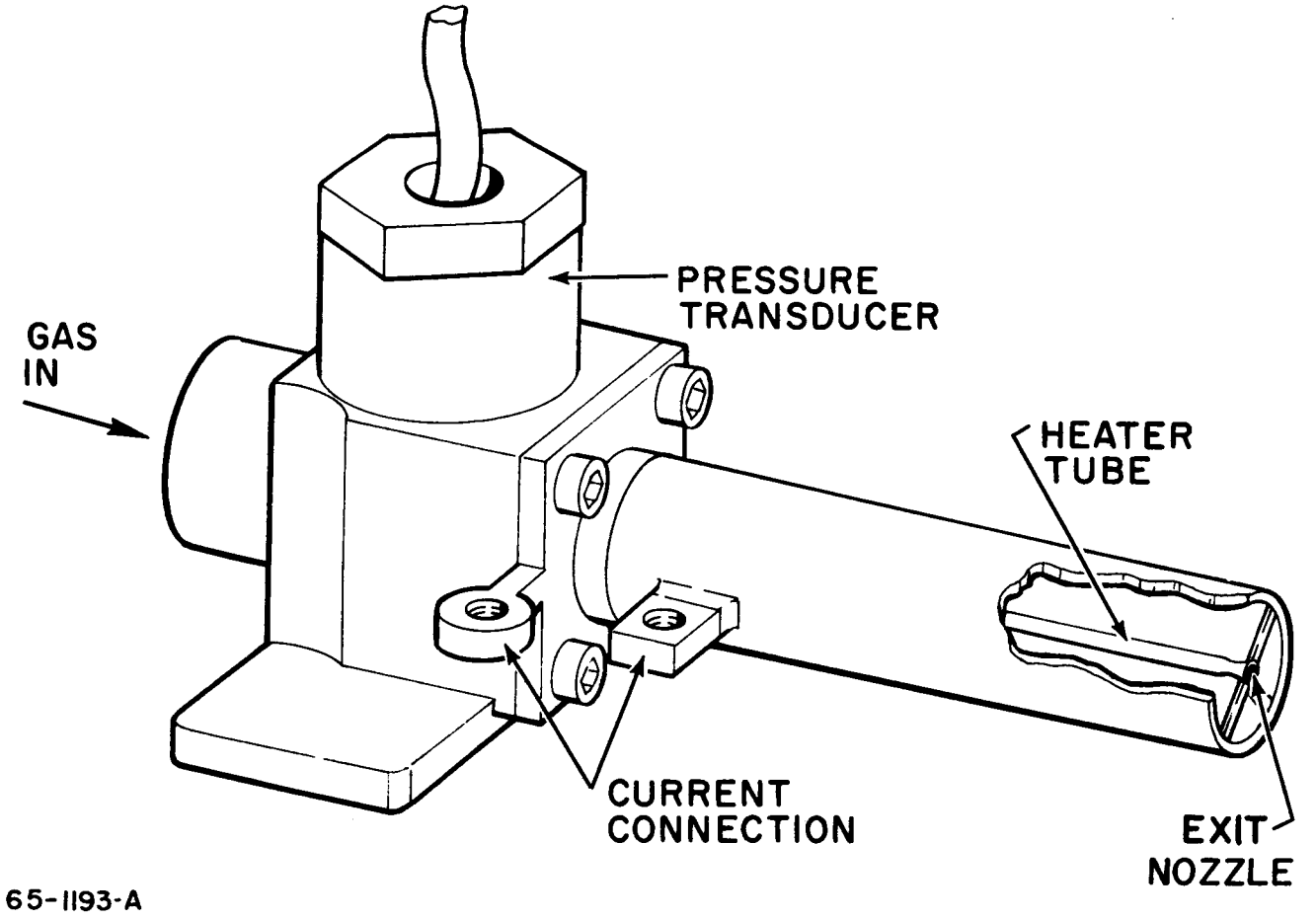

Figure 3.14 SCHEMATIC DIAGRAM OF AN EXPERIMENTAL FAST HEAT-UP THRUSTOR

TABLE 3.3

SUMMARY OF PERFORMANCE CHARACTERISTICS OF HEATER-NOZZLE ELEMENTS USED IN INITIAL RESISTOJET ACS TESTS AT NASA LEWIS

Engine Description		
Designation	6-A	7-A
Table Motion	Clockwise	Counterclockwise
Heater Element Length, inches	1.25	1.25
Heater Element, OD, inches	0.022	0.024
Heater Element, ID, inches	0.013	0.013
Nozzle Throat Diameter, inches	0.006	0.006
Heater Material	Molybdenum	Molybdenum
Heater Resistance (Cold), ohms	0.036	0.028
Nominal Performance		
Chamber Pressure, psia	14	14
Thrust Level, μ lbs	360	300
Cold Flow, μ lbs/sec	4.3	3.6
Power Input, watts	10	10
Heater Resistance (Hot), ohms	0.11	0.12
Heater Current, amperes	9.5	9.1
Heater Voltage, volts	1.05	1.1
Hot Flow Rate, μ lbs/sec	2.4	2.0
Cold Specific Impulse, sec	84	84
Hot Specific Impulse, sec	150	150

or

$$\tau_c = \tau_D \, \Delta t_D / \Delta t_c \tag{3.5}$$

5. Criteria for Soft and Hard-Limit Cycle Operation

For a fixed disturbance torque soft cycle operation is always obtained if the control impulse bit is less than a value given by[1,3]

$$(T_c \, \Delta t_c)_{soft} \leq 2 \sqrt{\tau_D \, \theta_c \, J} / \iota \tag{3.6}$$

where, θ_c (radians) is the control angle and the other quantities have been described previously. For example, at an input disturbance torque, τ_D, of 1000 dyne-cm, a vehicle moment of inertia, J, of 27-lb-ft-sec^2, a moment arm, ι, of 2 feet, and a control angle, θ_c, of 0.20 degree (or 3.5×10^{-3} radians), the control impulse bit, $(T_c \, \Delta t_c)_{soft}$, must be less than 2.64×10^{-3} lb-sec; for a 4 second pulse, (Δt_c = 4 seconds), the thrust level for soft-cycle operation must be less than 0.66×10^{-3} pounds (660 micropounds).

For a fixed disturbance torque hard cycle operation is always obtained if the control impulse bit is greater than a value given by

$$(T_c \, \Delta t_c)_{hard} \geq 4 \sqrt{\tau_D \, \theta_c \, J} / \iota \tag{3.7}$$

For the conditions cited in the previous example the control impulse bit must be greater than 5.28×10^{-3} lb-sec for hard-cycle operation, and for a 4 second pulse the thrust level for hard-cycle operation must be greater than 1.32×10^{-3} pounds.

It follows from equation 3.6 that for a fixed impulse bit, $T_c \, \Delta t_c$, soft cycle operation is obtained for disturbance torques greater than a value given by

$$(\tau_D)_{soft} \geq (T_c \, \Delta t_c)^2 \, \iota^2 / 4 \theta_c \, J \tag{3.8}$$

Hard-cycle operation is obtained for disturbance torques less than a value given by

$$(\tau_D)_{hard} \leq (T_c \, \Delta t_c)^2 \, \iota^2 / 16 \, \theta_c \, J \tag{3.9}$$

To illustrate, for a thrust level, T_c, of 300×10^{-6} lbs, an impulse bit length, Δt_c, of 4 seconds, a vehicle moment of inertia of 27 lb sec^{2}ft, moment arm, ι, of 2 feet, and a control angle of 0.2 degree, soft-cycle operation will occur at disturbance torques greater than 200 dyne-cm; and hard-cycle operation at disturbance torques less than 50 dyne-cm. Either soft, hard, or a combination of soft and hard limit cycles can occur between these two limiting torque values. Analog computer solutions for this situation are presented in appendix B.

6. Table Acquisition

Figure 3.10 shows a portion of the sensor traces obtained during Test Run No. 1.*

An external 25 second clockwise slew command, indicated by the voltage signals on channels 5, 6, and 7 was transmitted to the table. The clockwise thrustor was operating at a nozzle box pressure (channel 5) of about 15.5 psia, and a nominal thrust level of about 400 x 10^{-6} pound. Following the clockwise slew command the table was put on automatic control.

As indicated in the trace of table position (channel 1) the table initially moved in the clockwise direction until it saturated the position sensor. The sensor saturates at about ±1.5 degrees; however, the system will still acquire out to about ±8 degrees. After the table control system was placed on "automatic control" the counterclockwise thrustor was activated and the table was decelerated in the counterclockwise direction. 2.*

Following activation of both the clockwise and counterclockwise thrustors the system passed into a soft-limit cycle. In this soft cycle, the counterclockwise disturbance torque of about 1000 dyne-cm (or 0.735 x 10^{-4} lb-ft) was counterbalanced by the control torque of 8 x 10^{-4} lb-ft (400 x 10^{-6} pound thrust at a 2-foot moment arm). The control impulse bit time, Δt_c, was 4 seconds, compared to the cycle time, Δt_D of about 50 seconds. The estimated duty cycle, i.e., τ_D / τ_c, is equal to about 0.09 compared to a measured duty cycle, i.e., $\Delta t_c / \Delta t_D$, equal to about 0.08.

7. Hard Limit-Cycle Operation

Figure 3.11 shows a typical series of sensor traces obtained during test run 1 and is illustrative of hard limit-cycle operation. The nozzle box pressure was 32.5 psia and the corresponding thrust level was 800 x 10^{-6} pound. The table counterclockwise disturbance torque, τ_D, was estimated to be about 1000 dyne-cm. The engine thrust level was thus sufficient to result in hard limit-cycle operation.

At the beginning of the control cycle the table was moving in a counterclockwise direction. As the table traveled passed the 0.20-degree inner control line the clockwise thrustor was activated and the direction of the table was reversed. The clockwise thrustor moved the table to the opposite control line, the counterclockwise thrustor was activated and the cycle was repeated.

* The noise on the position trace: i.e., channel 1, was associated with an rf interference problem and was eliminated in later runs. The valve chatter problem, after considerable investigation, has been clearly identified with test tank vibration, which, in turn results in light source vibration. Some success: e.g., figure 3.13, has been obtained in reducing valve chatter by strengthening the light source mount and decreasing control circuit sensitivity; however, the problem is not yet completely resolved.

** Due to line blockage the counter-clockwise thrustor produced only about 100 × 10^{-6} pounds or about 25 percent of its full thrust capability. As a result, the clockwise thrust time, Δt_c, necessary to reacquire the table was considerably longer than the original command disturbance pulse.

As indicated previously the counterclockwise thrustor for test run 1 was clogged and in this case at a chamber pressure of 32.5 psia the thrust level was reduced to about 200 x 10^{-6} pound from its nominal value of 800 x 10^{-6} pound (at 32.5 psia). Nevertheless as shown in figure 3.11 the system still controlled.

8. Soft Limit-Cycle Operation

Figure 3.12 shows typical soft limit cycle obtained during test run 1. The nozzle-box pressure has been reduced to about 15 psia and the resulting engine thrust is about 400 x 10^{-6} pound. At the 1000 dyne-cm counterclockwise disturbance torque level characteristic of test run 1 this thrust level is low enough to assure soft limit-cycle operation. Referring to figure 3.12, the clockwise control thrust is just sufficient to overcome the counterclockwise disturbance torque.

Figure 3.13 shows a typical soft limit cycle obtained during test run 3. To eliminate valve chatter the sensitivity of the control logic system was decreased by moving the control lines out to ±0.4 degree and the outer lines were moved out to ±0.6 degree; further, the light-source vibrations were reduced by strengthening the optical-source mount. As indicated in figure 3.13, these changes reduced the valve chatter problem. During this portion of the test run, the bearing pressure was at about 35 psia and the disturbance torque level was about 200 dyne-cm in the clockwise direction. It is noted that the disturbance torque level is quite sensitive to bearing pressure. During test run 1, the bearing pressure was about 45 psia and the disturbance torque level was about 1000 dyne-cm in the counterclockwise direction.

Other examples of hard and soft limit-cycle operation for the single-axis resistojet ACS, obtained on the impulse table, are presented in appendix C.

9. Future Operation of the Model I Resistojet ACS

In the next series of tests the Model I system will be operated with the inner control lines at ±0.2 degree and the outer lines at ±0.4 degree. The hysteresis on the Schmitt trigger circuit will be reset at 30 percent from the present value of about 10 percent to make the system less sensitive to either light source or table vibration. The table will be operated in the acquisition mode and in both soft and hard-limit cycles. The results will be compared to analog computer results similar to those described in appendix B.

D. MODEL II SINGLE-AXIS RESISTOJET ACS

As indicated, the primary objective underlying the initial single-axis resistojet attitude control system test has been to demonstrate the feasibility of applying the resistojet concept to the attitude control and station keeping of satellites. During the course of development, construction, and operation of the Model I

ACS a number of modifications which will make the Model I more suitable for test purposes have become apparent. The changes which have been incorporated into the Model II Resistojet ACS are indicated below:

1. The heater power supply has been modified to permit variation of the input power to the individual ACS engines over the range from 5 to 35 watts. The engine input power in the Model I ACS was uniquely fixed by the lead resistance and for a hot engine resistance of about 0.10 ohms was about 5 watts. (See reference 1, table IX). The power supply has been further modified to permit one power level during the warmup period, and another during actual gas ejection. The heater warm-up and operational power levels are varied by two separate potentiometers with screwdriver adjustment slots.

2. The control logic circuit has been adjusted so that the heater warmup time defined as the time period between power-on time and propellant on-time) can be varied from 1 to 10 seconds in 1-second increments. The heat-up time pulse is adjusted by a 10-position selector switch.

3. The control logic circuit has been further adjusted so that the fixed inner pulse width can be varied from 1 to 10 seconds in 1-second increments. The inner pulse width is adjusted by means of a 10-position selector switch. The length of the heat-up time and the inner pulse width can be varied independently of each other and offer 100 different combinations of heat-up time and inner pulse width.

4. The hysteresis of the Schmitt triggers will be preset at 40 percent.

5. A manually adjustable pressure regulator will be placed on the gas reservoir tank so that the engine pressure can be varied over the range from 1 to 30 psia. This will make it possible to obtain over an order of magnitude range in resistojet thrust level.

6. Provision has been made to measure the time rms voltage and rms current across the clockwise and counterclockwise thrustors. This will permit a direct estimate of the "true" power into the individual engines; this measurement is not possible with the Model I system. To review briefly, the power conditioning equipment inverts the battery supply dc power into 1000 cps ac; the high frequency results in a high efficiency and reduced output transformer size. Since the engine is supplied with high-frequency ac power, it is necessary to measure the rms voltage and current. The dc voltage and dc current into the power conditioner also will be measured which will permit determination of the overall efficiency of the power conditioner.

7. The light-sensor electronics will be modified to permit acquisition and a linear sensor output for angles up to ±8 degrees.

8. The commutator channel assignments have been changed and are summarized in table 3.4. All unused channels have been made available through an additional connector mounted on top of the signal conditioning package. The outputs from the signal conditioning amplifiers have been wired to test points mounted on the top of the unit.

The Model II resistojet ACS will provide a flexible tool for characterizing the performance of low-power resistojet systems over a wide range of operating conditions.

TABLE 3.4

TELEMETRY DATA CHANNEL LIST (COMMUTATOR CHANNELS) FOR MODEL II RESISTOJET ACS

Channel Number	Model I	Model II
1	Calibrated Voltage	Calibrated Voltage
2	Calibrated Voltage	Calibrated Voltage
3	Calibrated Voltage	Calibrated Voltage
4	Position Sensor Coarse	Position Sensor Coarse
5	Station Heater Monitor	Station Heater Monitor
6	CCW Heater Monitor	CCW Heater RMS Voltage
7	CW Heater Monitor	CW Heater RMS Voltage
8	Station Valve Voltage	Station Valve Voltage
9	Not Used	CCW Heater RMS Current
10	Not Used	CW Heater RMS Current
11	Not Used	Spare Connector 1
12	Not Used	Spare Connector 2
13	Not Used	Spare Connector 3
14	Not Used	Spare Connector 4

TABLE 3.4 (Cont'd)

Channel Number	Model I	Model II
15	Not Used	Spare Connector 5
16	NASA Telemetry Channels	NASA Telemetry Channels
17	NASA Telemetry Channels	NASA Telemetry Channels
18	NASA Telemetry Channels	NASA Telemetry Channels
19	NASA Telemetry Channels	NASA Telemetry Channels
20	NASA Telemetry Channels	NASA Telemetry Channels
21	NASA Telemetry Channels	NASA Telemetry Channels
22	NASA Telemetry Channels	NASA Telemetry Channels
23	NASA Telemetry Channels	NASA Telemetry Channels
24	NASA Telemetry Channels	NASA Telemetry Channels
25	NASA Telemetry Channels	NASA Telemetry Channels
26	NASA Telemetry Channels	NASA Telemetry Channels
27	NASA Telemetry Channels	NASA Telemetry Channels
28	NASA Telemetry Channels	NASA Telemetry Channels
29	Not Used	Spare Connector 6
30	Not Used	Spare Connector 7
31	Station Jet Temperature	Station Jet Temperature
32	Not Used	Spare Connector 8
33	Plenum Tank Temperature	Plenum Tank Temperature
34	Station Line Temperature	Station Line Temperature
35	Not Used	Spare Connector 9

TABLE 3.4 (Concl'd)

Channel Number	Model I	Model II
36	Not Used	Spare Connector 10
37	Not Used	Spare Connector 11
38	Ammonia Tank Pressure	Ammonia Tank Pressure
39	Plenum Tank Pressure	Plenum Tank Pressure
40	Station Nozzle Pressure	Station Nozzle Pressure
41	CW Jet Temperature	CW Jet Temperature
42	CCW Jet Temperature	CCW Jet Temperature
43	Not Used	Spare Connector 12

E. OVERALL OBJECTIVES AND FUTURE DIRECTION OF THE SINGLE-AXIS ATTITUDE CONTROL SYSTEM EVALUATION TESTS

The objectives of the single axis attitude control system tests include:

1. Verification of the compatibility of all the ACS components including the propulsion subsystem, power conditioner, control logic package, sensors, signal conditioner, and telemetry system.

2. Demonstration of the performance of the ACS in the acquisition control mode, and in soft and hard limit-control cycles. (The three-axis air bearing and the single-axis impulse table make it possible to observe ACS operation as a function of disturbance torque, r_D, acquisition angle, θ_i, and initial rate of angular acquisition, $\dot{\theta}_i$.)

3. Confirmation of the validity of the analog computer solutions pertinent to the performance of the ACS control logic system (see appendix B).

4. Comparison of the performance; i.e., total impulse, fuel consumption, and reliability, of different types of attitude control systems as a function of disturbance torque, acquisition angle, and angular acquisition rate.

5. Establishment of a technological base for the development of three-axis attitude control systems.

The future direction for the single-axis tests include the following:

1. Performance data, including total impulse requirements, and fuel consumption, will be obtained for the single axis resistojet attitude control system as a function of heater input power from 0 to 35 watts, and for different propellants. In this manner it will be possible to make a quantitative tradeoff between propellant weight and heater power-supply weight.

2. Performance data will be obtained as a function of the resistojet attitude control logic parameters including inner θ_c, and outer θ_c, the slope of the control logic lines, the Schmitt trigger hysteresis, H, and the disturbance torque, τ_D. This data will be compared to similar data obtained from the analog computer (see appendix B). Assuming that the air-bearing test data correlates with the analog computer results, the analog computer can then be used to obtain system performance data over a much wider range of input variables than would be feasible (due to time and cost considerations) on the single axis air bearing.

3. Exploratory studies will be carried out on the feasibility of charging the on-board battery power supply with solar voltaic cells. This would make it possible to perform extended system lifetests, and, further, to checkout the compatibility of the solar-cell power supply and battery-charging system with the other subsystem components.

IV. THREE-AXIS ATTITUDE CONTROL AND STATION KEEPING SYSTEM

As part of the present program a study is being carried out on the application of 5- to 50-watt resistojets to the attitude control and station keeping of satellites in the 500- to 1000-pound class. A preliminary development program and system weight breakdown have been prepared and are presented below.

A. PRELIMINARY PROGRAM PLAN FOR THE DEVELOPMENT OF A FLYABLE THREE AXIS RESISTOJET ACS AND STATION KEEPING SYSTEM

The six basic subsystems for a flyable three-axis resistojet attitude control and station-keeping system are indicated in table 4.1. The subsystems are, of course, the same as those for the laboratory single-axis systems described in the previous section; however, in this case, the hardware must all eventually be flight qualified.

1. The propulsion subsystem consists of the thrustors and propellant storage and feed system. The propulsion performance, i.e., thrust level, specific impulse, and overall electric to thrust power efficiency of the individual thrustors will be measured on the wire-in-tension thrust stand and the impulse table at pressure levels of less than 10^{-3} mm Hg. Ammonia is a prime contender as a possible resistojet working fluid because of its low storage pressure and resulting low tank weight. Potential problems of 0-g feed for liquid ammonia systems, the determination of reliable space-qualified techniques for regulation of the ammonia storage pressure (order of 100 psia) to the operating nozzle-box pressure (order of 10 psia) and the establisment of valve reliability are under study.

TABLE 4.1

BASIC SUBSYSTEMS FOR A FLYABLE THREE-AXIS ATTITUDE CONTROL AND STATION-KEEPING SYSTEM

Propulsion
Control Logic
Power Supply and Power Conditioning
Sensors
Signal Conditioning
Telemetry

2. The control logic system will be developed using an existing analog computer. Results obtained from the analog computer for a single-axis system have been presented in appendix B. Due to uncertainties in the level of applied disturbance torque characteristic of the space environment, adaptive control system will be used to minimize fuel consumption and the total number of valve cycles. Briefly, the adaptive control system will vary the length of the impulse bit to assure soft limit-cycle operation independent of the applied disturbance torque. Preliminary studies of a possible adaptive control system suitable for a low-thrust ACS are presented in appendix D.

3. Referring to figure 4.1, the power supply and power conditioning subsystem will consist of a solar-cell array, battery charging equipment, battery pack, and power conditioning for the (a) propulsion system (including the resistojet heaters); (b) control logic package; (c) signal conditioner package; (d) sensors; and (e) telemetry package. The low-power, fast heat-up resistojet presents a power conditioning problem because of the low resistance ($\sim$0.10 ohm) and voltage requirement ($\sim$1 volt) of the heater elements. In the present single-axis tests, the battery voltage was inverted to 1 kilocycle ac and stepped down from 24 volts to 1 volt using a torroidal transformer. The power supply and power conditioning subsystem will be initially bench tested before being integrated with the other subsystem components.

4. Sensors for the three-axis system will be selected either by or in conjunction with NASA Lewis. The sensors will be representative of the present state of the art.

5. As in the case of the present single-axis system the signal conditioning package will be compatible with NASA Lewis supplied telemetry equipment.

6. Again, as in the case of the present single axis tests, the telemetry package will be supplied by NASA Lewis.

7. All the subsystems will be individually bench tested. Total system performance will be evaluated on the three-axis air bearing at NASA Lewis. These tests will permit a compatibility checkout of the individual resistojet ACS susbsystems. The three-axis system compatibility checkout will be analogous to the work currently being carried out on the single-axis tests, which has been described in the previous section. Further, as indicated previously for the single-axis tests, it may also be possible to include an on-board solar array for battery charging, and thus permit extended lifetests.

8. Some subsystems compatibility testing of the type described in appendix C can also be carried out on the impulse table. Finally, appendix

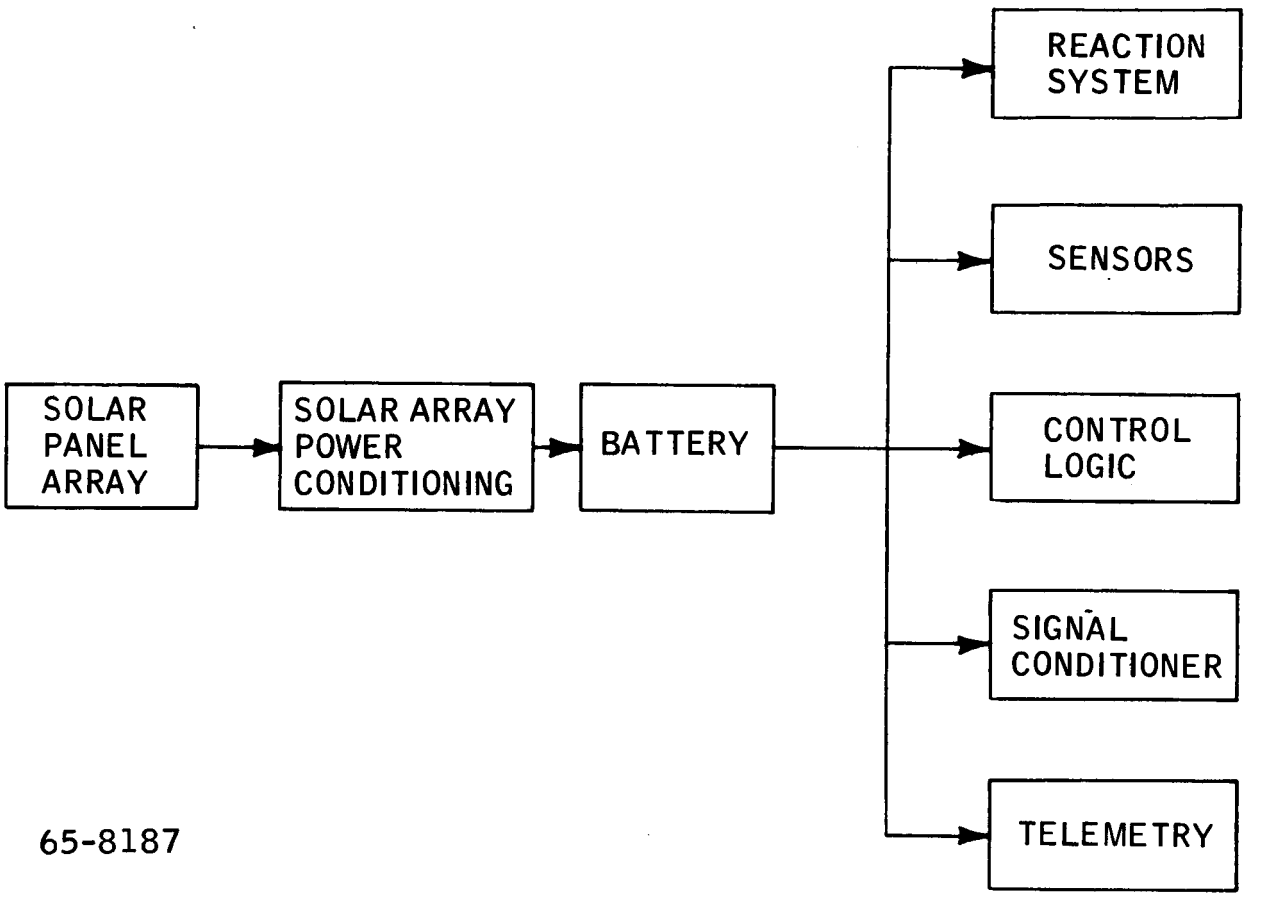

Figure 4.1 POWER SUPPLY AND POWER CONDITIONING SUBSYSTEM

E presents a brief description of the Avco RAD Astrolab, which is presently being installed, and is designed for evaluation of ACS subsystem compatibility, with particular emphasis on sensor performance.

B. WEIGHT ESTIMATES FOR A FLYABLE ORBIT AND ACS

Preliminary weight estimates of the ACS and station-keeping system for a 500-pound satellite similar to that described in the first quarterly report[3] are presented below. These estimates are being continually revised and performed for a variety of missions. The present calculations are for a synchronous satellite.

1. Weight of Resistojet Power Conditioning Equipment

A schematic of the power conditioning circuit is presented in figure 4.2. The electric input power which can originate either from a battery pack or directly from solar panels is inverted from dc to 1000 cps ac by means of an oscillator and amplifier. The amplifier is, in turn, connected to the primary winding of a transformer, which steps down the amplifier output voltage (order of 24 volts) to a voltage compatible with the resistojet voltage (order of 1 volt). To avoid line I^2R losses, a separate voltage stepdown transformer will be located at each resistojet. The resistojet heater element can thus be directly coupled to the secondary of the transformer with negligible line losses. Table 4.2 presents estimated values of the weight of 24-volt to 1-volt stepdown transformers for operation at 1000 cps. These figures are not to be taken as definitive, and work is proceeding in this area.

It is probable that a single amplifier and oscillator can be used for the entire system, although this point must be examined further. Estimated values of the oscillator-amplifier combination are shown in table 4.3 as a function of power level. The weight of the oscillator is, or course, negligible compared with the amplifier. The specific power values (lbs/watt) tend to be smaller at the higher power inputs. Again the values presented in table 4.3 are preliminary and still being examined.

TABLE 4.2

ESTIMATED WEIGHTS FOR THE RESISTOJET VOLTAGE STEPDOWN TRANSFORMER

Power Input (watts)	Transformer Weight (pounds)
5	0.20
25	0.50
100	1.00

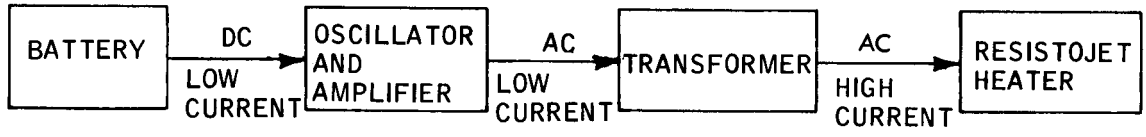

65-8188

Figure 4.2 SCHEMATIC OF RESISTOJET POWER CONDITIONING CIRCUIT

TABLE 4.3

ESTIMATED WEIGHT FOR THE OSCILLATOR AMPLIFIER PACKAGE

Power Input (watts)	Oscillator-Amplifier Package (pounds)
5	0.40
25	1.25
100	3.00

2. Weight of Resistojet Engine

The weight of the resistojet engine heater, structure, and solenoid valve is 0.04 pound.

3. Resistojet Engine Performance

For the present exercise the performance of the resistojet will be assumed to be 400 x 10^{-6} pound thrust, at 15 watts input power, and 175 seconds specific impulse (see reference 1, figure 17). The valves require 2 watts of power to operate. The overall efficiency of the power conditioning system, defined as the ratio of transformer power output to amplifier power input will be assumed to be equal to 70 percent. The required power input is then about 25 watts to operate both the engine heater and the valve.

4. Mission Assumptions

The basic mission assumptions are shown in table 4.4.

5. System Weight Comparison

Assuming that 400 x 10^{-6} pound thrust is the maximum which can be tolerated by the spacecraft, table 4.5 presents a weight comparison between a cold ammonia system operated at a specific impulse of 65 seconds and a hot system operated at a specific impulse of 175 seconds. The ammonia propellant feed and storage system is assumed to be equal to 0.10 of the propellant weight. Each system is assumed to have 12 engines. The specific weight of the solar power supply is assumed to be 0.25 lb/watt.

Referring to table 4.5 it is noted that the hot engine system offers nearly a 130-pound weight advantage over the cold system.

TABLE 4.4

BASIC ASSUMPTIONS FOR THE SYNCHRONOUS SATELLITE MISSION

Disturbance Torque	500 dyne-cm
Limit Cycle	Soft
Mission Time	3 years
Attitude Control Impulse Requirements	5265 lb-sec
Station Keeping Impulse Requirements	7920 lb-sec
Total Impulse Requirements	13,185 lb-sec

TABLE 4.5

WEIGHT COMPARISON BETWEEN A COLD AND HOT AMMONIA ATTITUDE CONTROL AND STATION-KEEPING SYSTEM, SYNCHRONOUS SATELLITE

Item	Cold (pounds)	Hot (pounds)
Engine - Valves (12)	0.5	0.5
Ammonia Propellant	200.0	75.0
Tankage	20.0	7.5
Solar Power Supply	0.8	6.3
Oscillator-Amplifier	---	1.3
Stepdown Transformer (12)	---	5.0
Control Logic Package	1.5	1.5
Total System	222.8	97.1

V. DIRECTIONS FOR FUTURE RESEARCH AND DEVELOPMENT

A. THRUST MEASUREMENT SYSTEM

The impulse balance will be mounted in a 4-foot by 8-foot tank which is connected to a 32-inch diffusion pump. This will permit semicontinuous operation at pressures less than 1 micron of mercury. Comparisons will be made between thrust measurements made on the wire-in-tension thrust stand, and thrust measurements made in the impulse table.

B. RESISTOJET THRUSTOR DEVELOPMENT

1. The experimental study of hot- and cold-nozzle performance in the thrust range from 10^{-6} to 10^{-3} pound will be continued. The study will involve a comparison of actual and "ideal" nozzle performance as a function of nozzle-throat diameter, nozzle-area ratio, nozzle-chamber pressure and back pressure, and nozzle temperature. A comparison will be made of experimental and analytically predicted nozzle behavior.

2. The experimental study of fast heat-up heater performance will be continued. Particular consideration will be given to increasing the resistance of the heater element in order to make it more compatible with the solar-cell power conditioning equipment.

3. Exploratory studies will be continued on other resistojet concepts and the use of propellants other than ammonia for application to a variety of attitude control and station-keeping missions.

C. SINGLE-AXIS ACS

1. Evaluation of the resistojet ACS Model I at NASA Lewis will be continued. Emphasis will be placed on eliminating vertical motion between the table and the light source; this should, in turn, eliminate the valve chatter problem. Performance of the control system will be studies as a function of acquisition angle, $\theta_{initial}$, acquisition rate, $\dot{\theta}_{initial}$, and disturbance torque, τ_D . Direct measurements will be made of the fuel requirements for acquisition and hard and soft limit-cycle operation as a function of power input to the resistojet thrustors.

2. Comparison will be made between the control system performance results obtained on the air bearing with control system performance results obtained on an analog computer.

3. The Model II resistojet ACS will be delivered and checked out at NASA Lewis. The Model II resistojet ACS will have an acquisition capability up

to 8 degrees, and provisions will be provided for manually adjusting the heater power (5 to 35 watts), the heater warmup time (1 to 10 seconds), and the pulse width of the inner lines (1 to 10 seconds). Measurements will also be made of the power input to the power conditioning equipment, and the power input to the heater element. The Model II system will make it possible to check out a variety of resistojet designs and control logic concepts.

D. DESIGN AND DEVELOPMENT OF A FLYABLE THREE-AXIS PROTOTYPE ACS AND STATION-KEEPING SYSTEM

1. Studies of a resistojet three-axis ACS and station-keeping system will be continued. Emphasis will be placed on the design of lightweight power conditioning equipment to transfer power from the solar-cell power supply to the low-resistance resistojet engines.

2. A review will be made of the current status of control valves and regulators for low pressure (order of 10 atms), low flow rate (order of μlbs/sec) propellant storage and feed systems. A feasibility study will be made of the possibility of using a porous plug for gas regulation in place of a mechanical gas regulator which has moving parts.

VI. REFERENCES

1. John, R. R., and D. Morgan, Resistojet Research and Development Phase II, Second Quarterly Report on Contract NAS 3-5908, Avco RAD SR-65-44, January 20, 1965.

2. Vaeth, J. E., Vapor Jet Control of Space Vehicles, IRE Transactions on Automatic Control, 1962.

3. John, R. R. and S. Bennett, Resistojet Research and Development - Phase II, First Quarterly Report on Contract NAS 3-5908, Avco RAD SR-64-290, November 25, 1964.

4. Tinling, B. E., Measured Steady-State Performance of Water Vapor Jets for Use in Space Vehicle Attitude Control Systems, NASA Technical Note D-1302, May, 1962, Ames Research Center.

5. Jonath, A. D., Gasdynamic Problems in Low Pressure Microthrust Engines, AIAA Propulsion Joint Specialist Conference, Colorado Springs, Colo., June 14-18, 1965.

APPENDIXES

APPENDIX A

LEAD NETWORK CHARACTERISTICS FOR THE RESISTOJET SINGLE AXIS ATTITUDE CONTROL SYSTEM

1. INTRODUCTION

A block diagram of the basic control logic for the Model I and II resistojet attitude control systems is given in figure A.1. The position sensor provides a voltage signal, $\theta(t)$, which is directly proportional to the angular error at a time t. The response of the position sensor is illustrated in figure A.2. This sensor has a linear response (± 2 percent) over a range of ± 1 degree of angular error with a null at zero-degree angular error. For positive angular errors, the voltage output is negative as shown. Outside the linear range, a nonlinear response occurs out to an angle which represents the maximum sensor output; from figure A.2 this angle is about ± 2.5 degrees and represents the maximum useful range of the sensor. For angular errors larger than 2.5 degrees, the signal output gradually decreases approaching a value of zero at an angle of ± 10 degrees. In the linear range of the sensor, the sensitivity is about 180 millivolts per degree of angle.

The voltage signal from the position sensor is amplified by a preamp with a gain K to give an output signal $K\theta(t)$. This signal is in exact phase with the input signal to the preamp, $\theta(t)$.

The preamp output represents the input signal to the lead network which is the basic control element of the resistojet control logic system. The lead network provides an output signal $Z(t)$, to the switching networks which then control the pulsing of the appropriate resistojets. If the output signal, $Z(t)$, equals and exceeds the lower of two preset values, the switching network provides a resistojet pulse of preset duration in the proper direction. If $Z(t)$ equals and exceeds the larger of the two preset values, the appropriate resistojet is turned on and remains on continuously until $Z(t)$ is reduced below this larger value. (Hysteresis will make the dropout voltage of the switch slightly less than the pullin voltage.) The operation of the resistojet pulsing to provide attitude control of the satellite is thus directly related to the output signal $Z(t)$ of the lead network. It is the purpose of the remaining discussion to investigate the relationship between the input signal, $K\theta(t)$, and the output signal $Z(t)$, for the lead network being used in the control logic of the Models I and II resistojet control systems.

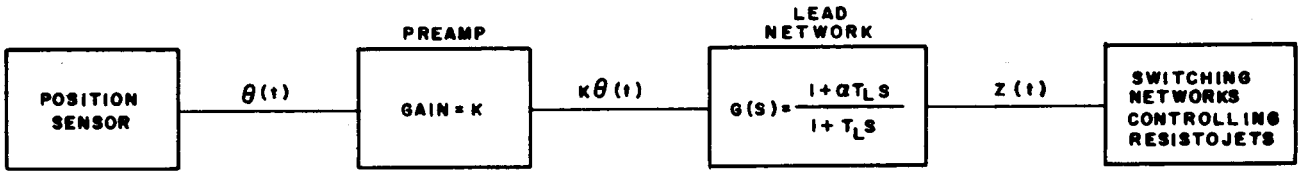

65-8189

Figure A.1 BASIC CONTROL LOGIC DIAGRAM FOR RESISTOJET ATTITUDE CONTROL SYSTEM

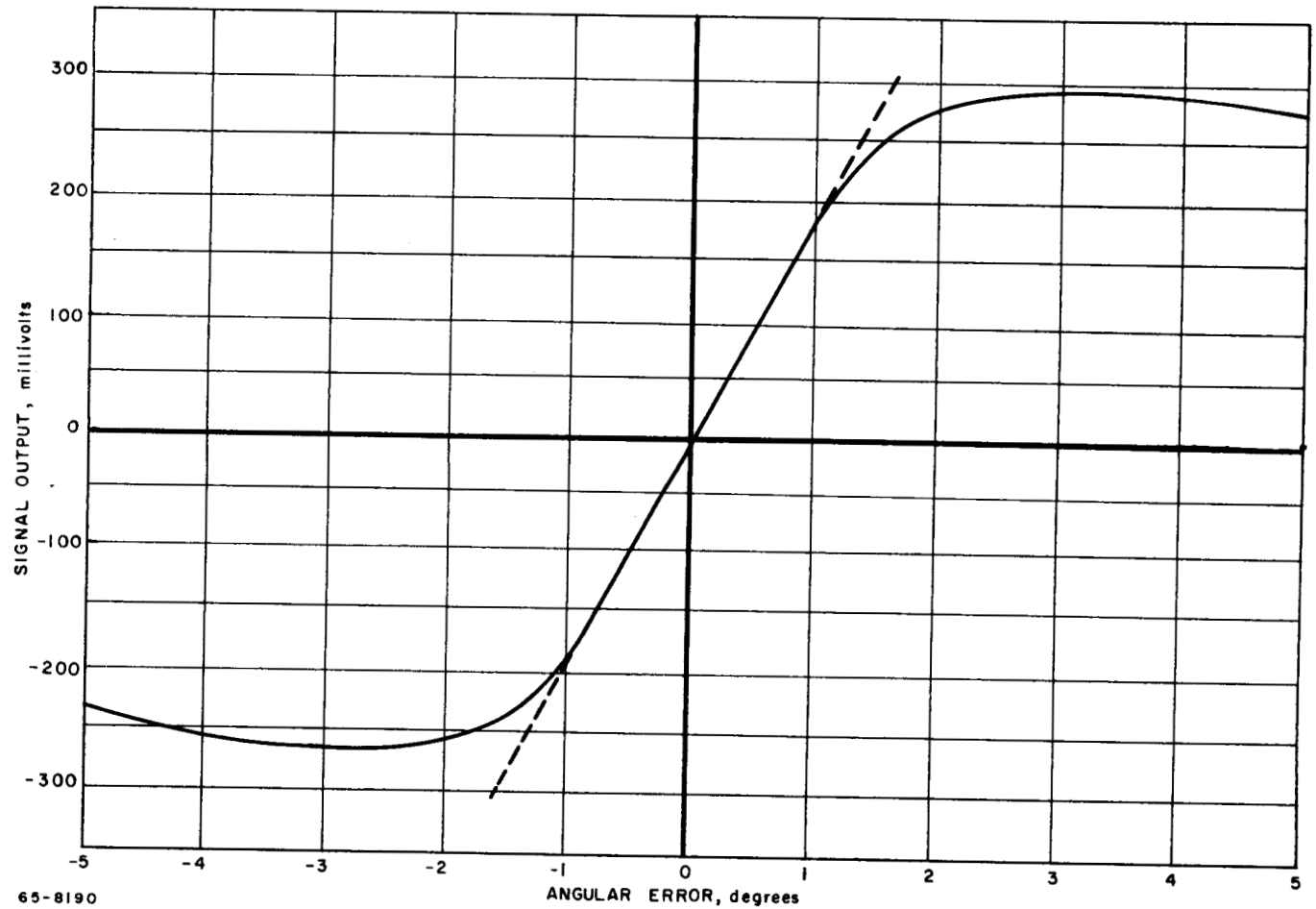

Figure A.2 SIGNAL OUTPUT FROM POSITION SENSOR AS FUNCTION OF ANGULAR ERROR

2. LEAD NETWORK CHARACTERISTICS

The characteristics of operation of the lead network are contained in the transfer function, G(s):

$$G(s) = \frac{1 + a\,\tau_L\,s}{1 + \tau_L\,s} \qquad (A.1)$$

where

a = constant of lead network, dimensionless

τ_L = constant of lead network, seconds

s = complex frequency variable

The transfer function is the ratio of the Laplace transform of the output signal to the Laplace transform of the input signal. The type of control represented by this transfer function is widely used in process control systems and is frequently referred to as "proportional plus derivative of error" control; in other words, the control element output depends not only on the absolute angluar error, $\theta(t)$, but also on the rate with which the angular error is changing, $d\theta(t)/dt$.

From the definition of the transfer function, equation (A.1) can be rewritten as:

$$\frac{Z(s)}{K\theta(s)} = \frac{1 + a\,\tau_L\,s}{1 + \tau_L\,s} \qquad (A.2)$$

where

$Z(s)$ = Laplace transform of $Z(t)$

$\theta(s)$ = Laplace transform of $\theta(t)$

Or as:

$$Z(s) = \frac{K}{\tau_L} \frac{1}{s + (1/\tau_L)} \theta(s) + aK \frac{s}{s + (1/\tau_L)} \theta(s) \qquad (A.3)$$

The output signal $Z(t)$ which is the inverse of $Z(s)$ thus depends on the function $\theta(s)$ which in turn depends on the variation of $\theta(t)$ with time. The solution for $Z(t)$ will be derived for two special cases to illustrate this dependence, the first in which $\theta(t)$ varies as a step increase followed by a linear increase with time and the second in which $\theta(t)$ varies sinusoidally with time.

a. Step Increase in Angle Followed by a Linear Change of Angle with Time (Constant Rate of Rotation)

In a hard limit cycle with zero disturbance torque, the drift phase of the limit cycle takes place with a constant rate of rotation. The angle at anytime with an initial step increase can thus be written as:

$$\theta(t) = 0 \qquad t < 0$$

$$\theta(t) = \theta_o + \psi t \qquad t \geq 0 \qquad (A.4)$$

where

θ_o = step increase in angle at t = zero

$\psi = \frac{d\theta}{dt}$ = rate of rotation

The case of constant ψ corresponds to the drift phase of the limit cycle with zero disturbance torque.

The Laplace transform of (A.4) is:

$$\theta(s) = \frac{\theta_o}{s} + \frac{\psi}{s^2} \qquad (A.5)$$

Substitution of this relation into (A.3) gives:

$$Z(s) = \frac{1}{s + (1/\tau_L)} aK\theta_o + \frac{1}{s[s + (1/\tau_L)]} \left[\frac{K\theta_o}{\tau_L} + aK\psi\right] + \frac{1}{s^2[s + (1/L)]} \frac{K\psi}{\tau_L} \qquad (A.6)$$

Taking the inverse of this relation and algebraic simplification results in:

$$Z(t) = K\left\{(a-1)(\theta_o - r_L\psi)\,e^{-t/r_L} + \psi t + [\theta_o + r_L\psi(a-1)]\right\} \qquad (A.7)$$

For $t \gg r_L$ this relation simplifies to:

$$Z(t) = K\{(\theta_o + \psi t) + (a-1)\,r_L\,\psi\}$$

$$= K\left\{\theta(t) + (a-1)\,r_L\,\frac{d\theta(t)}{dt}\right\} \qquad (A.8)$$

This expression, which is the same as that given in the second quarterly report illustrates the dependence of $Z(t)$ on both $\theta(t)$ and $d\theta(t)/dt$ and justifies the description of this type of control as "proportional plus derivative of error control".

Rewriting equation (A.8):

$$\frac{d\theta(t)}{dt} = \frac{Z(t)/K}{(a-1)\,r_L} - \frac{1}{(a-1)\,r_L}\,\theta(t) \qquad (A.9)$$

Switching occurs when $Z(t) = Z_{sw}$ so that the control line is represented by:

$$\left(\frac{d\theta}{dt}\right)_c = \frac{Z_{sw}/K}{(a-1)\,r_L} - \frac{1}{(a-1)\,r_L}\,\theta_c$$

$$\left(\frac{d\theta}{dt}\right)_c = \frac{\theta_{co}}{(a-1)\,r_L} - \frac{1}{(a-1)\,r_L}\,\theta_c \qquad (A.10)$$

Equation (A.7) can be used to obtain the response for a step change in $\theta(t)$ alone and for a linear increase of $\theta(t)$ alone starting from $\theta(t) = 0$. For the step change, ψ in equation (A.7) is set equal to zero giving:

$$Z(t) = K\theta_o\left[(a-1)\,e^{-t/r_L} + 1\right] \qquad (A.11)$$

At $t = 0$, $Z(t) = K\theta_o\,a$

For $t \gg r_L$, $Z(t) = K\theta_o$

For the linear increase alone, set θ_o of equation (A.7) equal to zero giving:

$$Z(t) = K\psi\left\{(a-1)\,\tau_L\left[1 - e^{-t/\tau_L}\right] + t\right\} \qquad \text{(A.12)}$$

At $t = 0$, $Z(t) = 0$

For $t \gg \tau_L$, $Z(t) = K\psi\left[(a-1)\tau_L + t\right] = K\left[\theta(t) + (a-1)\tau_L\,\psi\right]$

b. Sinusoidal Variation of Angle with Time

The usual way of expressing the response of a control element is to present the response to a sinusoidal variation in the input to the control element. The response is generally given in the form of the ratio of peak output magnitude to peak input magnitude versus frequency and the phase angle versus frequency. The response of the lead network to a sinusoidal input can be considered, to a first approximation, as the response to a symmetrical hard limit cycle with zero disturbance torque. This is illustrated in the sketch of figure A. 3.

The response to a sinusoidal input can be obtained directly from the transfer function by substituting $j\omega$ for s in the transfer function where $j = \sqrt{-1}$.

Thus:

$$G(j\omega) = \frac{1 + (a\,\tau_L\,\omega)j}{1 + (\tau_L\,\omega)\,j}$$

$$= \frac{1 + a(\tau_L\,\omega)^2}{1 + (\tau_L\,\omega)^2} + j\,\frac{a\,\tau_L\,\omega - \tau_L\,\omega}{1 + (\tau_L\,\omega)^2} \qquad \text{(A.13)}$$

The magnitude of this relation is given by:

$$G = \sqrt{\left[\frac{1 + a(\tau_L\,\omega)^2}{1 + (\tau_L\,\omega)^2}\right]^2 + \left[\frac{a\,\tau_L\,\omega - \tau_L\,\omega}{1 + (\tau_L\,\omega)^2}\right]}$$

$$= \sqrt{\frac{1 + (a\,\tau_L\,\omega)^2}{1 + (\tau_L\,\omega)^2}} \qquad \text{(A.14)}$$

The phase angle is obtained from:

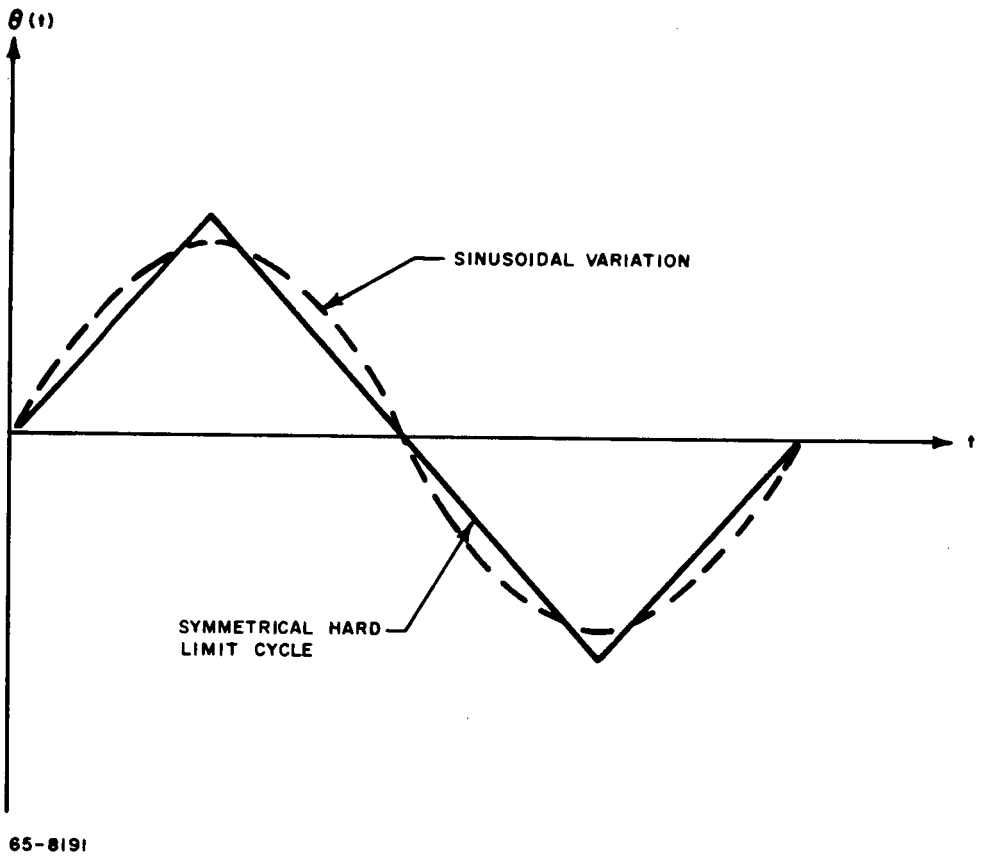

Figure A.3 COMPARISON OF HARD LIMIT-CYCLE OPERATION WITH SINUSOIDAL VARIATION OF ANGLE WITH TIME

$$\tan\phi = \left[\frac{a\tau_L\,\omega - \tau_L\,\omega}{1+(\tau_L\,\omega)^2}\right] \Big/ \left[\frac{1+a(\tau_L\,\omega)^2}{1+(\tau_L\,\omega)^2}\right]$$

$$= \frac{\tau_L\,\omega\,(a-1)}{1+a\,(\tau_L\,\omega)^2} \qquad \text{(A. 15)}$$

The phase angle is defined as $\phi = (\omega t)_1 - (\omega t)_2$ as illustrated in figure A. 4.

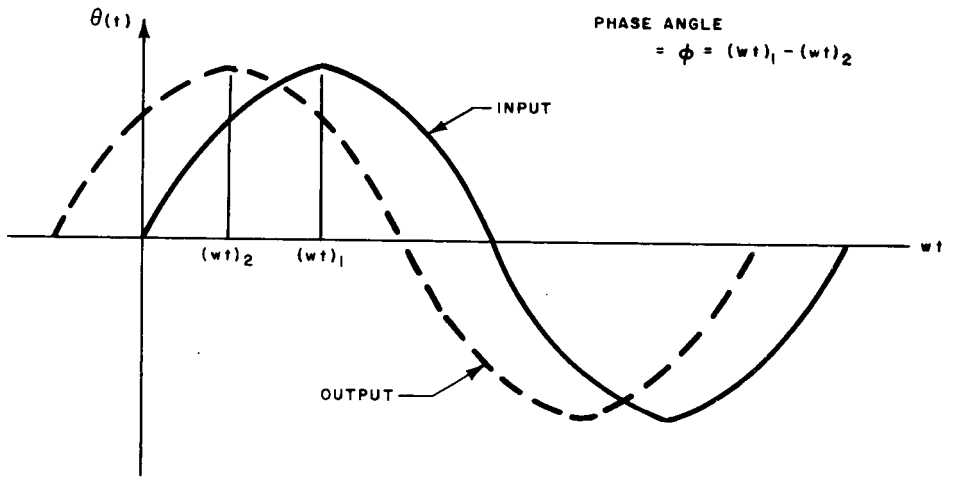

65-8192

Figure A.4 ILLUSTRATION OF PHASE ANGLE DEFINITION

The sketch of this figure is for a positive phase angle; from equation A. 15, it is apparent that the phase angle is positive for the Model I and II resistojet control systems. A positive phase angle means the response "leads" the input as illustrated in figure A. 4; hence, the expression "lead network".

The lead network response has been calculated and plotted for several values of a and τ_L. In figures A. 5 and A. 6, the ratio of output peak magnitude to input peak magnitude and the phase angle respectively are presented as a function of the dimensionless frequency, $\tau_L\,\omega$, for a's of 10, 20, and 30. The amplitude ratio at large frequencies is seen to be equal to a and drops to one at low frequencies. The point at which the peak amplitude ratio is approached occurs for a constant $\tau_L\,\omega$ of about 2π for all a's or when:

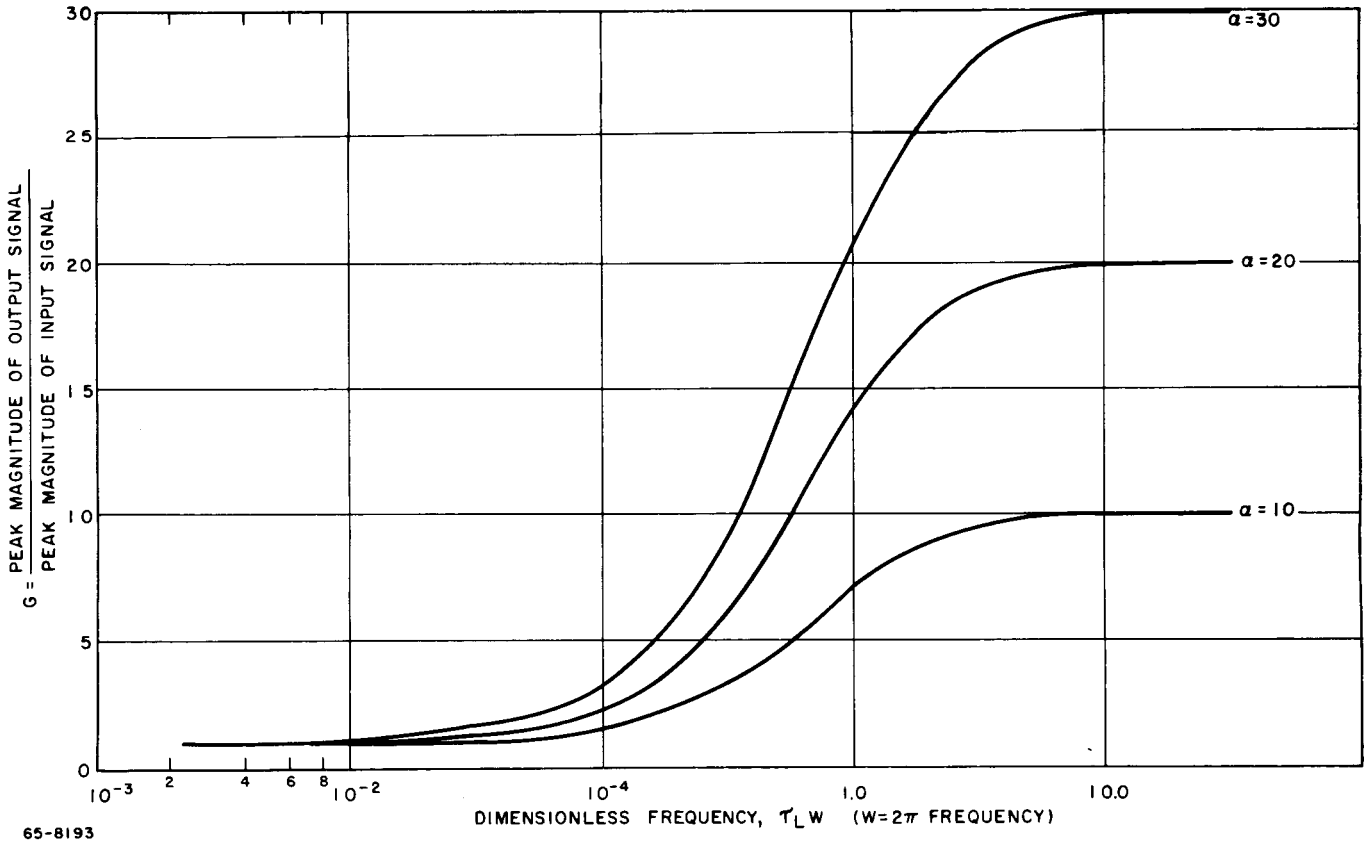

Figure A.5 RATIO OF PEAK OUTPUT MAGNITUDE TO PEAK INPUT MAGNITUDE VERSUS DIMENSIONLESS FREQUENCY

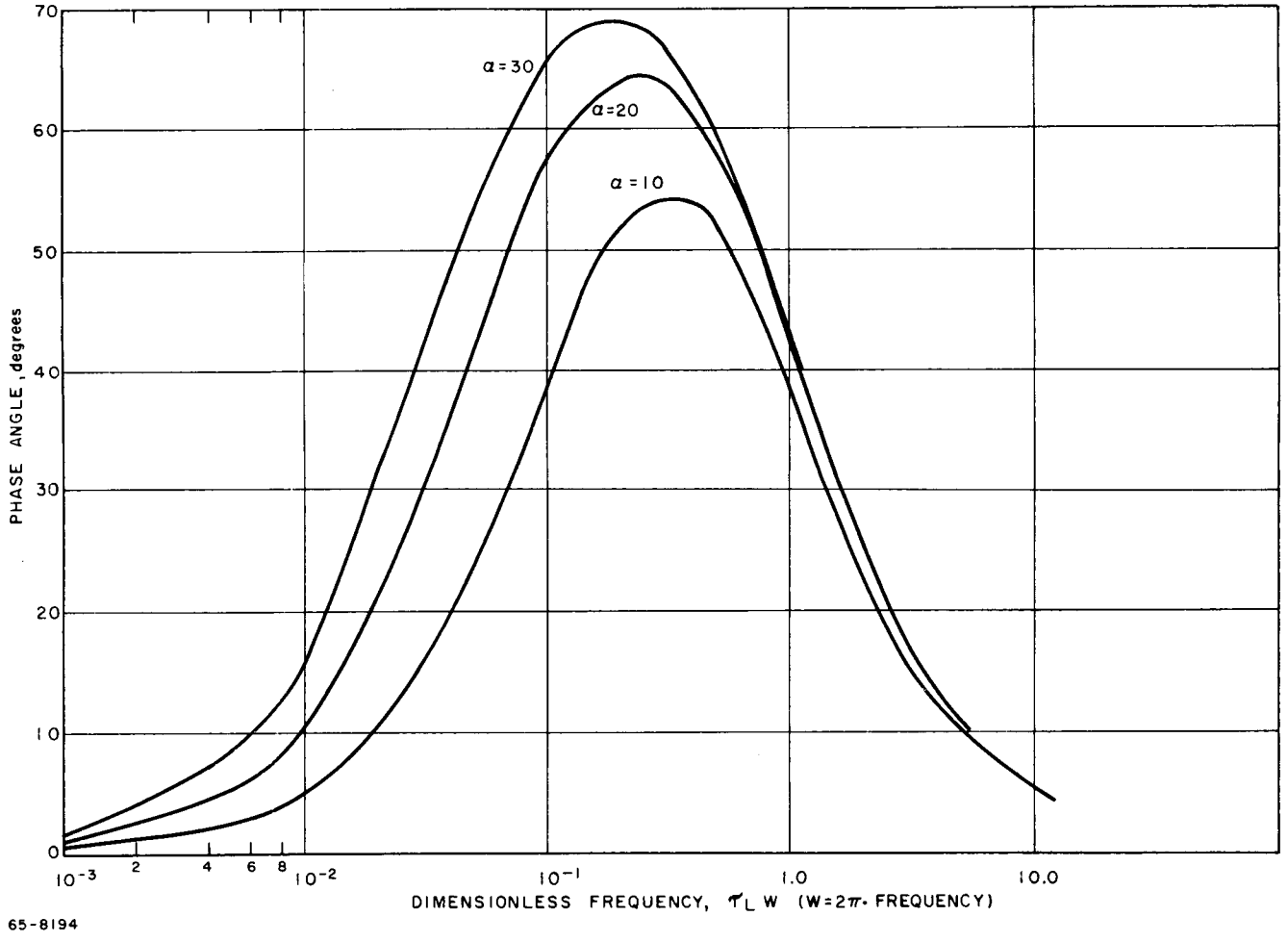

Figure A.6 PHASE ANGLE VERSUS DIMENSIONLESS FREQUENCY

$$f(G \to \alpha) = \frac{\omega}{2\pi} = \frac{1}{\tau_L} \qquad \text{(A. 16)}$$

At the low frequencies, the point at which the amplitude ratio approaches one is dependent on α as well as τ_L and can be obtained by expanding equation (A. 14) and throwing away higher order terms:

$$G \cong \sqrt{1 + (\alpha \tau_L \omega)^2} \quad , \quad \tau_L \omega \ll 1 \qquad \text{(A. 17)}$$

For different α's, the amplitude ratio thus has the same value when:

$$\alpha \tau_L \omega = \text{Constant} \qquad \text{(A. 18)}$$

or when:

$$f = \frac{\omega}{2\pi} = \frac{\text{Constant}}{2\pi \alpha \tau_L} \qquad \text{(A. 19)}$$

From figure A. 5, G = 1. 4 with $\tau_L \omega = 0.1$ and $\alpha = 10$; the constant in the above equations for this G is thus $\alpha \tau_L \omega = 1$ and:

$$f(G \to 1) = \frac{1}{2\pi \alpha \tau_L} \qquad \text{(A. 20)}$$

From figure A. 6, it is apparent that the phase angle increases with increasing α. Also, the frequency of peak phase angle lowers by about a factor of 2 as α is increased from 10 to 30.

The preceding plots illustrated the effect of α; in figure A. 7, the amplitude ratio is plotted versus cycle time for an α of 10 and for τ_L's of 2 and 5 seconds. The effect of increasing τ_L is to increase the limit cycle time (or decrease the frequency) at which the response of the lead network is strongly rate dependent. In figure A. 8, the amplitude ratio is plotted versus ω for an α of 20 and τ_L's of 1, 2, and 5 seconds.

3. CIRCUIT FOR LEAD NETWORK

The control circuit with the transfer function given by equation (A. 1) consists basically of two resistors and one capacitor wired as illustrated in figure A. 9 . The transfer function of this circuit is

$$\frac{V_{bc}(s)}{V_{ac}(s)} = \frac{1}{\alpha} \frac{1 + \alpha \tau_L s}{1 + \tau_L s} \qquad \text{(A. 21)}$$

where

$$\alpha = 1 + \frac{R_1}{R_2} \qquad \text{(A. 22)}$$

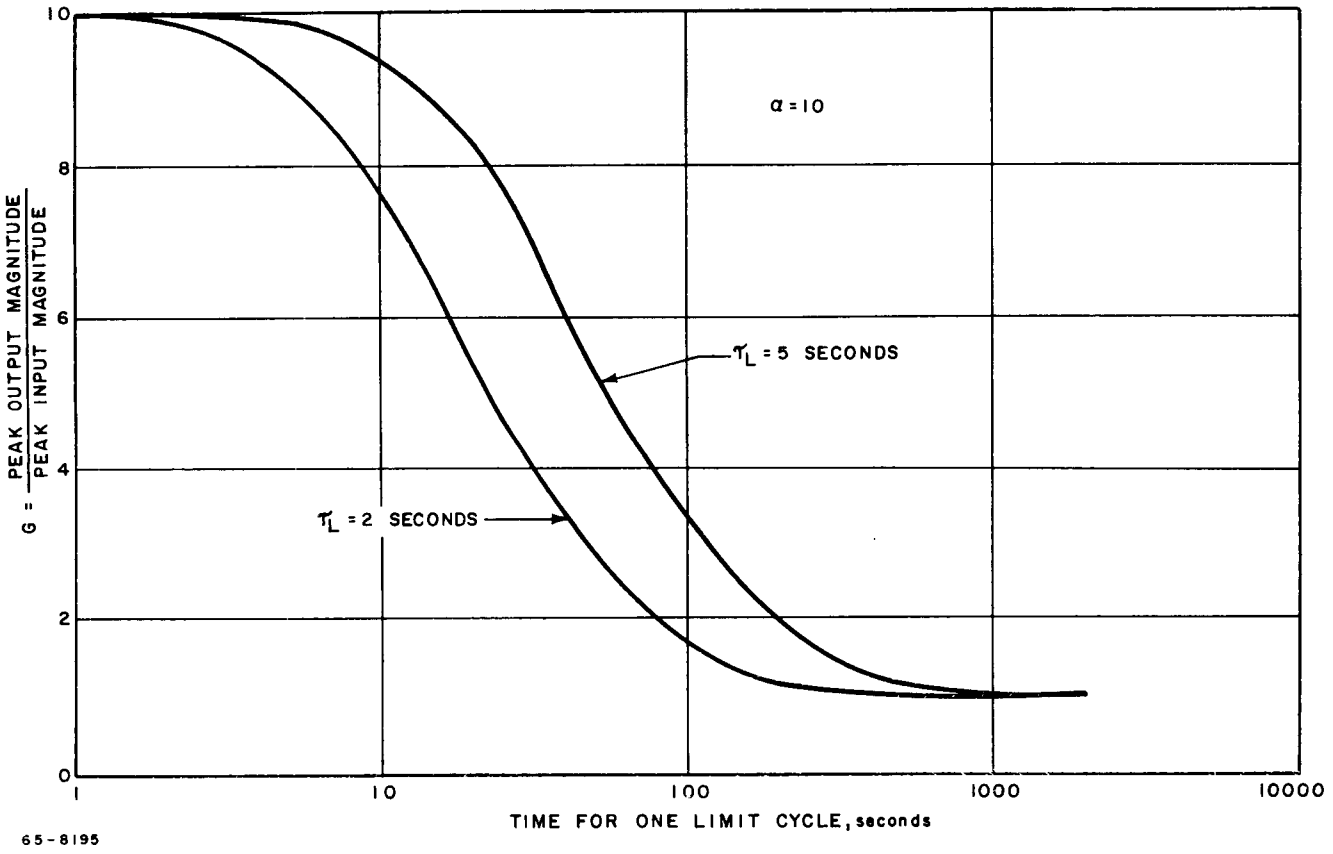

Figure A.7 RATIO OF PEAK OUTPUT MAGNITUDE TO PEAK INPUT MAGNITUDE VERSUS TIME OF ONE CYCLE

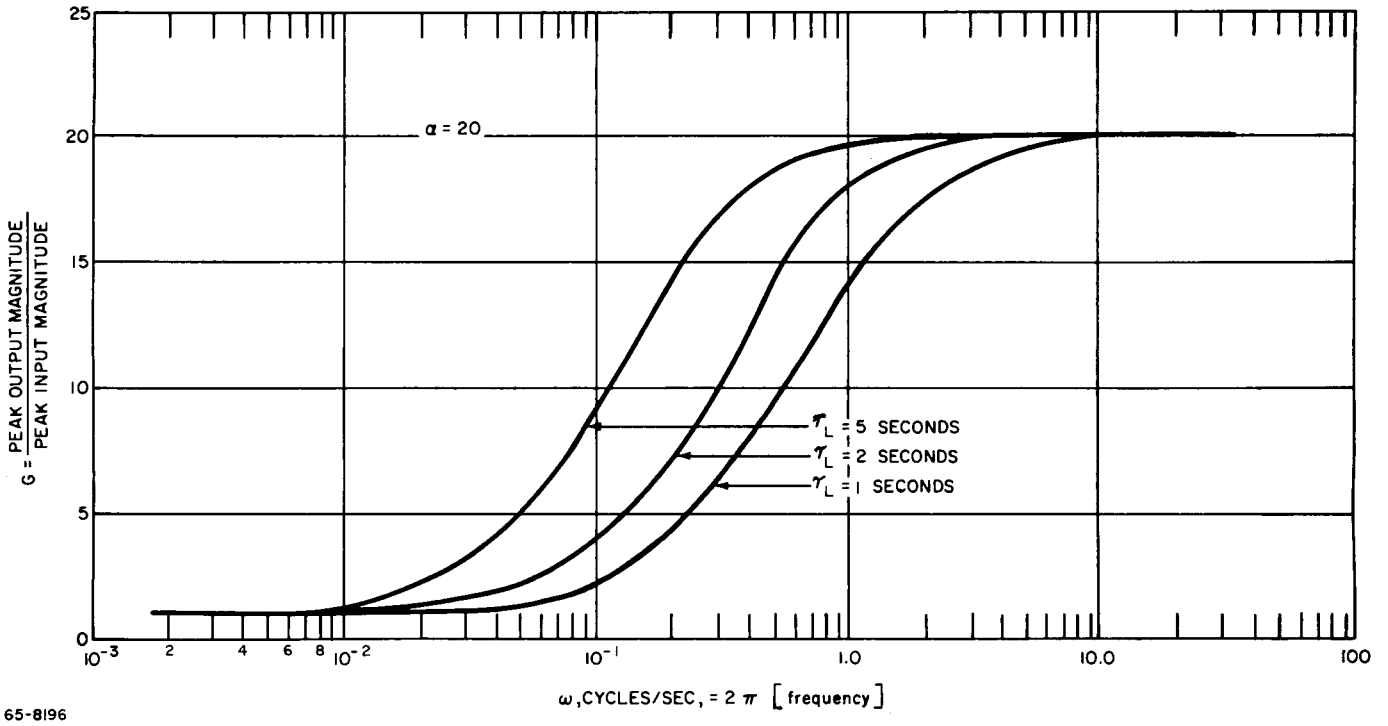

Figure A.8 RATIO OF PEAK OUTPUT MAGNITUDE TO PEAK INPUT MAGNITUDE VERSUS ω

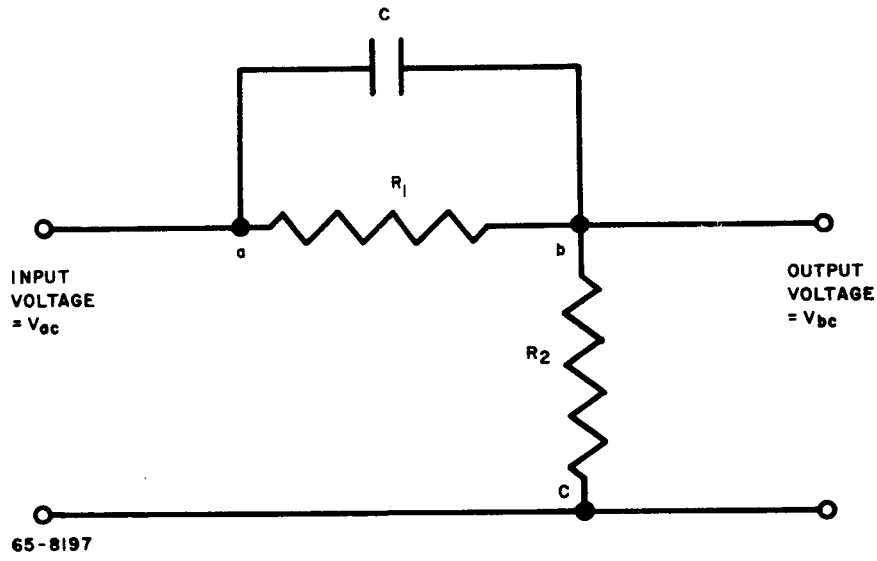

Figure A.9 CIRCUIT FOR LEAD NETWORK

$$\tau_L = \frac{R_2 R_1}{R_1 + R_2} C \qquad \text{(A. 23)}$$

This transfer function is identical to that of equation (A. 1) if an amplifier with a gain of a is added to the input. For the control logic of the Model I and Model II systems, nominal characteristics are:

$C = 100$ microfarads

$R_1 = 200{,}000\ \Omega$

$R_2 = 22{,}000\ \Omega$

Substitution gives

$a = 10.09$

$\tau_L = 1.982$ seconds

as the nominal lead network constants for the Model I and II resistojet attitude control systems.

APPENDIX B

ANALOG CALCULATIONS OF DUTY CYCLE VERSUS DISTURBANCE TORQUE

1. INTRODUCTION

To determine more precisely the effect of disturbance torque on the duty cycle for the Model I and II resistojet attitude control systems, additional analog computer calculations have been performed. These calculations were performed for two acquisition angles, 2.25 and 3.40 degrees, with the following other variables:

τ_R = control torque = 0.6×10^{-3} ft-lb = 8130 dyne-cm

J = moment of inertia = 27 slug ft^2

H = hysteresis of switching network = 15 percent

a = lead network constant = 10

τ_L = lead network constant = 2 seconds

t_R = fixed pulse duration for control by inner lines = 4 seconds

For these calculations, three output plotters were used. Two x-y plotters were used, one with a scale to follow in the phase plane the acquisition and the other with a blownup scale to follow in great detail in the phase plane the limit cycle performance. The third plotter was a strip chart recorder on which the following variables were continuously plotted throught a run:

Error Signal

Angular Acceleration, $d^2\theta/dt^2$

Angular Rate, $d\theta/dt$

Angular Error, θ

Total Time

In figures B.1, B.2 and B.3, typical plots from a run are presented.

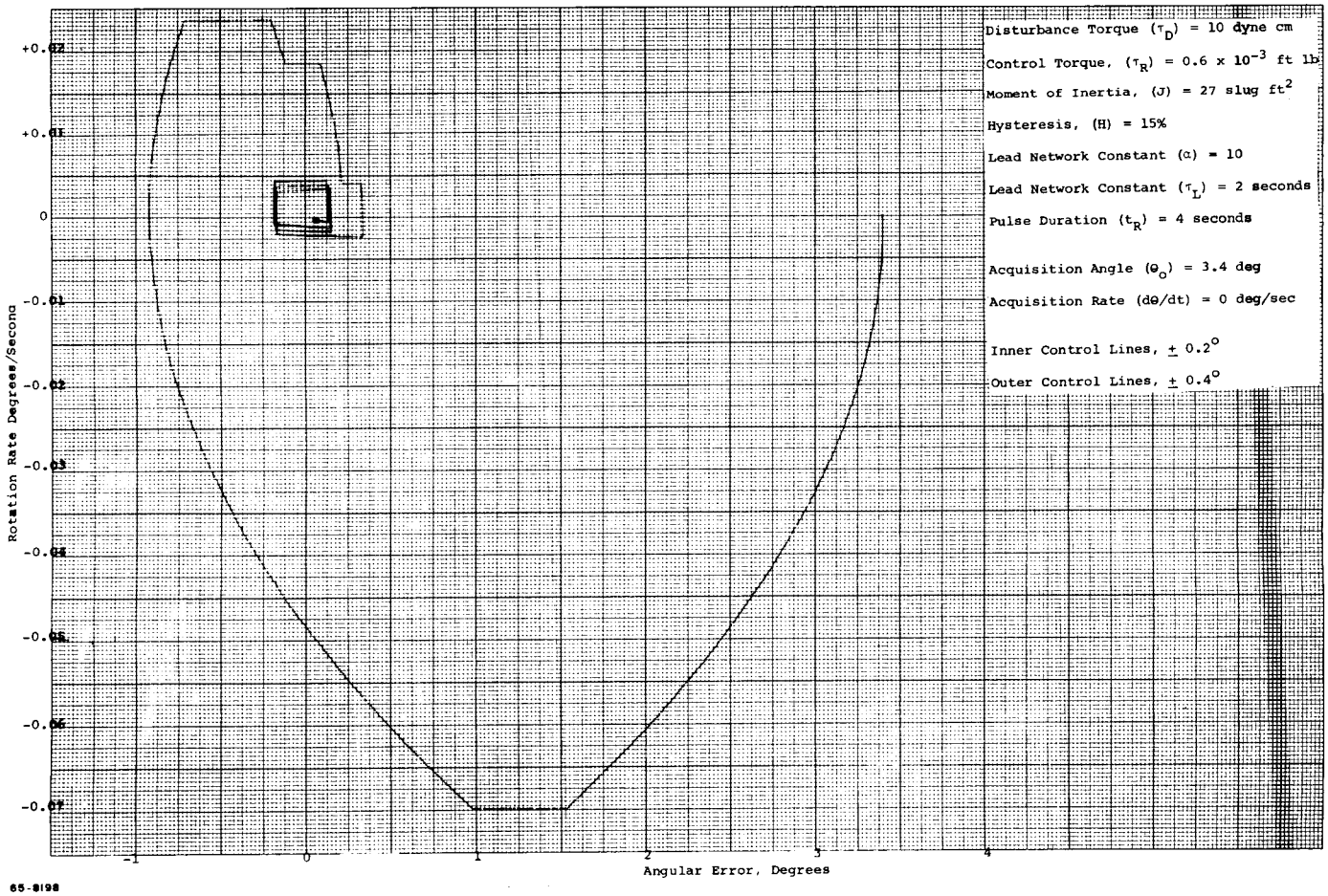

Figure 8.1 VEHICLE ACQUISITION IN THE PHASE PLANE

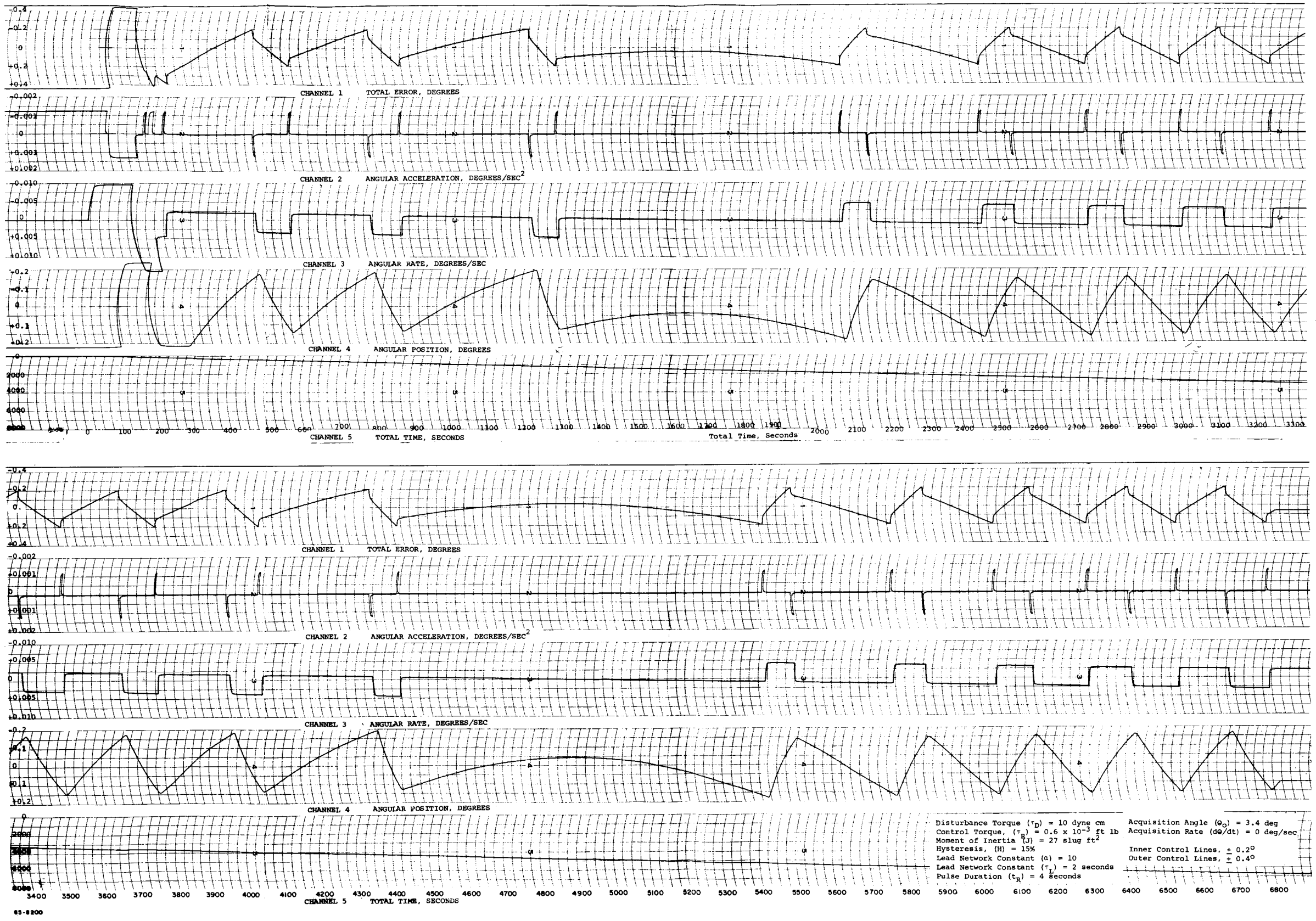

Figure B.3 STRIP CHART RECORD OF SYSTEM PERFORMANCE

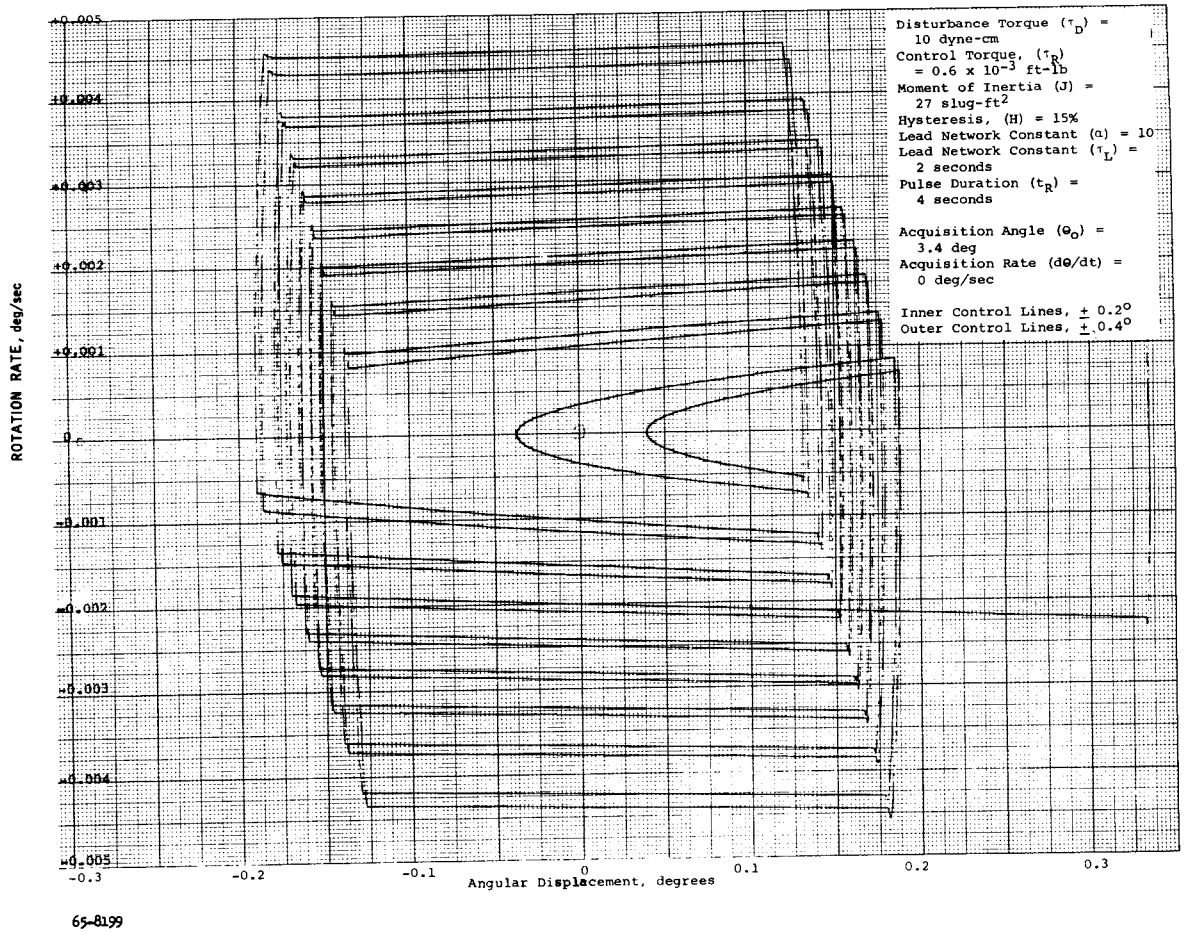

Figure B.2 VEHICLE LIMIT-CYCLE CONTROL IN THE PHASE PLANE

2. LIMIT-CYCLE PERFORMANCE AS FUNCTION OF DISTURBANCE TORQUE

From the strip chart record, the duty cycle for all runs was calculated; the duty cycle as a function of disturbance torque is presented in figures B. 4 and B. 5 for acqusition angles of 3.4 and 2.25 degrees, respectively. The most striking feature of these plots is that real discontinuities exist in the plots of duty cycle versus disturbance torque. In some cases, a change in the disturbance torque of as little as 0.25 dyne-cm resulted in a change in the duty cycle of two to three at the boundary between soft and hard limit-cycle operation. As the disturbance torque decreased, the frequency of occurrence of these discontinuities increases but their amplitude decreases.

The reason for these discontinuities can be seen with reference to some limit-cycle plots for the case of 3.4-degree acquisition angle. In figures B. 6 and B. 7, the phase plane plots are given for disturbance torques of 110 and 90 dyne-cm, between which the control goes from soft limit-cycle control to hard-limit control consisting of basically one hard-limit cycle coupled with one soft-limit cycle. From disturbance torques of 90 to 39, no discontinuities occur and the duty cycle decreases from a peak value of 0.0374 at 100 dyne-cm to 0.0135 at 38 dyne-cm. The limit-cycle plots for disturbance torques of 70, 39, and 37 are presented in figures B. 8, B. 9, and B. 10. For a disturbance torque of 70, the soft limit-cycle branch is larger than at 90 dyne-cm resulting in a decreased duty cycle. In both of these cases, the cycle is slowly nulling to a limit cycle which would retrace itself and have the shape illustrated in figure B. 11.

At 39 dyne-cm, the solf-limit part of the cycle has almost reached the opposite control line. The system is now much slower nulling than for the higher disturbance torques (70 and 90); thus, if the run were continued long enough, the two soft-limit and hard-limit branches would approach one another and merge into one retraceable cycle similar to that sketched in figure B. 11, except with a larger soft limit-cycle branch.

As the disturbance torque is reduced slightly below 39 dyne-cm, a point is reached where the soft-limit branch just reaches the opposite control line and triggers the opposing resistojet. When this occurs, a step increase in the duty cycle occurs. For a disturbance torque of 37 dyne-cm, this has occurred and a completely different type of limit cycle control occurs. Comparison of the limit cycles for 37 and 39 dyne-cm illustrates dramatically the difference 2 dyne-cm of disturbance torque can make. For 37 dyne-cm, the cycle has not nulled, but appears to be nulling to a cycle with one soft limit branch and two hard-limit branches for a repeating cycle.

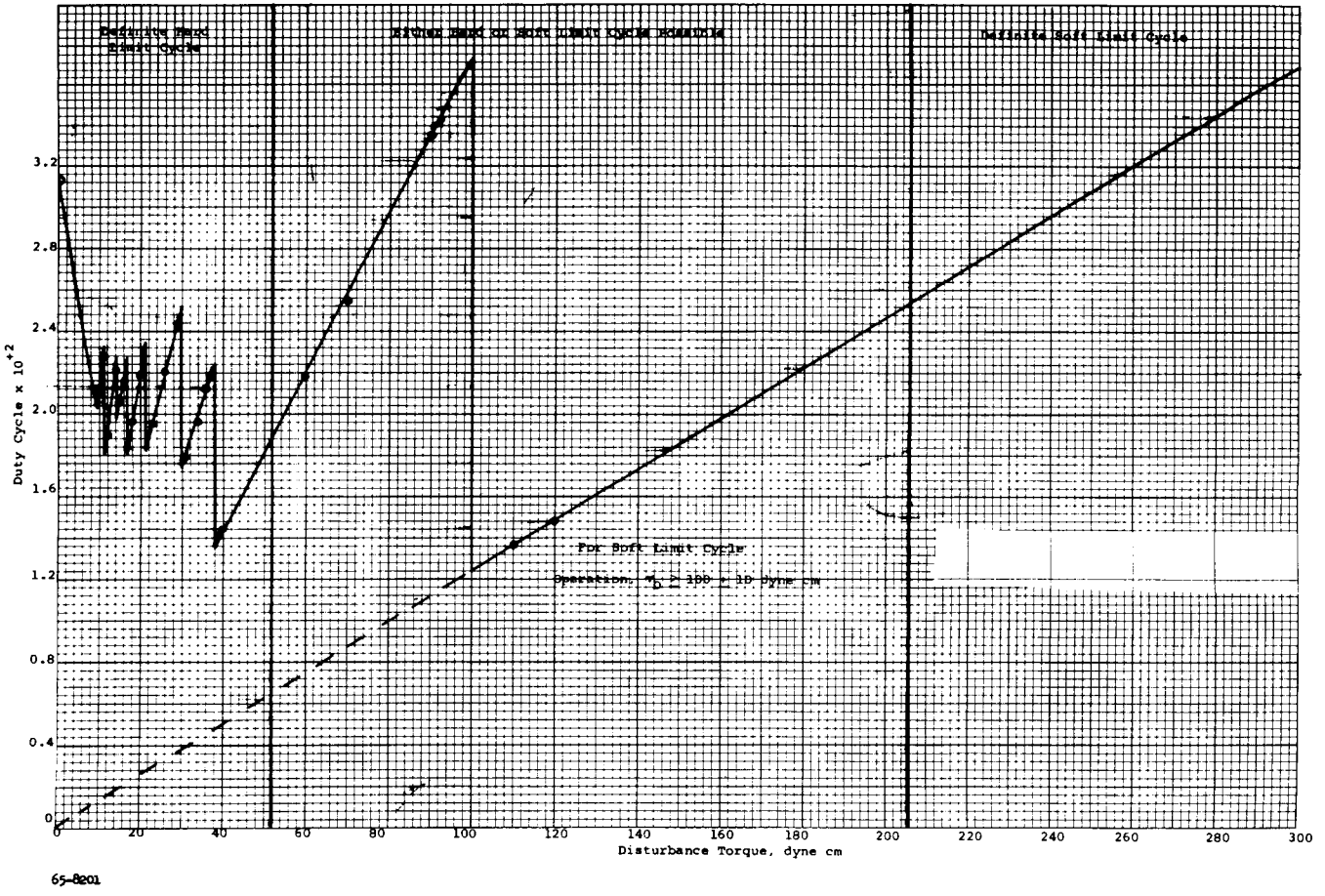

Figure B.4 DUTY CYCLE VERSUS DISTURBANCE TORQUE, θ_o = 3.4 DEGREES, $\dot{\theta}_o = 0$

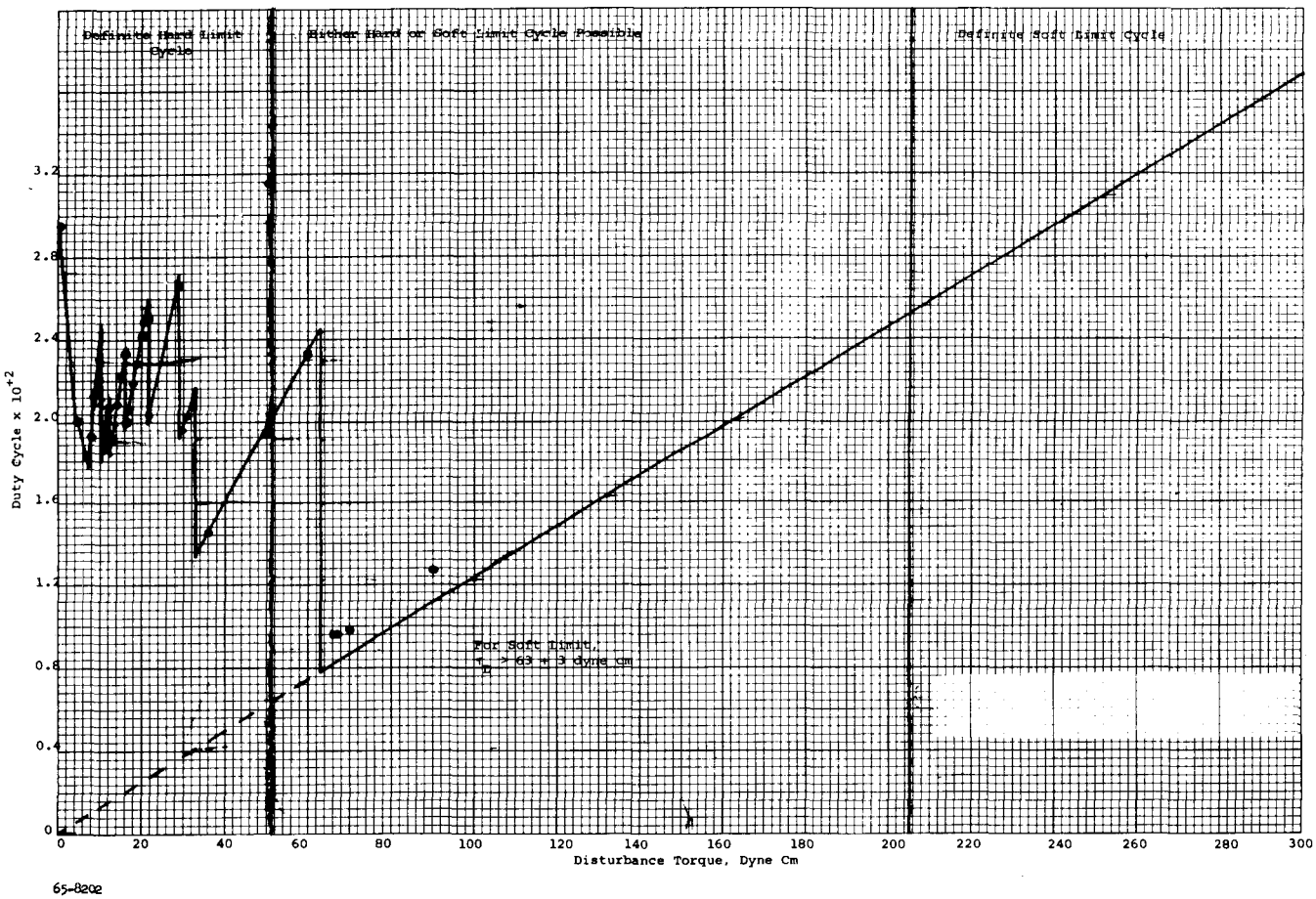

Figure B.5 DUTY CYCLE VERSUS DISTURBANCE TORQUE, θ_o = 2.25 DEGREES, $\dot{\theta}_o = 0$

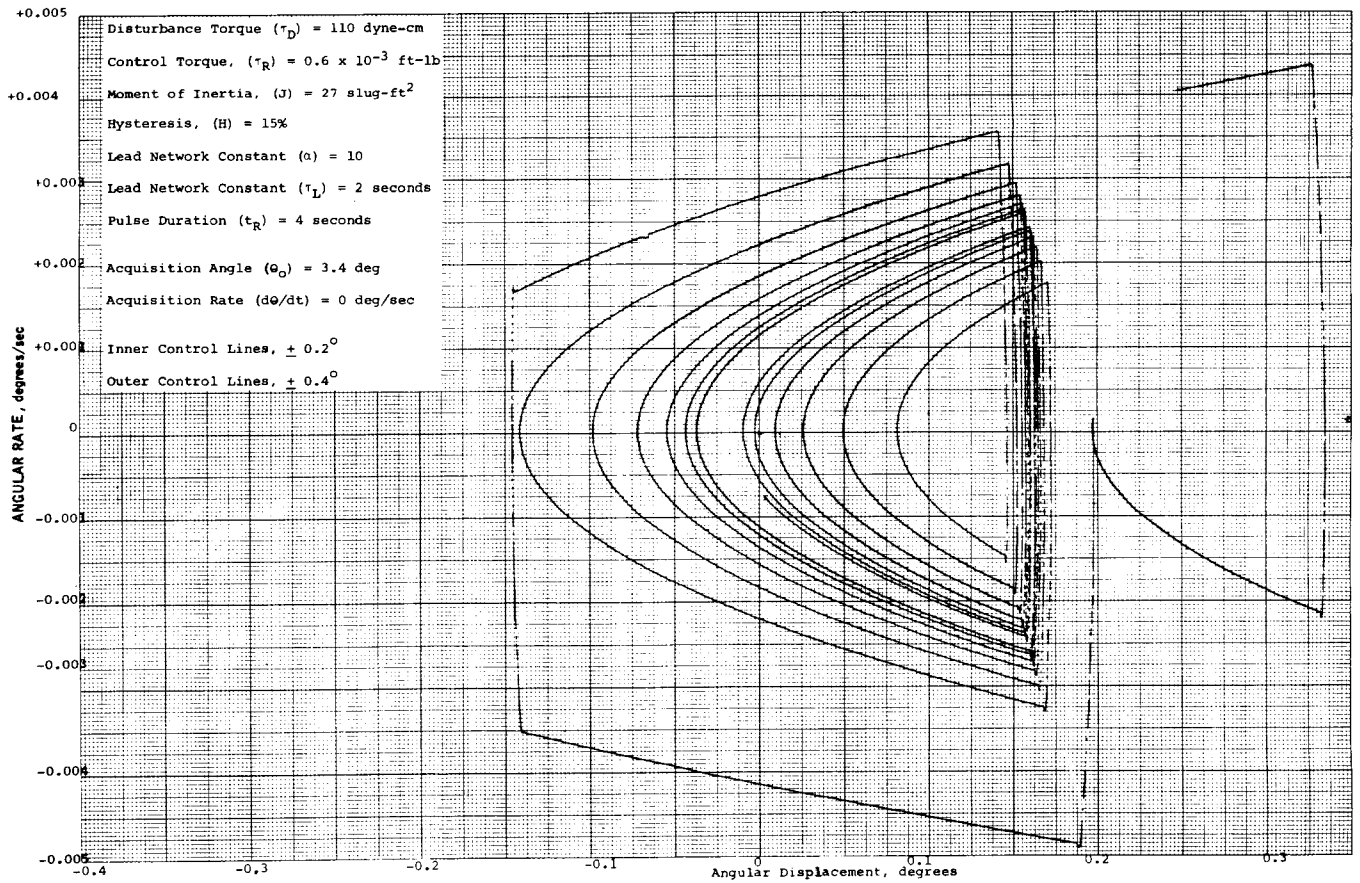

65-8203

Figure B.6 LIMIT CYCLE FOR DISTURBANCE TORQUE OF 110 DYNE-CM

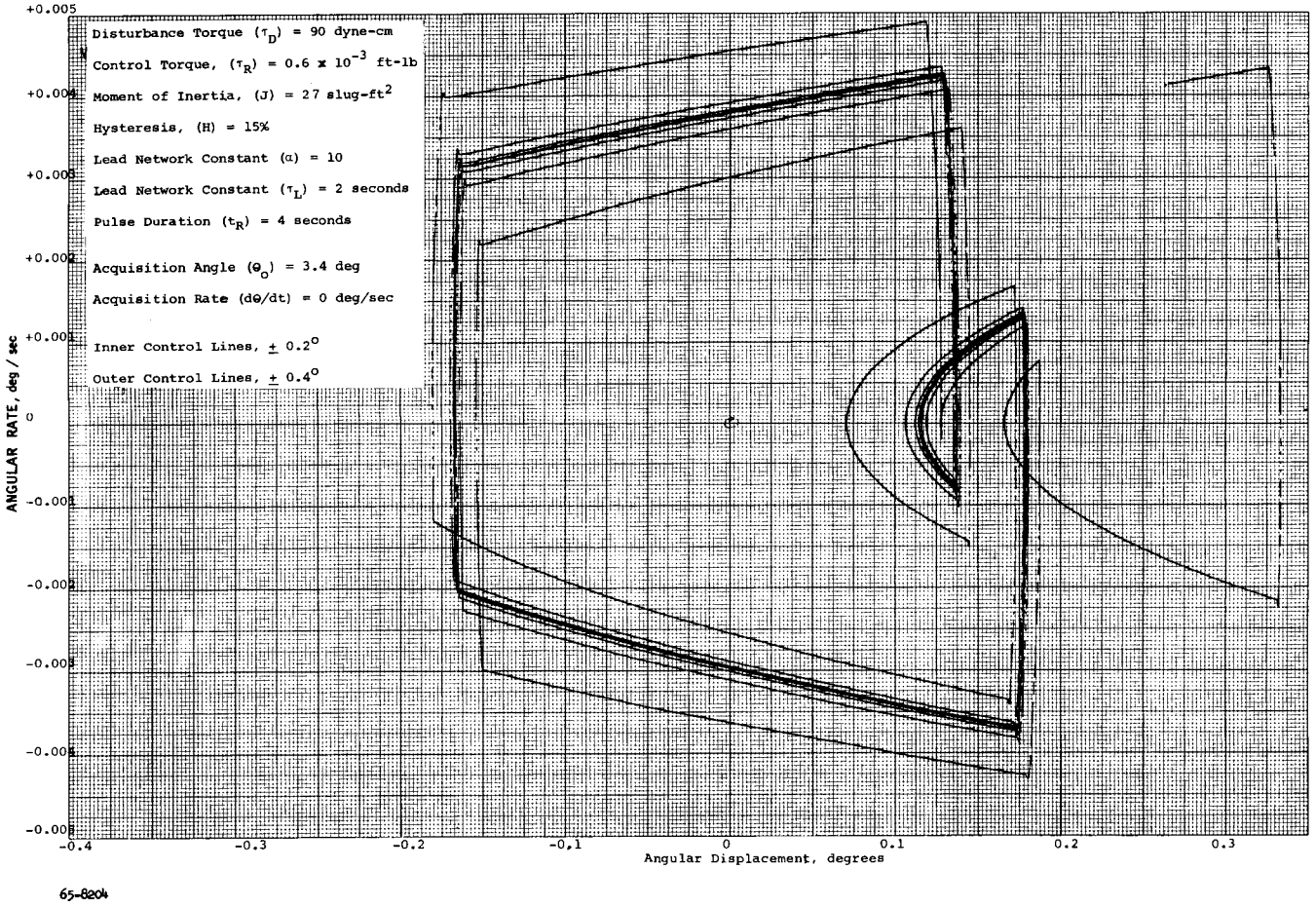

Figure B.7 LIMIT CYCLE FOR DISTURBANCE TORQUE OF 90 DYNE-CM

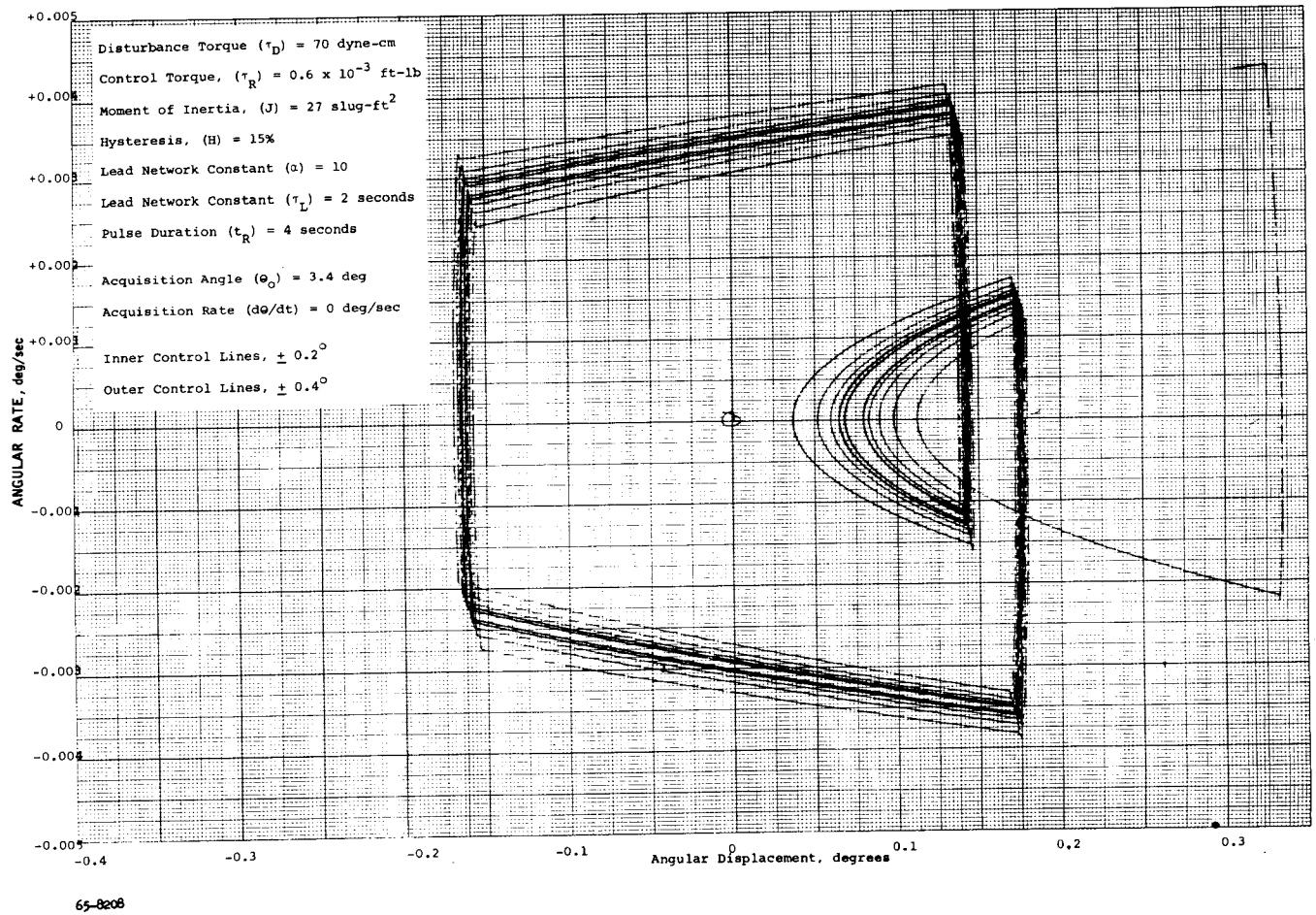

Figure B.8 LIMIT CYCLE FOR DISTURBANCE TORQUE OF 70 DYNE-CM

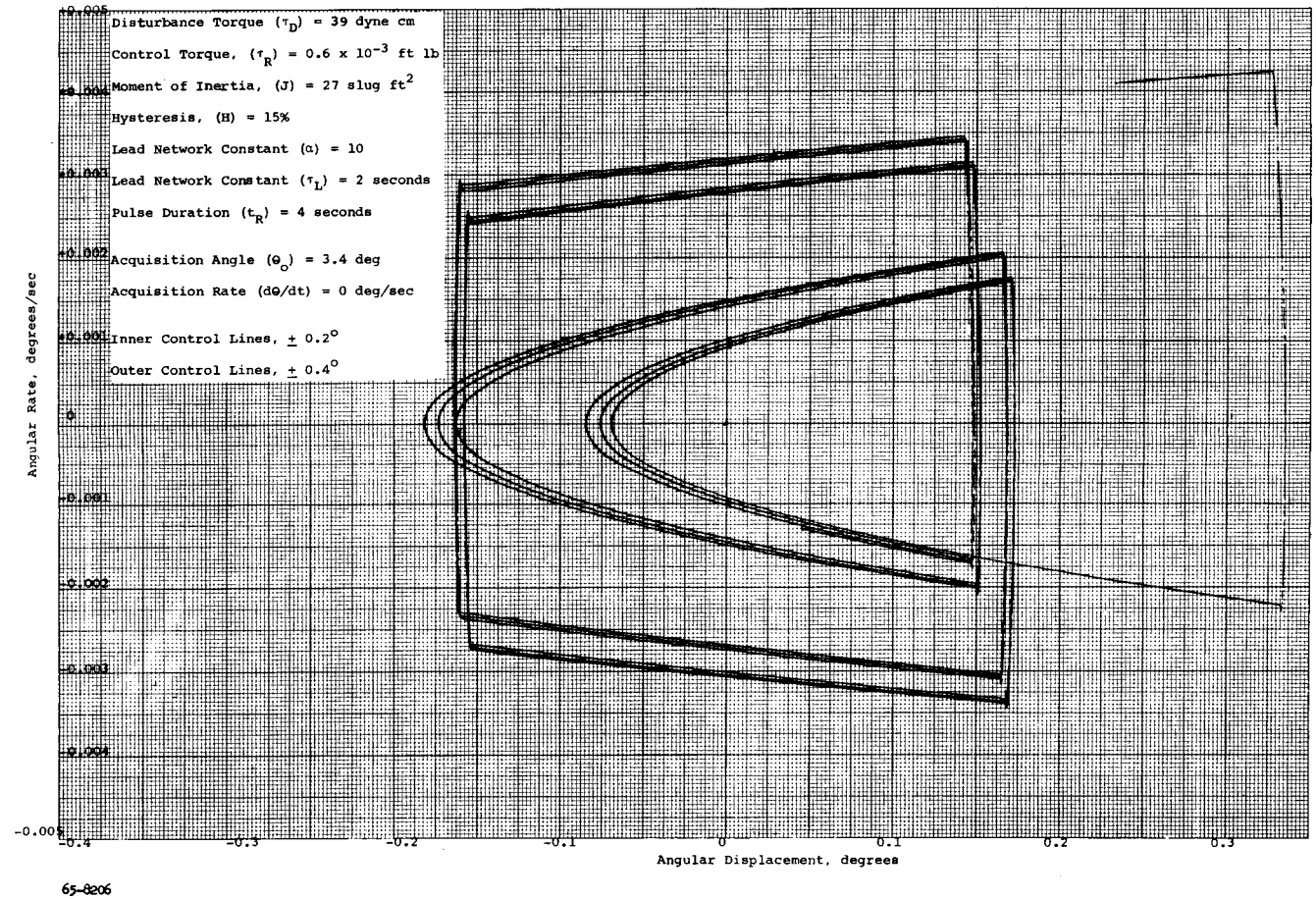

Figure B.9 LIMIT CYCLE FOR DISTURBANCE TORQUE OF 39 DYNE-CM

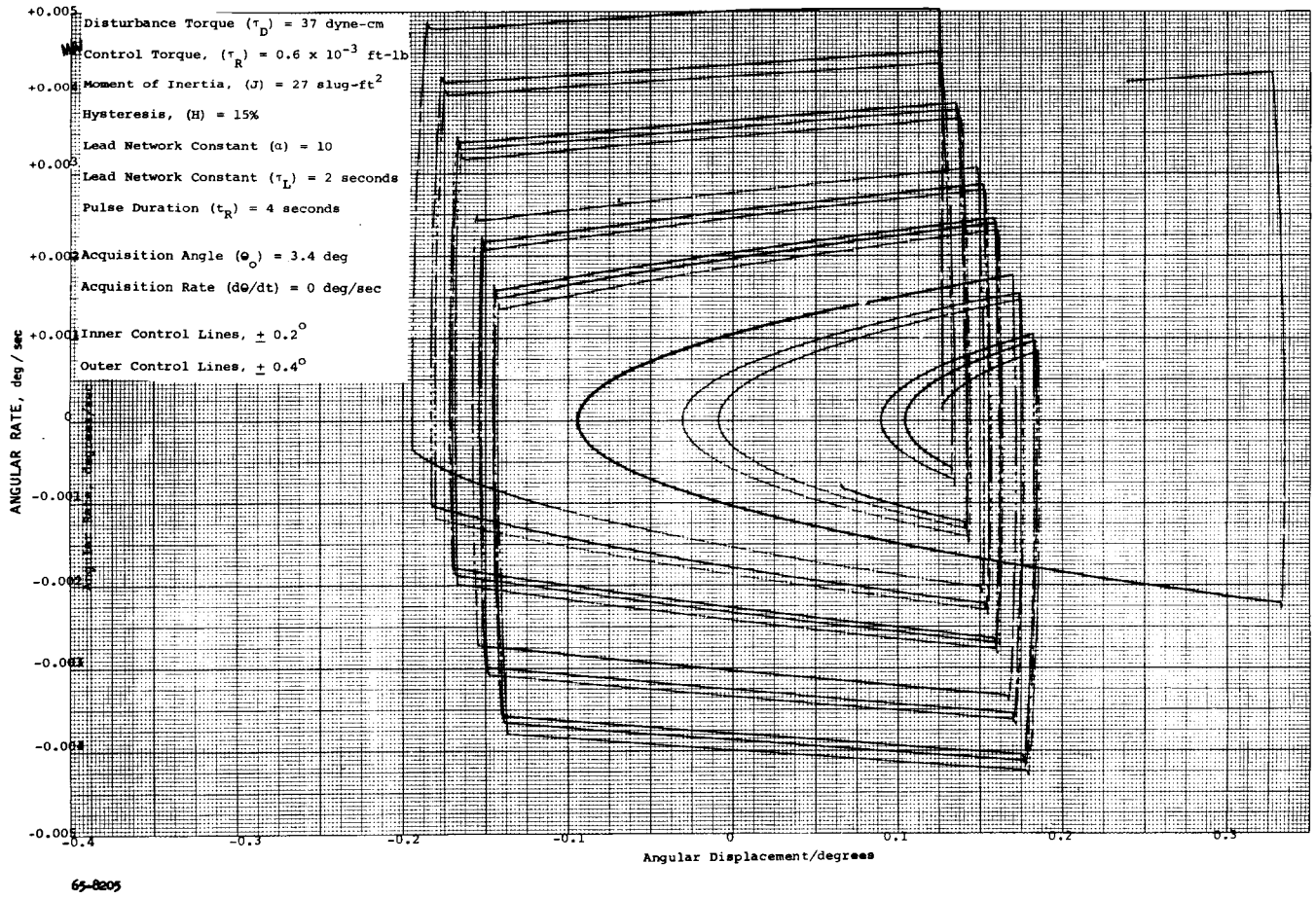

Figure B.10 LIMIT CYCLE FOR DISTURBANCE TORQUE OF 37 DYNE-CM

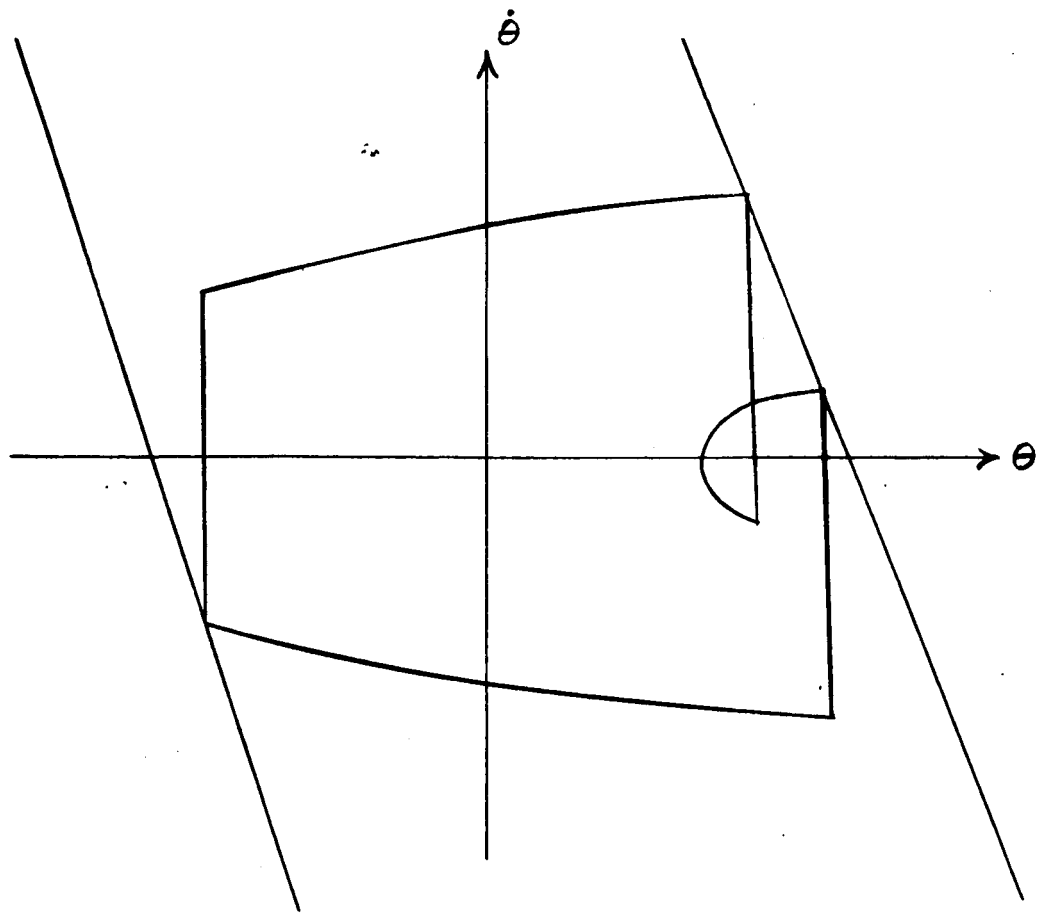

Figure B.11 SKETCH OF NULLED LIMIT CYCLE

For lower disturbance torques, very complex cycles are obtained. In figure B.2, for example, a plot is presented of a complete repeating cycle for a disturbance torque of 10 dyne-cm. The complete repeating cycle consists of two soft-limit branches and 16 hard-limit branches.

The limit cycle for zero disturbance torque always consists of one repeating hard-limit cycle as would be expected and as illustrated in figure B.12.

Comparison of figures B.4 and B.5 illustrates the effect of acquisition angle on the disturbance torque at which control changes from soft limit-cycle control to hard-limit control. In both plots, the regions of definite hard limit and definite soft limit-control are presented. It is seen that at an acquisition angle of 2.25 degrees, soft-limit cycle is maintained down to 63 ± 3 dyne-cm, while for an acquisition angle of 3.40 degrees, the limit cycle changes from soft to hard at a disturbance torque of 100 ± 10 dyne-cm. The maximum duty cycle is 0.0374 for θ_o = 3.4 degrees, whereas it is only. 0.0294 for θ_o = 2.25 degrees.

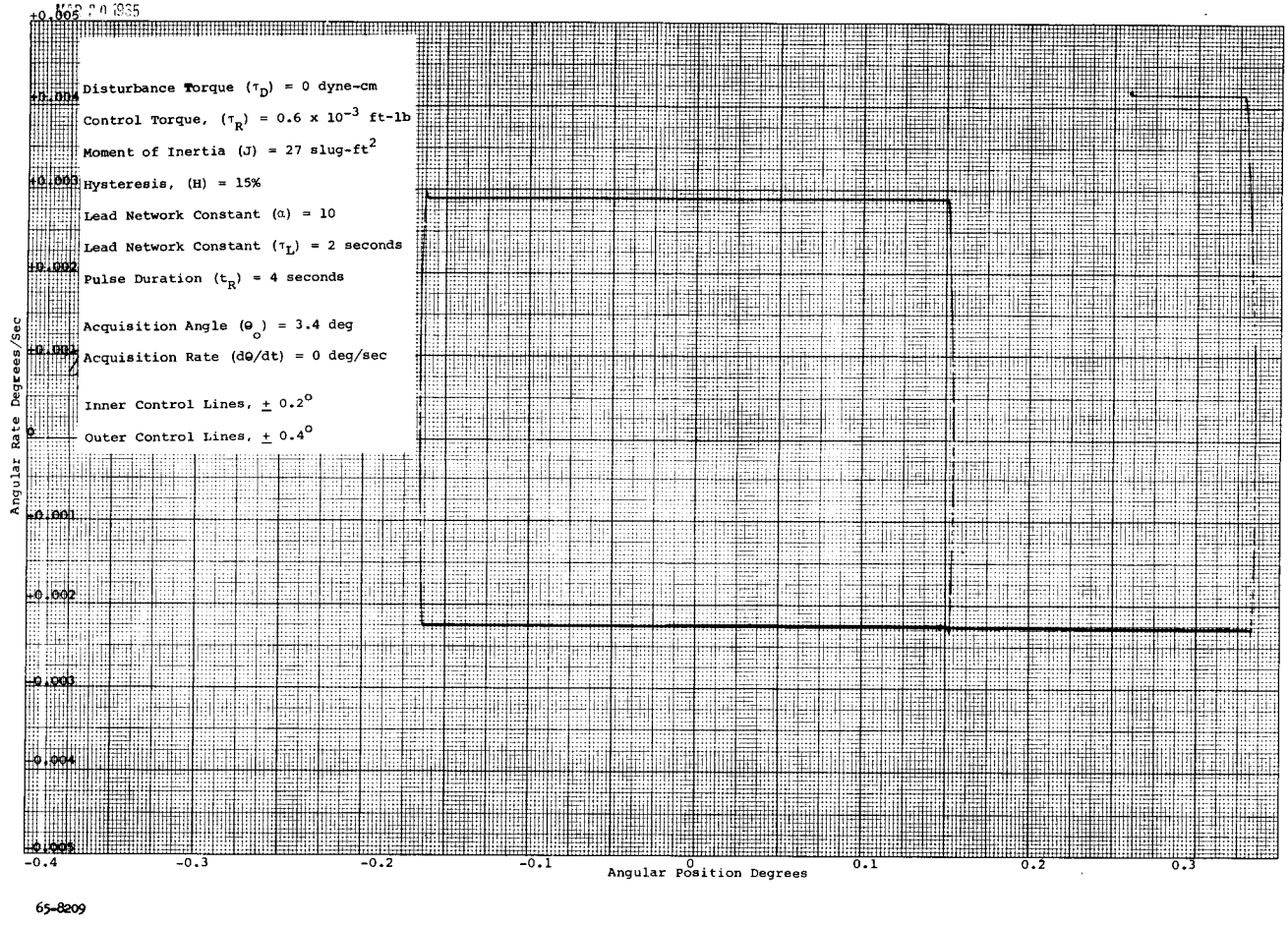

Figure B.12 LIMIT CYCLE FOR DISTURBANCE TORQUE OF ZERO DYNE-CM

APPENDIX C

PERFORMANCE OF THE SINGLE AXIS RESISTOJET ATTITUDE CONTROL SYSTEM ON THE IMPULSE BALANCE

The impulse balance is attractive for checkout of single-axis ACS because of the possibility of systematically varying the acquisition angle, $\theta_{initial}$, acquisition rate, $\dot{\theta}_{initial}$, and disturbance torque, τ_D . In the present test setup, data are transmitted from the table by lightweight wires; the number of wires and thus the amount of data which can be transmitted must be held to a minimum because of the possibility of introducing disturbance torques into the system. For the initial tests only the clockwise and counterclockwise valve signals, and the angular position and total angular error signals have been transmitted.

Figure C. 1 illustrates a hard-limit cycle, obtained on the impulse table for a negligible disturbance torque ($\tau_D \cong 0$ dyne-cm), and a control thrust of about 124×10^{-6} pound.

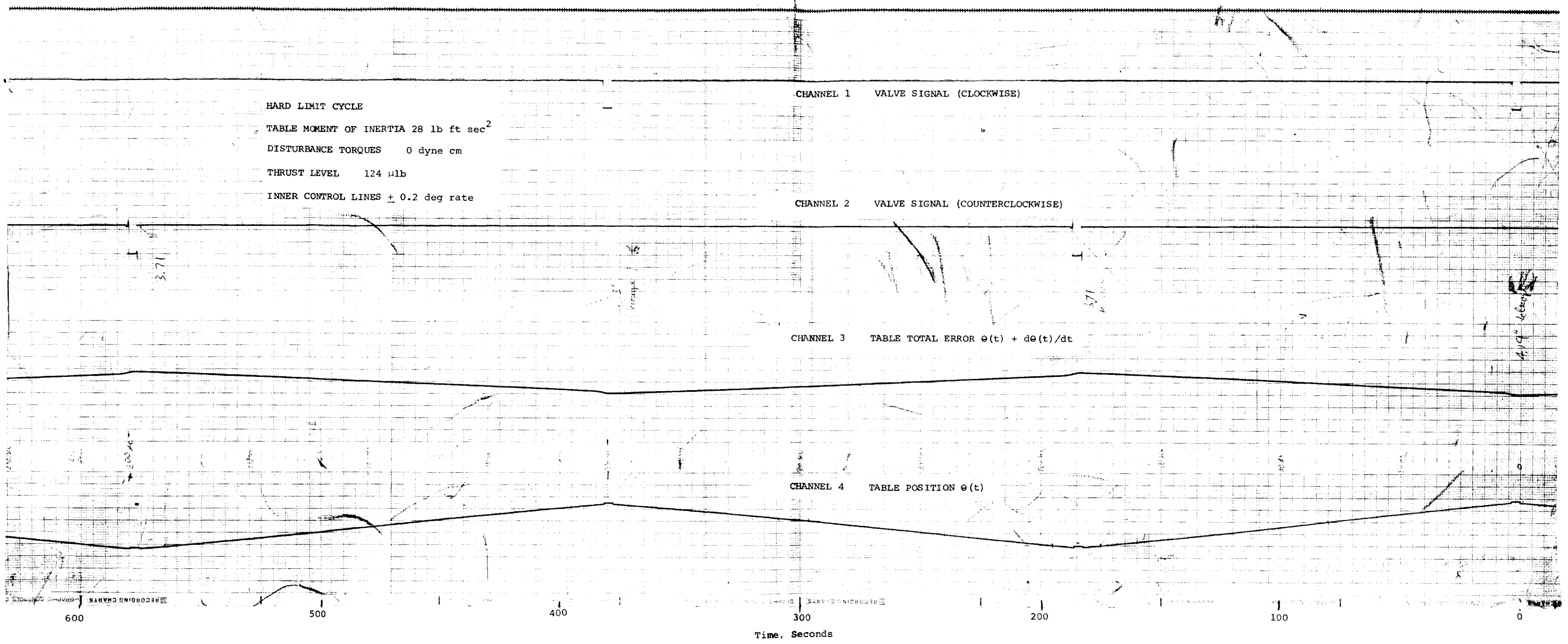

Figure C.1 RECORD OF SINGLE-AXIS RESISTOJET ACS TEST ON IMPULSE BALANCE

APPENDIX D

ADAPTIVE ATTITUDE CONTROL SYSTEM

1. INTRODUCTION AND BACKGROUND

The disturbance torque which a satellite will encounter cannot be predicted with any precision at the present time. Thus, the attitude control system must be designed to handle a range of disturbance torques extending from zero up to some estimated maximum possible disturbance torque which represents with a high degree of confidence the maximum disturbance torque the system could possibly receive. The objective of an ACS design evaluation is to arrive at the system which provides attitude control over the entire mission duration with a minimum total system mass and maximum reliability. As will be discussed below, this objective requires an adaptive control system, that is, one which automatically changes certain system parameters to provide satisfactory limit cycle operation of the system regardless of what the actual disturbance torque may be.

The adaptive control system should thus be designed to insure that (1) the propellant mass is sufficient for the entire mission for whatevever disturbance torque is encountered between zero and the estimated maximum possible value, and (2) the pulsing frequency of the system is minimized.

The need for an adaptive control system is further illustrated by figure D. 1 where a typical plot of duty cycle versus disturbance torque is sketched. With the control torque fixed, the fixed pulse duration for control on the inner lines would be set at a value to give soft limit cycle operation with a minimum pulsing rate with the maximum possible disturbance torque. Analog computer simulation of the control system would then be used to generate the curve of figure D. 1. The design point as illustrated is for soft limit cycle operation with the maximum possible disturbance torque. The duty cycle on which the propellant consumption rate, and hence propellant mass required for the entire mission, is based is $(D_{SL})_{max}$. At some disturbance torque lower than the maximum possible value, the limit cycle with $(t_R)_{max}$ will jump into hard limit cycle operation with a corresponding large increase in the duty cycle. As illustrated, the duty cycle with no change in thrust characteristics exceeds $(D_{SL})_{max}$ over a large range of disturbance torques, and if no adaptive control action were taken, that is, both the control torque and the pulse duration remained fixed, the propellant mass in the design would have to be based on $(D_{HL})_{max}$ rather than on $(D_{SL})_{max}$. The ratio of $(D_{HL})_{max}$ to $(D_{SL})_{max}$ (or of the propellant masses) might be as much as a factor of 2 to 3 based on analog computer simulation of the control system (see figures B. 4 and B. 5 of appendix B).

Adaptive control action for $\tau_D < (\tau_D)_{max}$ can be applied by reducing either or both the control torque and the pulse duration. The discussion below is based

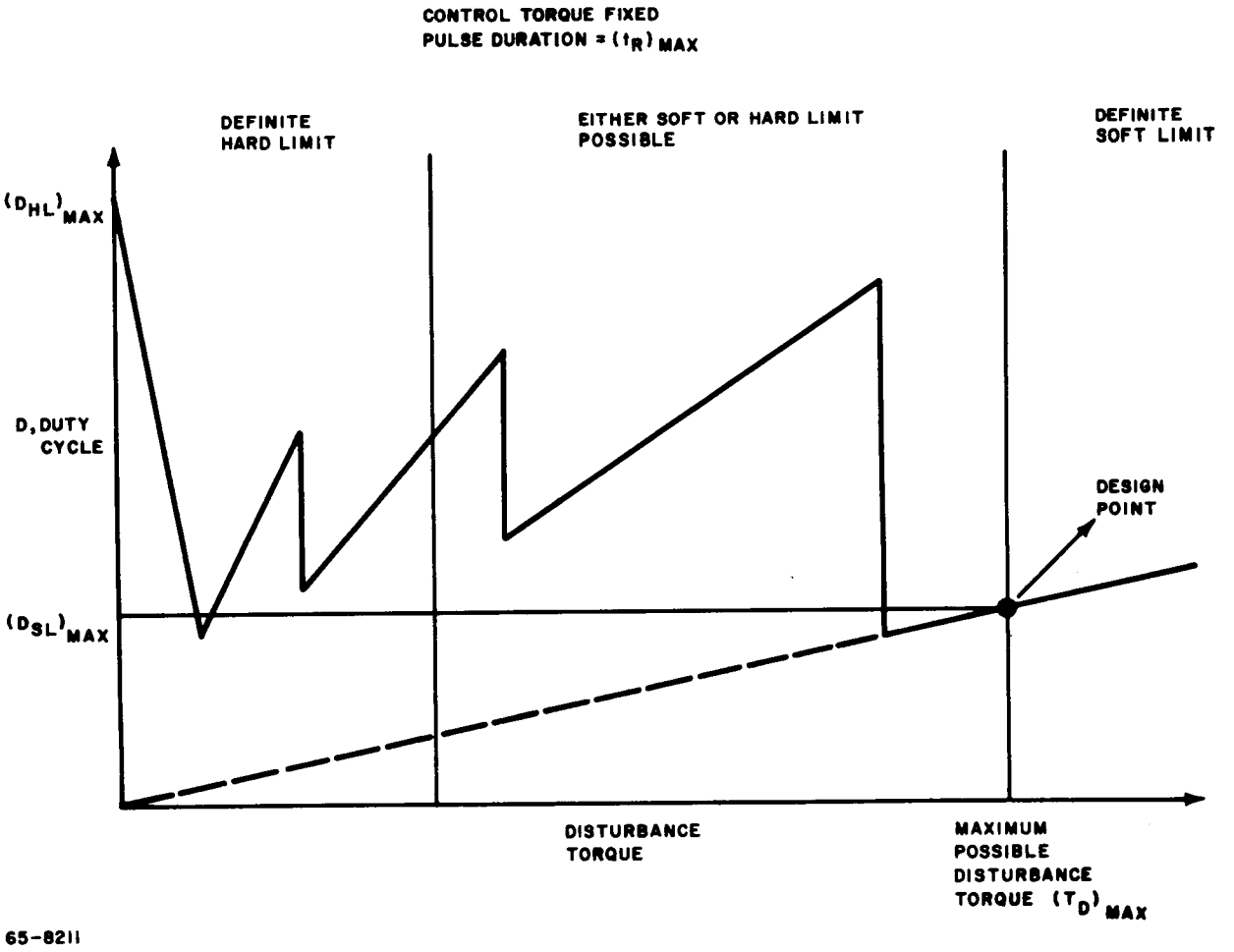

Figure D.1 DUTY CYCLE VERSUS DISTURBANCE TORQUE FOR MAXIMUM PULSE DURATION

on reduction of the pulse duration as the adaptive control mechanism with a fixed control torque. In figure D. 2, the variation of duty cycle with disturbance torque is illustrated for three pulse durations with the control torque fixed. The curve for $(t_R)_{max}$ is the same as that sketched in figure D. 1. If a disturbance torque of $(\tau_D)_2$ were encountered and no change made in t_R, a duty cycle of $(D_{HL})_2 > (D_{SL})_{max}$ would occur which is unacceptable. If the pulse duration were automatically decreased to some value $(t_R)_v$, soft limit cycle operation would occur with a disturbance torque of $(\tau_D)_2$ and a duty cycle $(D_{SL})_2 < (D_{SL})_{max}$ would occur which is acceptable. With a pulse duration of $(t_R)_v$, however, a lower disturbance torque than $(\tau_D)_2$ could still result in hard limit cycle operation with a duty cycle greater than $(D_{SL})_{max}$. At some pulse duration $(t_R)_{min}$, however, the duty cycle for the fixed control torque will not be greater than $(D_{SL})_{max}$ for all disturbance torques. Thus, this pulse duration represents the minimum pulse duration required to insure that a propellant mass based on $(D_{SL})_{max}$ is sufficient for the entire mission. Thus, a possible adaptive control system is one which varies stepwise the pulse duraction, $(t_R)_v$, between two limits, $(t_R)_{max}$ and $(t_R)_{min}$. Depending on the particular system, it might be desirable to decrease t_R below $(t_R)_{min}$ to minimize the pulsing frequency for low disturbance torques.

The question might be asked as to why the pulse duration was not preset at a constant value of $(t_R)_{min}$ since this insures that the propellant mass based on $(D_{SL})_{max}$ is sufficient for the entire mission. Another consideration of importance from a reliability point of view, however, is the pulsing frequency of the resistojets which should be minimized for maximum reliability. Thus, if the pulse duration were set at $(t_R)_{min}$ and the actual disturbance torque were $(\tau_D)_{max}$, the limit cycle would follow a path in the phase plane like that illustrated in figure D. 3A and the pulsing frequency would be very high.

If the pulse duration were $(t_R)_{max}$, however, the path followed would be like that illustrated in figure D. 3B and the pulsing frequency would be minimized. The pulsing frequency for soft limit cycle operation is given by:

$$f = \frac{\tau_D}{t_R \tau_R} \qquad (D.1)$$

and thus, for a fixed τ_D and τ_R, f varies inversely with t_R so long as soft limit cycle operation is maintained. In addition to this factor, a pulse duration $(t_R)_{min}$ might not be sufficient to hold the limit cycle control on the inner lines with a disturbance torque $(\tau_D)_{max}$ and the control would jump to the outer back-up lines.

In summary, an adaptive control system is required if it is desired to minimize the propellant mass required for a given mission and, at the same time, minimize the pulsing frequency of the system for any disturbance torque between zero and an estimated maximum possible disturbance torque.

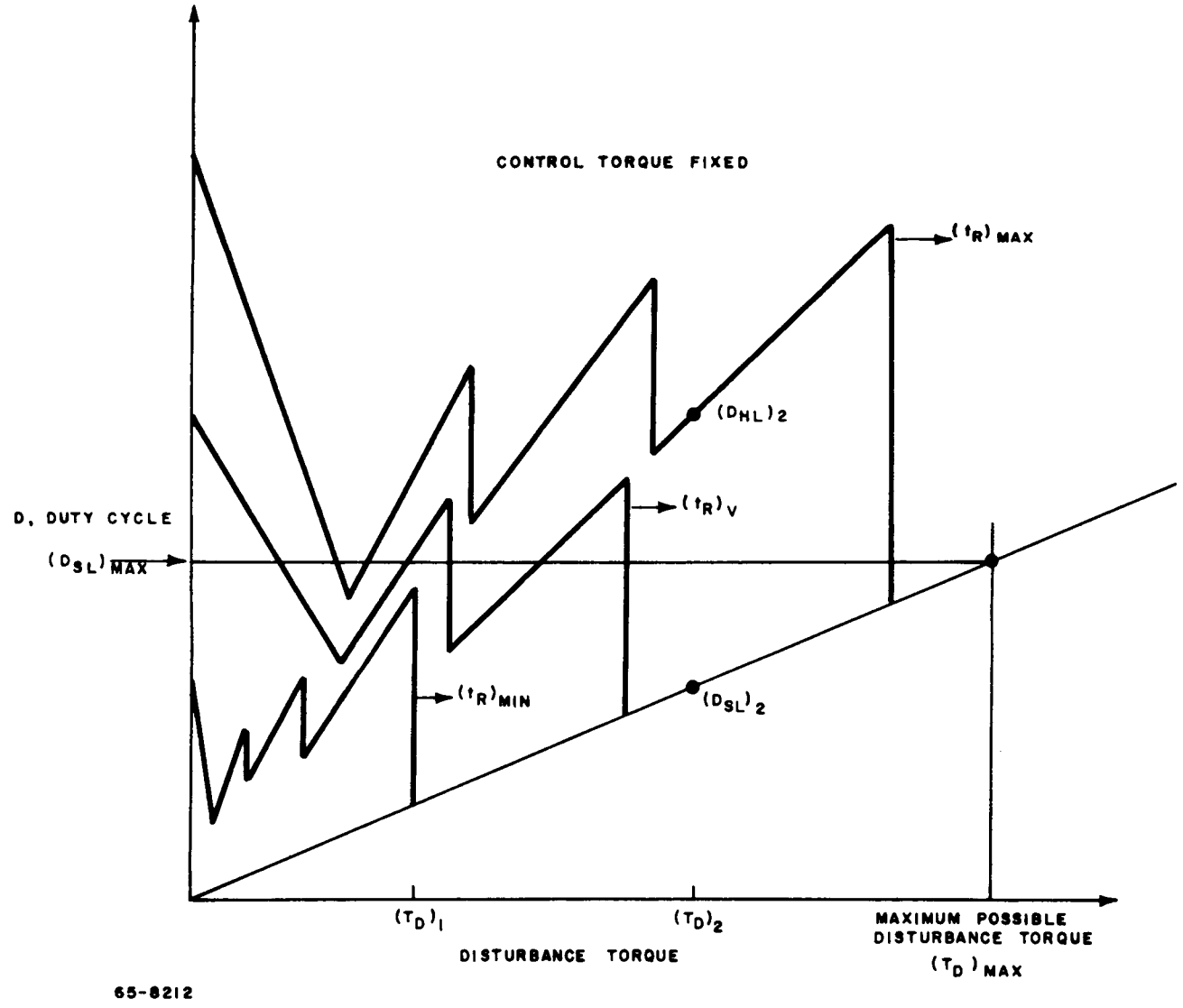

Figure D.2 SKETCH ILLUSTRATING MINIMUM PULSE DURATION

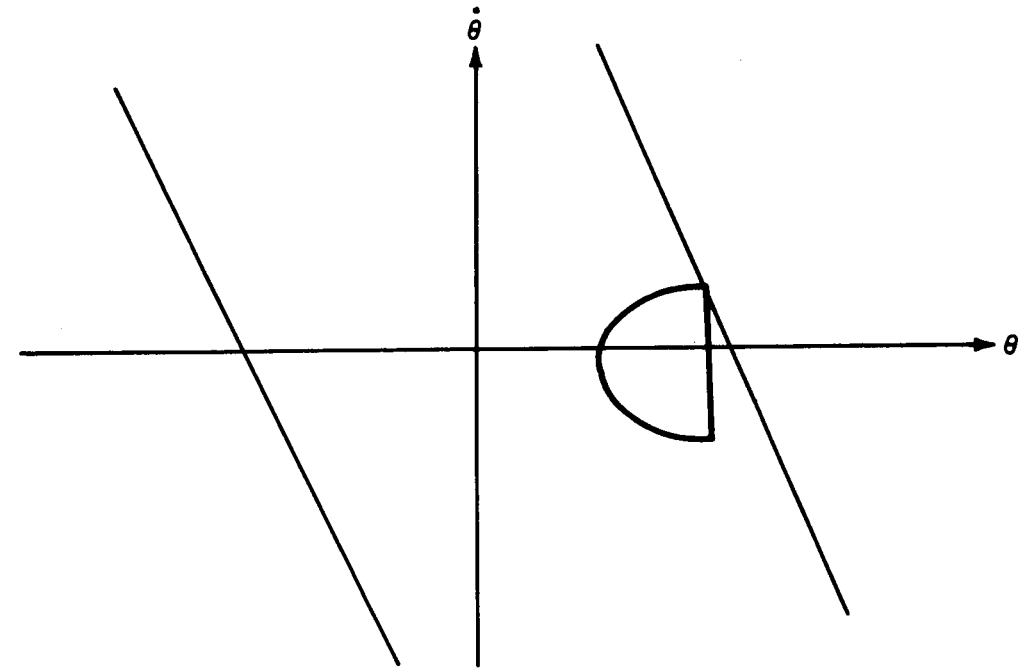

A PULSE DURATION = $(t_R)_{MIN}$
DISTURBANCE TORQUE = $(T_D)_{MAX}$

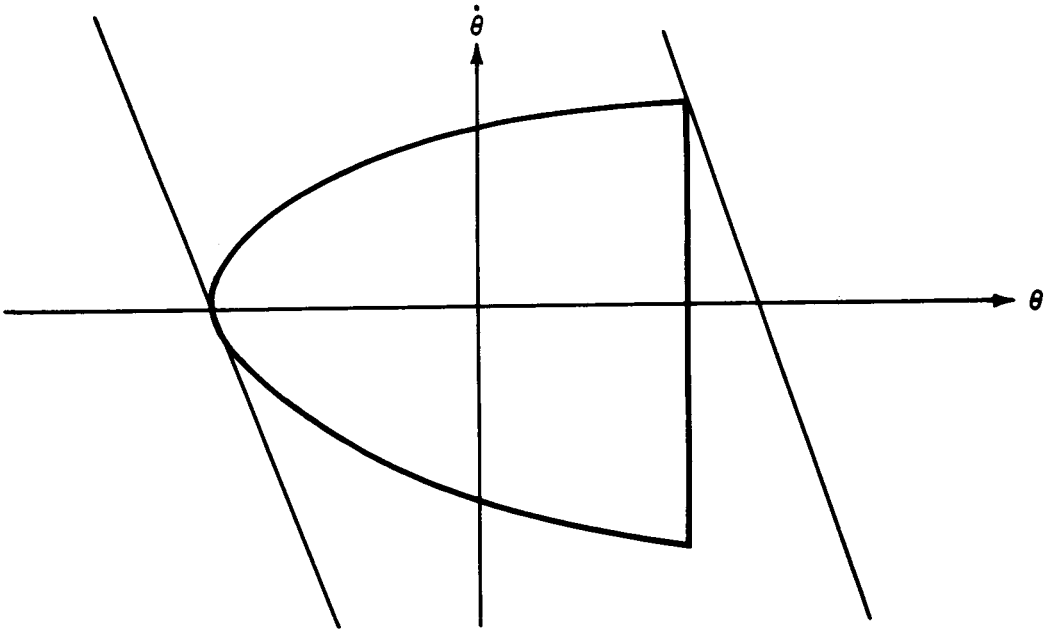

B PULSE DURATION = $(t_R)_{MAX}$
DISTURBANCE TORQUE = $(T_D)_{MAX}$

65-8213

Figure D.3 PHASE PLANE PATH FOLLOWED BY SYSTEM WITH DISTURBANCE TORQUE $(\tau_D)_{MAX}$ AND PULSE DURATIONS OF $(t_R)_{MIN}$ AND $(t_R)_{MAX}$

2. PROPOSED ADAPTIVE CONTROL SYSTEM

As discussed above, an adaptive control system is required to insure sufficient propellant mass to fulfill the entire mission and at the same time to minimize the pulsing frequency of the system. The following discussion describes conceptually an adaptive control system for this purpose which would involve some simple additions to the present control logic system as used in the Single Axis Tests. The proposed method involves the stepwise variation of the pulse duration on the inner control lines in response to the mode of resistojet pulsing; the mode of resistojet pulsing in turn depends directly on the disturbance torque for a given set of thrustor characteristics. If preferable, the control action could be variation of the control torque by variation of the plenum pressure or a combination of variation of both the plenum pressure (control torque) and the pulse duration. The pulse duration should be easier to vary however and can be instantaneously changed whereas a decrease in the plenum pressure can be made only gradually as the pressure is reduced by pulsing of the resistojets.

It is assumed that the control torque and maximum pulse duration have been established based on the estimated maximum possible disturbance torque, $(\tau_D)_{max}$. Analog computer calculations have also established a $(t_R)_{min}$ which insures sufficient propellant mass for any disturbance torque between zero and $(\tau_D)_{max}$.

The system during acquisition will have the fixed pulse duration for the inner lines set at the maximum value, $(t_R)_{max}$. This will insure control within the desired error limits, though with a hard limit cycle except for disturbance torques very near $(\tau_D)_{max}$. In the hard limit cycle, the opposing clockwise and counterclockwise resistojets will be pulsed each cycle, an unacceptable condition with a pulse duration of $(t_R)_{max}$. When this occurs, the pulse-on-duration of both resistojets will automatically be decreased by a predetermined amount. A possible circuit to perform this function might conceptually be as illustrated in figure D. 4. If hard limit cycle operation occurs, both the CW and CCW resistojets will be pulsed. The two memory circuits would then simultaneously pass signals to the "and" circuit which requires both inputs before passing a signal. A signal would then pass to the pulse duration control which would automatically decrease the pulse duration by one step. The memories would simultaneously be erased. If a hard limit cycle still occurred, the above process would be repeated and the pulse duration decreased until either soft limit-cycle operation occurred or the minimum pulse duration, $(t_R)_{min}$ was reached. While $(t_R)_{min}$ would be set at a value low enough to guarantee that the propellant mass was sufficient for the entire mission, it might or might not be desirable to set $(t_R)_{min}$ below this value to minimize the pulsing frequency if very low disturbance torques were encountered. Analog computer calculations would be used to determine a satisfactory value of $(t_R)_{min}$. The minimum possible value of $(t_R)_{min}$ is set by the time for thrust buildup and decay which is about 50 milliseconds for the present system.

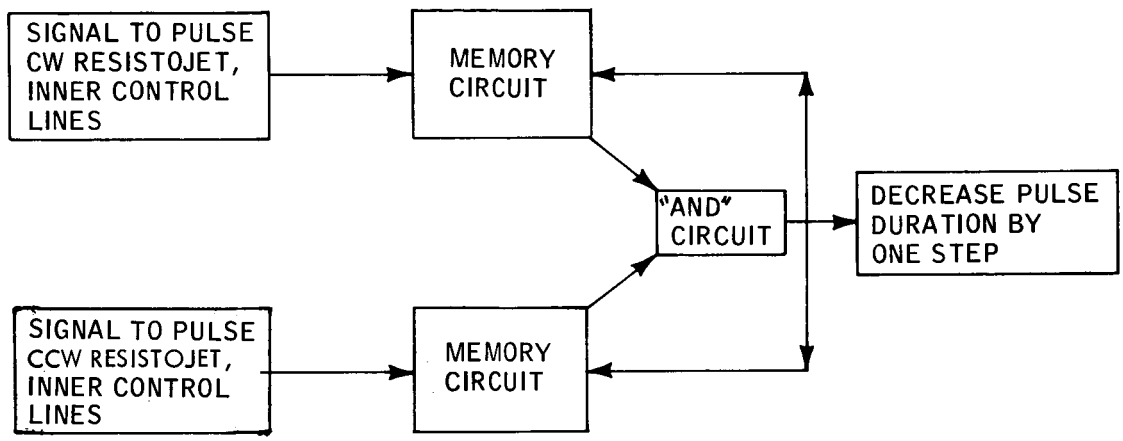

65-8214

Figure D.4 BLOCK DIAGRAM OF CIRCUIT TO AUTOMATICALLY DECREASE PULSE DURATION BY ONE STEP WHEN HARD LIMIT-CYCLE OPERATION OCCURS

Suppose now that the system has automatically adjusted t_R either to $(t_R)_{min}$ or to a value where soft limit-cycle operation occurs and an increase in the disturbance torque occurs. This increase in disturbance torque, if no corrective action occurs and the system is in soft limit-cycle operation, produces a decrease in the cycle time resulting in more frequent pulsing. If the disturbance torque becomes sufficiently large, the control may jump out of the inner control lines and transfer to the outer backup lines unless the pulse duration is increased. To handle the situation of a large step increase in the disturbance torque, with transfer of control to the backup lines, the pulse duration produced by the backup lines must always be sufficiently large to handle the estimated maximum possible disturbance torque. Thus, the minimum on-time for a pulse controlled by the backup lines should be set at $(t_R)_{max}$ by selection of the proper value of the lead network delay constant, τ_L. This should insure that control will jump back to the inner control lines even if an unusally large step increase in τ_D occurs so long as τ_D is not larger than $(\tau_D)_{max}$. If the system does jump out of the inner control lines, large disturbance torques will have encountered and t_R on the inner lines should be reset to $(t_R)_{max}$ as illustrated in figure D.5.

If the disturbance torque increases slowly or levels off at some higher value, control will not jump out of the inner lines. It will be desirable to increase the pulse duration of the inner lines to minimize the pulsing frequency without leaving soft limit cycle operation. For example, consider the sketch, of figure D.6. The limit cycle as sketched with the solid lines would have a very low cycle time and high pulsing rate. The cycle time is given by either:

$$t_t^2 = 8(\theta_c - \theta_o)\left(\frac{\tau_R}{\tau_R - \tau_D}\right)^2 \frac{J}{\tau_D} \qquad (D.2)$$

or:

$$t_t = t_R \frac{\tau_R}{\tau_D} \qquad (D.3)$$

It is desirable to increase the pulsing time to give a limit cycle such as that illustrated by the dotted line. As an arbitrary criterion of satisfactory versus unsatisfactory limit cycle behavior, satisfactory operation is defined as a limit cycle in which θ_o (θ at $\dot{\theta} = 0$) is less than or equal to zero, that is, the limit cycle represented by the dotted line. If $\theta_o \geq 0$ as for the solid line, it is desirable to increase the pulse duration to reduce the pulsing frequency.

The circuit illustrated by the block diagram of figure D.7 will accomplish this objective. Referring to the CW resistojet, a quantity $\Delta = \theta_o - \theta$ is calculated continuously. This output goes to a switching network which passes a signal only if $\Delta \geq \theta_c$. The output from the switching network erases a memory circuit as shown. The memory is activated by a signal to pulse the CW resistojet. The signal from the memory passes through a fixed time delay to an "and" circuit. The signal for pulsing the resistojet also passes to this "and" circuit.

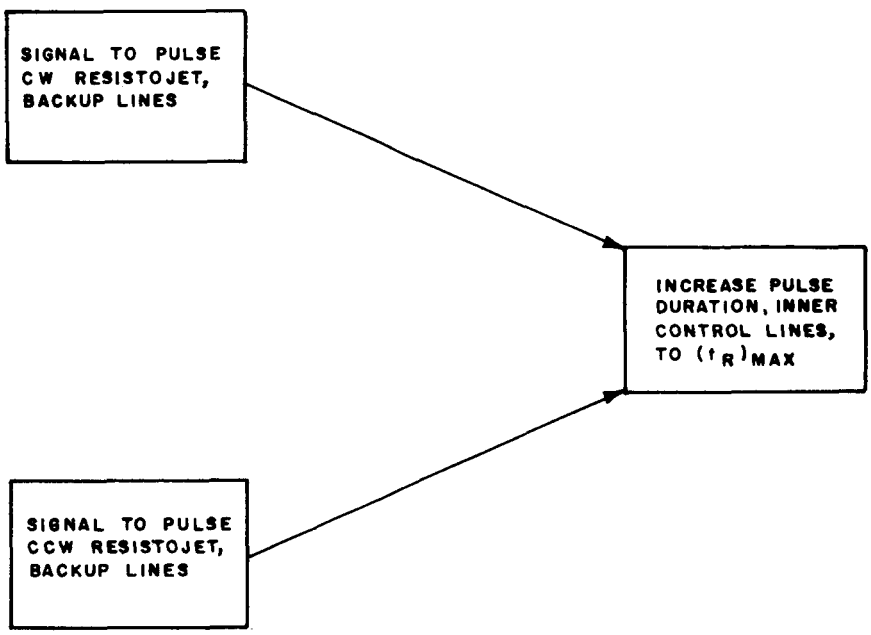

Figure D.5 INCREASE IN FIXED PULSE DURATION TO $(t_R)_{MAX}$ IF CONTROL JUMPS TO BACKUP LINES

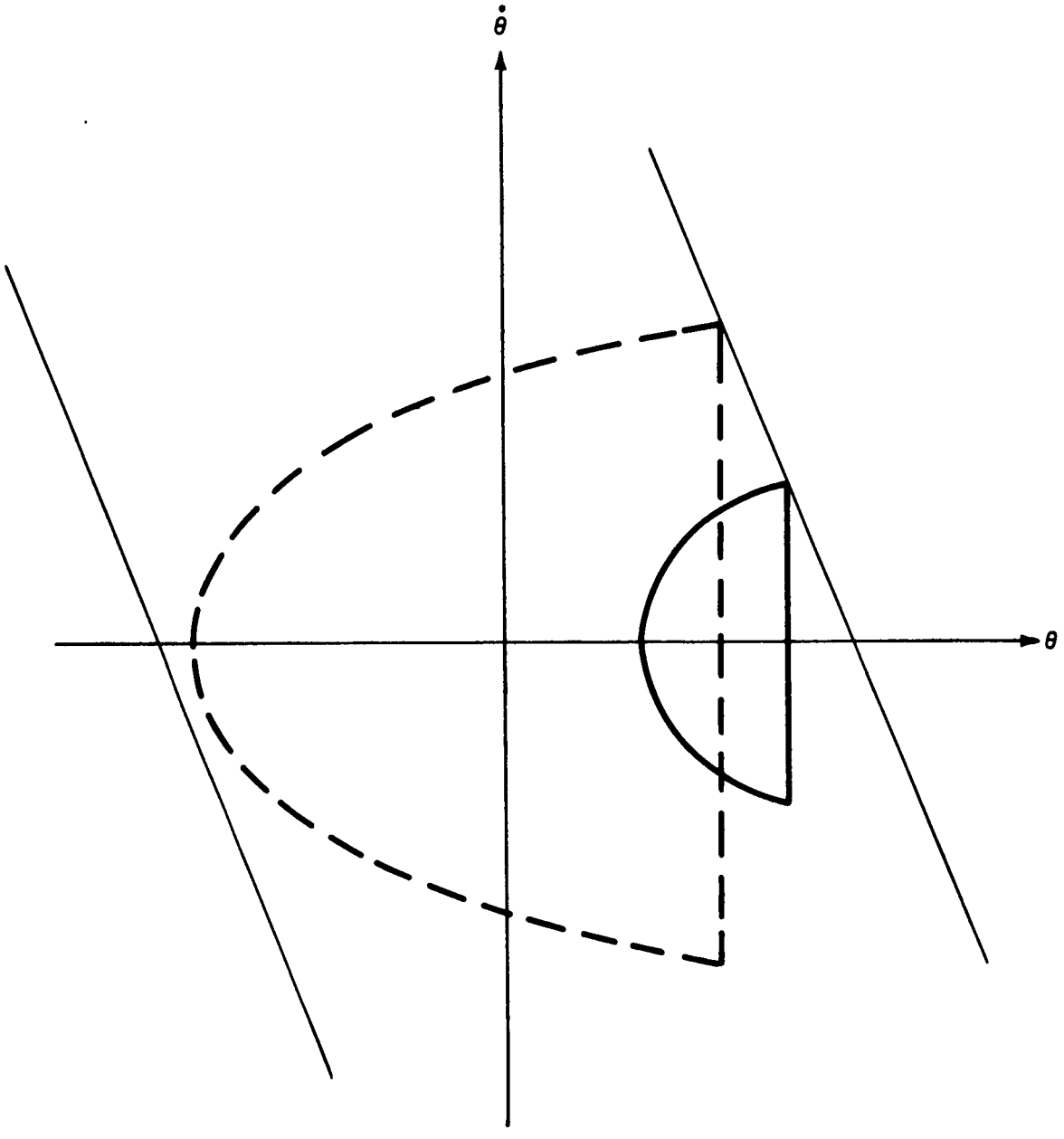

65-8216

Figure D.6 SKETCH ILLUSTRATING SOFT LIMIT-CYCLE OPERATION WITH LOW- AND HIGH-PULSING RATES

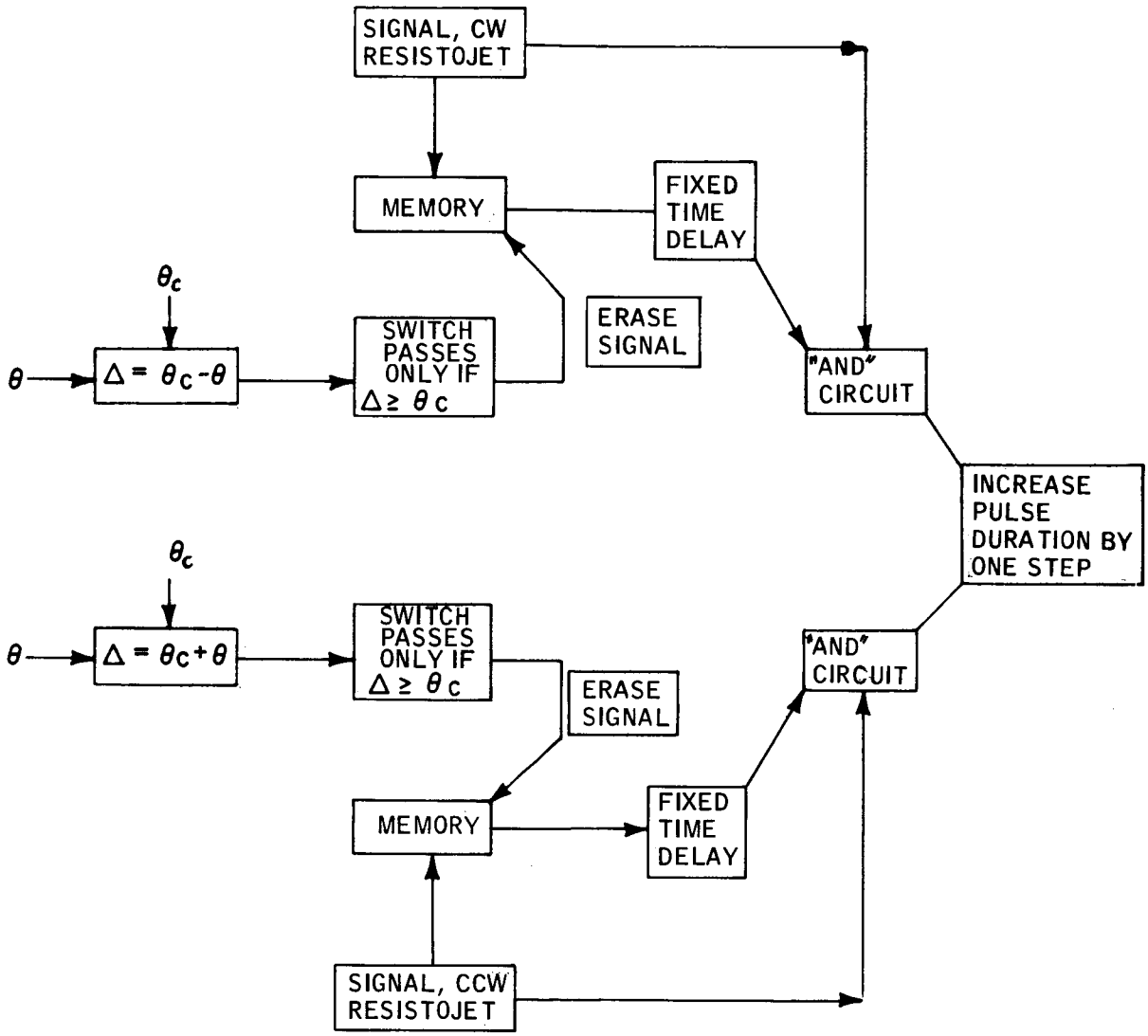

Figure D.7 LOGIC FOR INCREASING PULSE DURATION IN SOFT LIMIT-CYCLE OPERATION TO REDUCE PULSING RATE

If both signals are received simultaneously by this circuit, the pulse duration is increased by one step. Suppose now, the memory is vacant and the CW resistojet pulses ($\theta = \theta_c$, $\Delta = 0$). The memory is activated. After the preset time delay, the "and" circuit is activated by the signal from the memory. The disturbance torque decreases θ thereby increasing Δ. If Δ does not exceed θ_c during the cycle, the memory stays activated and the next signal to pulse the CW resistojet increases the pulse duration by one step. If Δ does exceed θ_c, the memory is erased, the succeeding signal to pulse the CW resistojet cannot pass the "and" circuit, and the pulse duration remains constant. The CCW resistojet operates as above except $\Delta = \theta_c + \theta$.

The stepwise increase in pulse duration cannot be too large; otherwise, the system will be thrown into hard limit cycle operation. It can be shown that θ_c is given by the following relation:

$$\theta_c - \theta_o = \frac{1}{8} \frac{(\tau_R - \tau_D)^2}{J \tau_D} t_R^2 \qquad \text{(D. 4)}$$

Let

t_{R1} = pulse duration when $\theta_o = 0$

t_{R2} = pulse duration when $\theta_o = -\theta_c$

Then;

$$\frac{\theta_c}{2\theta_c} = \frac{(t_{R1})^2}{(t_{R2})^2} \qquad \text{(D. 5)}$$

or:

$$\frac{t_{R2}}{t_{R1}} = \sqrt{2} \qquad \text{(D. 6)}$$

This represents the maximum ratio by which the pulse duration should be increased with the criterion used above for increasing the pulse duration when $\Delta \geq \theta_c$.

3. SELECTION OF THE CONTROL TORQUE LEVEL

As discussed previously, the attitude control system design should be based on the estimated maximum possible disturbance torque which the satellite could ever encounter. A necessary condition on the control torque is therefore:

$$\tau_R > (\tau_D)_{max} \qquad \text{(D. 7)}$$

A system with a control torque just slightly greater than the disturbance torque would not function in a satisfactory fashion however. Consider the sketch of figure D. 8. The system drifts with a given disturbance torque, τ_D, across the control line to point (a) as shown. At point (a) the resistojet is either pulsed on for a preset time duration producing an impulse bit (inner control lines for the Model I and II systems) or pulsed on continuously until the system is driven back across the control line (backup lines for the Model I and II systems). In either case, the path followed in the phase plane plot during the time of thrust application is strongly dependent on the difference between the control torque, τ_R, and the disturbance torque, τ_D ; the angular acceleration is given by:

$$\frac{d^2\theta}{dt^2} = -\frac{\tau_R - \tau_D}{J} \qquad \text{(D. 8)}$$

Referring to the figure D. 8 now, if $\tau_R = \tau_D$, the system will follow the path (a) to (b) and the angular error will continue to increase at a constant rate of rotation. If τ_R is only slightly greater than τ_D, the rate of rotation will decrease only slightly with time, and, for continuous thrust, the system will follow the path (a) to (c). Since the control line should be set so that $\pm \theta_{co}$ is only slightly less than the allowable angular error, the allowable error will obviously be exceeded when the control torque is only slightly greater than the disturbance torque. The control torque should thus be set at some level considerably in excess of the maximum expected disturbance torque.

As the control torque is further increased relative to the disturbance torque, a value is reached where the slope in the phase plane initially after thrust start-up is equal to the slope of the control line and the path (a) to (d) is followed. For very large control torques, the path followed will essentially be an almost vertical line on the phase plane plot as represented by the path (a) to (e).

It is suggested that a reasonable criterion for the minimum control torque is given by the condition that the slope in the phase plane of the path followed by the system immediately after thrust is turned on must be equal to the slope of the control line. A relation for the minimum control torque based on this criterion will now be derived. Integrating equation (D. 8) with $\dot{\theta} = d\theta/dt$ and $\theta = \dot{\theta}_1$ at $t = 0$ gives:

$$\dot{\theta} - \dot{\theta}_1 = -\frac{\tau_R - \tau_D}{J}\, t \qquad \text{(D. 9)}$$

Now,

$$\frac{d\dot{\theta}}{d\theta} = \frac{d\dot{\theta}}{dt} \cdot \frac{dt}{d\theta} = \frac{1}{\dot{\theta}} \frac{d\dot{\theta}}{dt} \qquad \text{(D. 10)}$$

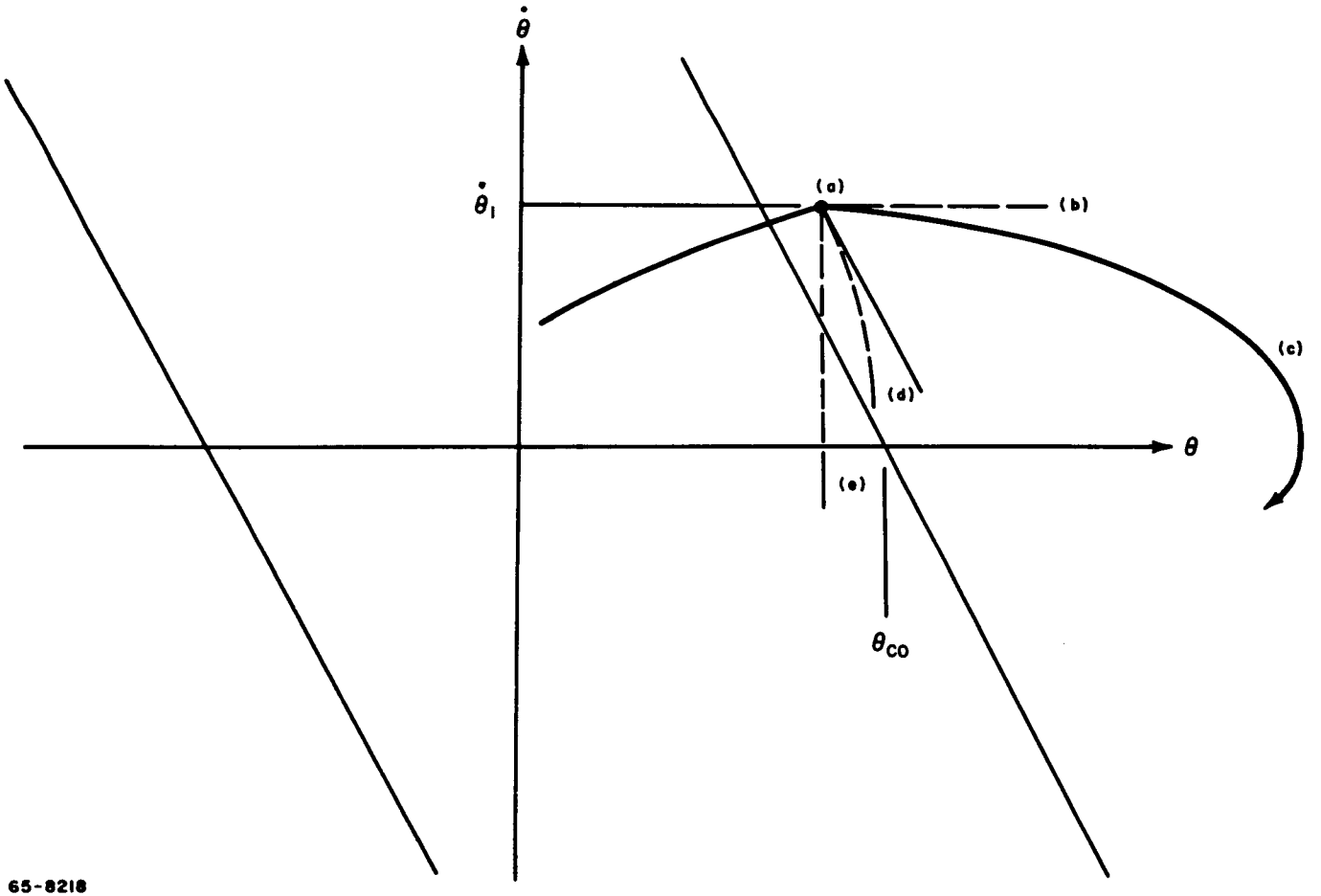

Figure D.8 SKETCH ILLUSTRATING PHASE PLANE PATHS FOLLOWED FOR DIFFERENT CONTROL TORQUE LEVELS

Substituting and letting $t = 0$ gives the slope in the phase plane of the path followed by the satellite at the moment thrust is turned on:

$$\left(\frac{d\dot{\theta}}{d\theta}\right)_{t=0} = -\frac{\tau_R - \tau_D}{J\,\dot{\theta}_1} \tag{D.11}$$

A relation for $\dot{\theta}_1$ must now be derived. This relation is based on the maximum value of $\dot{\theta}_1$ for a soft limit cycle which occurs when the impulse delivered is sufficient to just drive the system to the opposite control line as illustrated in figure D. 9.

Integrating equation (D. 8) from (2) to (1) with $\tau_R = 0$ and neglecting the small difference between θ_1 and θ_{co} gives:

$$\frac{d\theta}{dt} = \frac{\tau_D}{J}\,t \tag{D.12}$$

$$\theta + \theta_{co} = \frac{\tau_D}{2J}\,t^2 \tag{D.13}$$

When $\theta = +\theta_{co}$, $t = t_c$ and, from (D. 13):

$$t_c = 2\sqrt{\frac{\theta_{co}\,J}{\tau_D}} \tag{D.14}$$

Substitution of this relation into (D. 12) gives:

$$\dot{\theta}_1 = 2\sqrt{\frac{\theta_{co}\,\tau_D}{J}} \tag{D.15}$$

Substitution into equation (D. 11) and setting:

$$\left(\frac{d\dot{\theta}}{d\theta}\right)_{t=0} = -\frac{1}{(a-1)\tau_L} \tag{D.16}$$

where $\frac{1}{(a-1)\tau_L}$ is the control line slope gives:

$$\tau_R = \tau_D\left[1 + \frac{2\sqrt{\frac{\theta_{co}\,J}{\tau_D}}}{(a-1)\,\tau_L}\right] \tag{D.17}$$

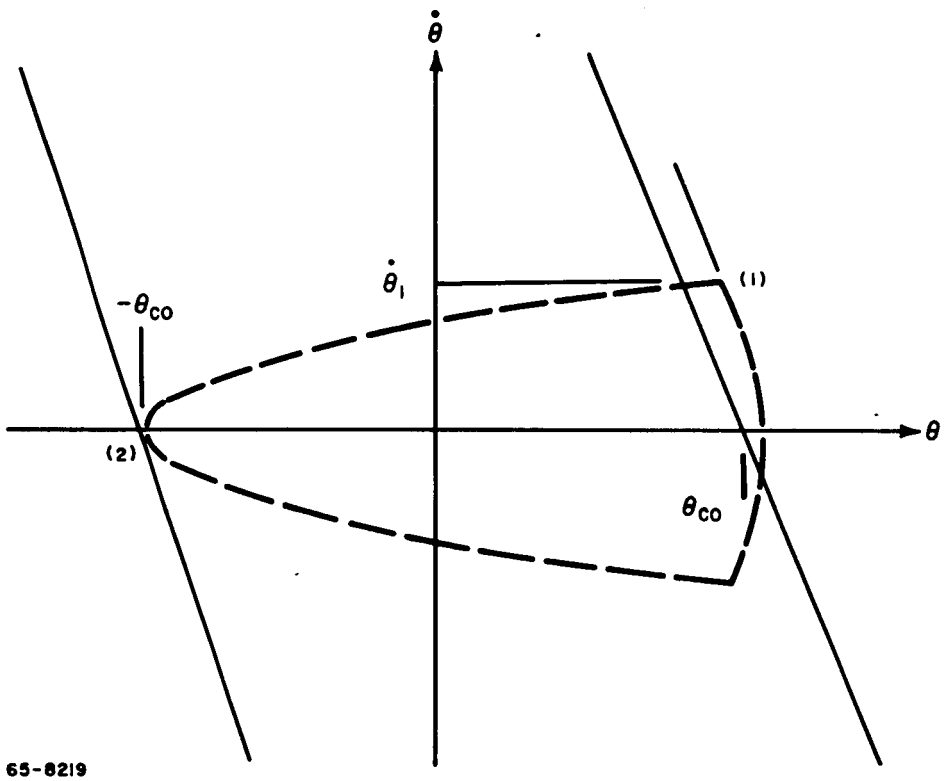

Figure D.9 ILLUSTRATION OF SOFT LIMIT CYCLE WITH MAXIMUM IMPULSE

With $(\tau_D)_{max}$ representing the estimated maximum possible disturbance torque, the permissible criterion for the minimum limit of τ_R, the control torque, is:

$$\tau_R \geq (\tau_D)_{max} \left[1 + \frac{2\sqrt{\frac{\theta_{co}\, J}{(\tau_D)_{max}}}}{(\alpha - 1)\, \tau_L} \right] \qquad \text{(D. 18)}$$

As an illustration, for the Model I system:

θ_{co} = 0.2°

J = 27 slug ft^2 = 3.66 x 10^8 gmm cm^2

α = 10

τ_L = 2 seconds

Substitution gives:

$$\tau_R \geq [(\tau_D)_{max} + 125.8\sqrt{(\tau_D)_{max}}] \qquad \text{(D. 19)}$$

With $(\tau_D)_{max}$ of 1600 dyne cm,

$\tau_R \geq$ 6630 dyne cm

The resistojets supplied to NASA Lewis have a nominal thrust of 0.3 x 10^{-3} pounds which with a moment arm of two feet provides a control torque of 8130 dyne cm and thus meets the criterion of equation (D. 18).

The maximum control torque will be based on the basic assumptions that an adaptive control system is used and that limit cycle control is maintained by fixed pulse duration operation of the resistojets. The criterion is based on maintaining soft limit cycle control down to some minimum disturbance torque, $(\tau_D)_{min}$, below which it is satisfactory for hard limit cycle operation to occur. This maximum control torque is directly dependent on the minimum pulse duration built into the control logic, $(t_R)_{min}$. In the 2nd Quarterly Progress Report, it is shown that the criterion for definite soft limit cycle operation is:

$$t_R\, \tau_R \leq 2\sqrt{\tau_D\, \theta_{co}\, J} \qquad \text{(D. 20)}$$

Setting:

$$\tau_R = (\tau_R)_{max}$$

$$t_R = (t_R)_{min}$$

$$\tau_D = (\tau_D)^{SL}_{min}$$

Equation, (D.20) becomes:

$$(t_R)_{min}\ (\tau_R)_{max} \leq 2\sqrt{\theta_{co}\, J\, (\tau_D)^{SL}_{min}} \qquad \text{(D.21)}$$

As an example, with $J = 27$ slug ft^2

$$(\tau_D)^{SL}_{min} = 10 \text{ dyne-cm}$$

$$\theta_{co} = 0.2°$$

$$(t_R)_{min} = 0.1 \text{ seconds}$$

the value for $(\tau_R)_{max}$ is computed to be:

$$(\tau_R)_{max} = 286000 \text{ dyne-cm}$$

In summary, the control torque selected for attitude control should lie within the range:

$$\left\{(\tau_D)_{max}\left[1 + \frac{2\sqrt{\frac{\theta_{co}\, J}{(\tau_D)_{max}}}}{(\alpha - 1)\ \tau_L}\right]\right\} \leq \tau_R \leq \left\{\frac{2}{(\tau_R)_{min}}\sqrt{\theta_{co}\, J\, (\tau_D)^{SL}_{min}}\right\} \qquad \text{(D.22)}$$

Within this range, other factors must be considered before a final desired value of the control torque is selected. Among these are the desire to use the same thrustors for despinning, acquisition, and station keeping as well as for attitude control and the desire to operate the resistojet under conditions of pressure, heater diameter, and nozzle configuration and dimensions which give a high specific impulse. These factors and their interrelationship can be considered quantitatively only when a specific satellite and mission are being considered.

APPENDIX E

CELESTIAL SIMULATOR AND TEST RANGE (ASTROLAB)

A celestial simulator or Astrolab is presently under construction at Avco RAD as part of an internally funded program. The purpose of the laboratory will be to evaluate complete spacecraft guidance and control systems. The basic laboratory is shown in figure E. 1.

Referring to figure E. 1 the attitude control system to be evaluated will be placed on the internal air bearing table. The table and air bearing are, in turn, located within a vacuum chamber. The attitude control system located on the air bearing table will include: (1) power supply and power conditioning equipment; (2) a reaction system, including propellant storage and feed; (3) control logic package; (4) sensors; and (5) signal conditioning equipment. The test range is 80 feet long and will contain a planet simulator, a star simulator, and a solar simulator. The combination of the three-axis air bearing, vacuum chamber, and celestial simulator will thus permit realistic evaluation of complete attitude control systems.

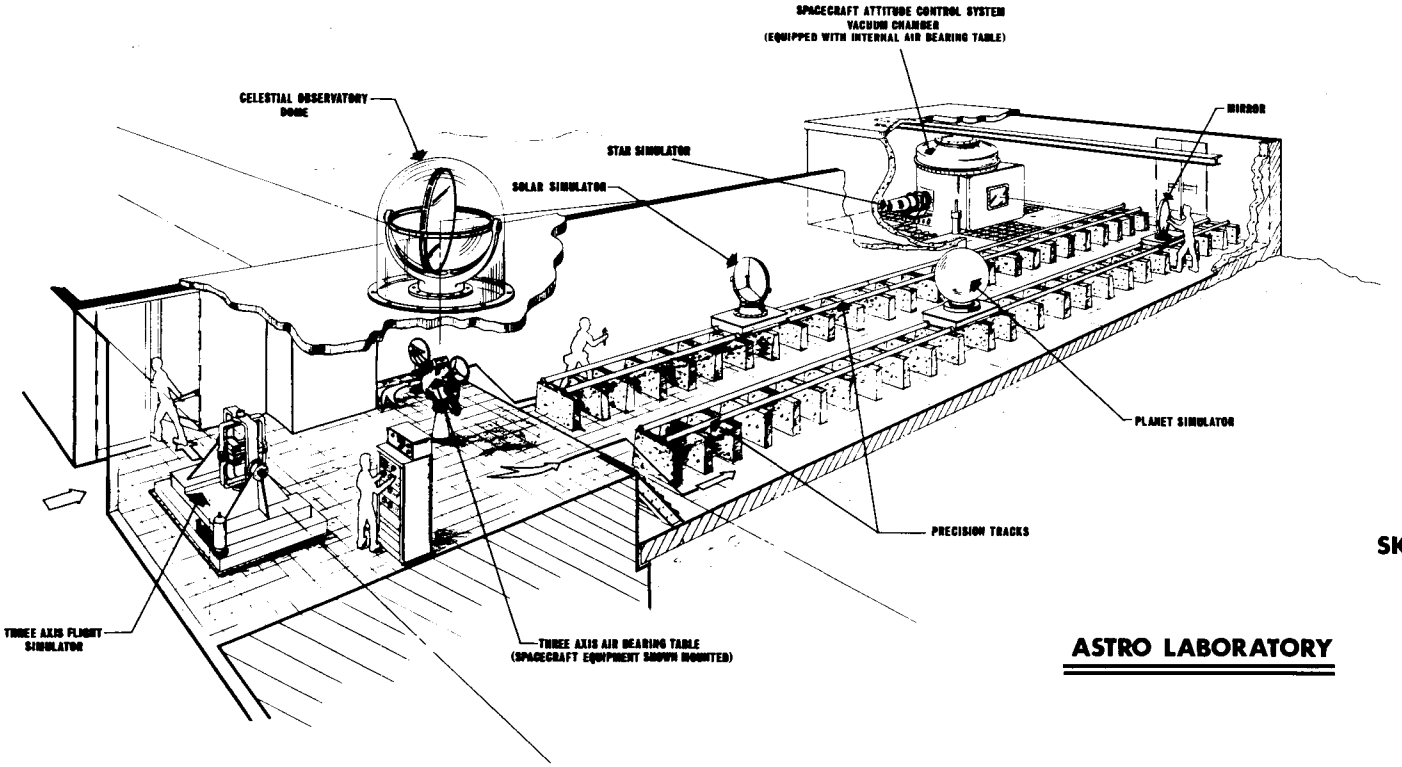

Figure E.1 AVCO RAD CELESTIAL SIMULATOR AND TEST RANGE (ASTROLAB)

DISTRIBUTION

Addressee	No. of Copies
NASA-Lewis Research Center	
21000 Brookpark Road	
Cleveland, Ohio 44135	
Attention: J. H. Childs	1
R. J. Rulis	3
H. Gold	1
R. Cybulski	1
NASA Headquarters	
FOB - 10B	
600 Independence Avenue, Northwest	
Washington, D. C. 20546	
Attention: RNT/J. Lazar	1
RNT/J. Mullen	1
NASA-Lewis Research Center	
21000 Brookpark Road	
Cleveland, Ohio 44135	
Attention: J. H. DeFord	1
H. R. Hunczak	2
J. Jack	1
N. Musial	1
Reports Control Office	1
Technology Utilization Office	1
Library	1
NASA Scientific and Technical Information Facility	
Box 5700	
Bethesda, Maryland 20014	
Attention: RQT-2448/NASA Representative	6
NASA Marshall Space Flight Center	
Huntsville, Alabama 35812	
Attention: Library	1
R-RP-DIR/G. Heller/Bldg. 4481	1
R-RP-DIR/Dr. E. Stuhlinger	1
R-RP-T/W. Jones/Bldg. 4488	1
MS-T/Dan Gates/Bldg. 4488	1
NASA-Ames Research Center	
Moffett Field, California 94035	
Attention: Library	1
DR. G. Goodwin	1

DISTRIBUTION (Cont'd)

Addressee	No. of Copies
NASA Goddard Space Flight Center Bldg. 6 Greenbelt, Maryland 20771 Attention: W. Isley/Code 623	1
Commander Aeronautical Systems Division Wright-Patterson AFB, Ohio 45433 Attention: AFAPL (APIE)/R. Supp AFAPL (APIE)/P. Lindquist	1 1
Aeronautical Systems Division Wright-Patterson Air Force Base, Ohio 45433 Attention: ASRMPE/F. L. 'Hommendieu	1
Electro-Optical Systems, Inc. 125 North Vinedo Avenue Pasadena, California Attention: Dr. R. Buhler Dr. J. Teem	1 1
General Electric Company Electric Space Propulsion Projects Evandale, Ohio Attention: Dr. M. L. Bromberg	1
Marquardt Corporation 16555 Saticoy Street Van Nuys, California Attention: R. Page	1
Gianinni Scientific Corporation 3839 South Main Street Santa Ana, California Attention: Adriano Ducati	1
Gianinni Scientific Corporation 3839 South Main Street Santa Ana, California Attention: Dr. Gabriel Gianinni	1

DISTRIBUTION (Cont'd)

Addressee	No. of Copies
Jet Propulsion Laboratory Pasadena, California 91103 Attention: G. Robillard	1
Thrust Systems Company 1641 Monrovia Costa Mesa, California Attention: W. Stoner	1
Ling-Temco-Vought, Inc. Advanced Systems, Astronautic Division Box 6267 Dallas, Texas 75222 Attention: F. T. Esenwein	1
Air Products and Chemicals, Inc. P.O. Box 538 Allentown, Pennsylvania 18101 Attention: R. Barclay	1
Arthur D. Little, Inc. Acorn Park Cambridge, Massachusetts 02140 Attention: A. Fowle	1
Beech Aircraft P.O. Box 631 Boulder, Colorado Attention: J. Bell	1
Garrett Corporation/Air Research 9851 Sepulveda Blvd. Los Angeles, California 90045 Attention: R. Fischer	1
TAPCO 7209 Platt Avenue Cleveland, Ohio 44104 Attention: Dr. P. Lawlor	1

DISTRIBUTION (Concl'd)

Addressee	No. of Copies
NASA-Langley Research Center Langley Station Hampton, Virginia Attention: Mike Ellis, MS 160	1
Jet Propulsion Laboratory California Institute of Technology 4800 Oak Grove Drive Pasadena, California Attention: John W. Stearns, Jr. MS 125-224	1
Dr. J. Lundholm Fairchild Aircraft Washington, D.C.	1
Central Files	1
Research Library (+ 1 reproducible)	50